TETRADENIA RIPARIA (HOCHST.) CODD (LAMIACEAE) AQUEOUS LEAF EXTRACT ENHANCED OXIDANT PRODUCTION AND NF-κB MEDIATED APOPTOSIS IN HEPATOCELLULAR CARCINOMA (HEPG2) CELLS

Seluleko Gcaba

Student number: 218045487

BMedSci Physiology (UKZN), BMedSci Honours in Medical Biochemistry (UKZN)

Submitted in fulfilment for the degree

MASTER OF MEDICAL SCIENCE (MEDICAL BIOCHEMISTRY)

School of Laboratory Medicine and Medical Sciences

College of Health Sciences

University of KwaZulu-Natal

Durban

2024

DECLARATION

This dissertation contains original work done by the author and has not been submitted to UKZN or any other tertiary institution for the purposes of obtaining an academic qualification, whether by myself or any other party. The use of work by others has been duly acknowledged in the text. The research described in this study was carried out in the Department of Medical Biochemistry and Chemical Pathology, School of Laboratory Medicine and Medical Science, Faculty of Health Sciences, University of KwaZulu-Natal, Durban, under the supervision of **Dr RB Khan** and **Dr HK Khumalo.**

SIGNED : _____ **DATE: 22 January 2025**

Mr S Gcaba

SIGNED : _____ **DATE: 22 January 2025**

Dr R Khan

SIGNED : _____ **DATE: 22 January 2025**

Dr H Kumalo

ACKNOWLEDGEMENTS

- I thank the Almighty God for this opportunity and for providing me with strength throughout the year.
- I would like to express my gratitude to **Miss VV Gcaba, Mrs PG Dube,** the **Gcaba** family, and **Miss NT Buthelezi** for being my biggest supporters and cheerleaders. I am honoured and will forever be grateful for your prayers and love.
- I would like to sincerely thank **Dr RB Khan** and **Dr HK Khumalo** for granting me this opportunity and for her guidance. To be supervised by someone like you is an answer to my prayers. Thank you for your encouragement and wise advice throughout the course of this thesis.
- I would also like to thank **Mr K Dumisa**, **Mr S Govender**, **Ms A Dlamini**, **Ms N Phakathi** and the whole **Department of Medical Biochemistry**. I couldn't have wished for more ideal peers with whom to discuss my research. You have been incredibly helpful and committed to your work. In happy times, we danced and gave thanks to God together, and in bad times, we prayed for better days and supported one another. You all made my life so much easier, so I'm glad I got to meet you.
- To my friends and extended family, I appreciate your support, encouragement, and prayers. I appreciate you constantly reminding me that God is good all the time. I want to express my gratitude to all my friends for always checking in on me and supporting me, as well as for showing love all the way. I sincerely value your friendship and thank God for every one of you.
- Gratitude to **College of Health Sciences Scholarship (CHS)** and **(Health and Welfare Sector Education and Training Authority) HWSETA** for funding my project.

TABLE OF CONTENTS

LIST OF ABBREVIATIONS

ΔΨM	Mitochondrial membrane potential
%	Percentage
AFB_1	Aflatoxin B_1
AFP	Alpha-fetoprotein
APAF-1	Apoptotic protease activating factor-1
APS	Ammonium persulfate
BCA	Bicinchoninic acid
BCL-2	B cell lymphoma-2
BSA	Bovine serum albumin
CCM	Complete culture medium
cIAP	Cellular -linked inhibitor of apoptosis protein
-COOH	Carboxyl
cPARP	Cleaved poly (ADP-ribose) polymerase
CST	Cell Signalling Technology
CYP	Cytochrome P450
DAMPs	Damage-associated molecular pattern
dH_2O	De-ionised water
DIABLO	Direct inhibitor of apoptosis-binding protein with low pI
DISC	Death inducing signalling complex
DMEM	Dulbecco's Modified Eagle Medium
DMSO	Dimethyl sulfoxide
DNA	Deoxyribonucleic acid
dNTP	Deoxynucleotide triphosphates
ETC	Electron transport chain
FADD	Fas-associated death domain
Fas	First apoptosis signal
Fas-L	Fas ligand
GPx	Glutathione peroxidase
GSH	Glutathione
GST	Glutathione transferase
GSTA2	Glutathione S-transferase A2

HBV	Hepatitis B virus
HCC	Hepatocellular carcinoma
HCC-CCA	Hepatocellular cholangiocarcinoma
HCV	Hepatitis C virus
HepG2	Hepatocellular carcinoma
H_2O_2	Hydrogen peroxide
HRP	Horse-radish peroxidase
HSC	Hepatic stellate cells
iCCA	Intrahepatic cholangiocarcinoma
IFN	Interferon
IKK	IκB kinase
IL	Interleukin
iNOS	Inducible nitric oxygen synthase
KCl	Potassium chloride
Keap1	Kelch-like ECH-associated protein 1
LDH	Lactate Dehydrogenase
LPS	Lipopolysaccharide
LPS-TLR	Lipopolysaccharide-Toll-like receptor
MAPK	Mitogen-activated protein kinase
MDA	Malondialdehyde
MLKL	Mixed lineage kinase domain-like
MOMP	Mitochondrial outer membrane permeabilization
NaCl	Sodium chloride
NADPH	Nicotinamide adenine dinucleotide phosphate hydrogen
NEDD	N-(1-naphthyl)- ethylenediamine
NEMO	NF-κB essential modulator
NF-κB	Nuclear factor kappa B
NH_2	Amino
$NO^{\bullet}$	Nitric oxide
NOS	Nitric oxygen synthase
Nrf2	Nuclear factor erythroid 2–related factor 2
O_2	Oxygen
$O_2^{\bullet-}$	Superoxide anion radical
OD	Optical density

$^{-}$OH	Hydroxyl
$^{\bullet}$OH	Hydroxyl radical
$^{\bullet}$ONOO	Peroxynitrite
PAMPs	Pathogen-associated molecular patterns
PS	Phosphatidylserine
RBD	Relative band density
RFU	Relative fluorescence units
RIPK	Receptor-interacting protein kinase
RLU	Relative light units
RNS	Reactive nitrogen species
ROS	Reactive oxygen species
RT	Room temperature
SDS	Sodium dodecyl sulfate
-SH	Thiol
SOD2	Superoxide dismutase 2
STAT	Signal transducer and activator of the transcription
TBA	Thiobarbituric acid
TBA-BHT	Thiobarbituric acid-butylated hydroxytoluene
TBARS	Thiobarbituric acid reactive substances assay
TCA	Tricarboxylic acid cycle
TEMED	Tetramethyl ethylenediamine
TNF	Tumour necrosis factor
TNF-α	Tumour Necrosis Factor alpha
TRADD	TNF associated death domain
TRAIL	TNF-related apoptosis-inducing ligand
TRALE	*T. riparia* aqueous leaf extract
T. riparia	*Tetradenia riparia*
TBS	Tris-buffered saline
TTBS	Tween-20 Tris-buffered saline
VCl_3	Vanadium chloride

LIST OF FIGURES

LIST OF TABLES

ABSTRACT

Introduction: Cancer has become a global health problem, contributing almost 20 million new cases and 10 million deaths worldwide in 2020. Ranked third globally, liver cancer accounted for 8.3% of the global cancer-associated mortality. Hepatocellular carcinoma (HCC) accounts for more than 90% of diagnosed primary liver cancer cases. Treatment may include chemotherapy, radiation therapy and liver transplant, but these treatments are expensive and induce serious adverse effects that reduce the efficacy of treatment. Medicinal plants are the suggested alternate treatment option attributed to anti-microbial, antioxidant and anti-inflammatory effects that may ameliorate the harsh side effects, but also demonstrate anti-cancer activity. *Tetradenia riparia* is a readily available South African shrub with medicinal and anti-cancer potential, but the mechanisms require elucidation. This study aimed to investigate the antioxidant and cell death mechanisms activated by *Tetradenia riparia* aqueous leaf extract (*TRALE*) in HCC (HepG2) cells.

Methods: HepG2 cells were treated with several concentrations of TRALE (0–3000 μg/ml) for a duration of 24 hours to assess the cell viability. The methylthiazol tetrazolium (MTT) assay was used to obtain an IC_{50}, which was used to treat the HepG2 cells for all subsequent assays. After treatment, mitochondrial activity was assessed as a measure of cell viability using luminometry for the ATP and mitochondrial membrane potential ($\Delta\Psi m$) assays. The cells were assayed for oxidative stress by quantifying free radical mediated membrane damage (TBARS, NOS and LDH cytotoxicity assays, and *iNOS* gene expression), and antioxidant response using luminometry (GSH, GSSG, ratio of GSH/GSSG), qPCR (*SOD2*, *catalase*, *GPx1*, *Nrf2*) and western blotting (HSP70). Induction of apoptosis was determined by luminometrically quantifying caspase-3/7, caspase-8, and caspase-9 activities. Furthermore, the Annexin V apoptosis and necrosis assay elucidated the cell death pathway. Protein expression of cIAP (Western blot) and qPCR for *NF-κB* and *BCL-2* were also evaluated.

Results: After a 24-hour exposure, *TRALE* conferred a dose-dependent reduction in cell viability that was associated with a notable drop in ATP at the IC_{50}. An increase in $\Delta\Psi M$ led to increased levels of ROS, which increased lipid peroxidation and RNS production despite downregulated *iNOS*. Elevated *SOD2* in response to ROS production enhanced the HepG2 cell's ability to convert superoxide radicals into H_2O_2, while *catalase* and *Gpx1* were upregulated to prevent harmful ROS formation and protect macromolecules from oxidative damage. Increased *GPx1* was associated with depletion of GSH and the GSH/GSSG ratio, but *Nrf2* was downregulated and HSP70 was similar to the control. The downregulation of *Nrf2* was associated with increased *NF-κB*. Initiator caspase-8 activation corresponded with downregulated cIAP, while downregulated *BCL-2* contributed to caspase-9

activation. In addition, activation of caspase-3/7 facilitated phosphatidylserine externalisation. Necrotic markers and LDH were decreased, suggesting that *TRALE* induced apoptosis in HepG2 cells. **Conclusion:** The decreased cell viability was associated with depletion of ATP, while ΔΨm contributed to ROS production that increased RNS and caused lipid peroxidation. Although GSH was depleted and *Nrf2* was downregulated, the upregulated *SOD2*, *catalase* and *Gpx1* suggest a response suggested a response to ameliorate oxidative stress as implied by unchanged HSP70. However, oxidants were still elevated and associated with increased *NF-κB*. Interestingly, *iNOS* expression was downregulated, thus *NF-κB* contributed to initiation of apoptosis that was associated with decreased *BCL-2* and cIAP, and increased caspase activity. In addition, necrosis was not evident. Therefore, the *TRALE*-treated HepG2 cells were more susceptible to apoptosis. Further studies are required to elucidate the role of NF-κB in *TRALE*-induced apoptosis.

KEYWORDS: *Tetradenia riparia*, liver cancer, HepG2 cells, oxidative stress, apoptosis.

CHAPTER 1 : INTRODUCTION

1.1 BACKGROUND

Cancer is a disease where the body's cells grow uncontrollably, potentially spreading to all parts of the body (Ferlay *et al.*, 2021). The fast-growing cells have the potential to develop into tumours and interfere with normal bodily functions. Cancer has emerged as a major global health issue, accounting for over 10 million deaths globally in 2020 and 2022 (Sung *et al.*, 2021;Bray *et al.*, 2024). There are different types of cancer, and one of the main causes of cancer-related fatalities globally is liver cancer. Liver cancer remains a burden as it accounted for an estimated 4.7% cancer cases and about 7.8% cancer deaths, globally in 2022 (Bray *et al.*, 2024). Primary liver cancer was ranked the 6th most diagnosed cancer and the 3rd leading cause of cancer death world-wide in 2022 (Bray *et al.*, 2024). Hepatocellular carcinoma (HCC) is the most prominent type of primary liver cancer, accounting for more than 90% of diagnosed cases (Sung *et al.*, 2021). The main risk factors for HCC include aflatoxin-contaminated foods, chronic infection with hepatitis B virus (HBV) or hepatitis C virus (HCV), heavy alcohol intake, smoking, excess body weight and type 2 diabetes (Shen *et al.*, 2020). The significant risk factors differ from region to region. Liver cancer treatment also varies but may include chemotherapy, transplant and, in some cases, radiation (Sung *et al.*, 2021). Many people have turned to herbal medicine for treatment due to the high cost of conventional cancer treatment (Anwanwan *et al.*, 2020), and over 80% of people in developing countries rely on herbal medicine for their primary healthcare (Mhlanga *et al.*, 2019). These methods have been linked to several side effects, such as extreme fatigue, severe bleeding after surgery, and increased risk of infection. Therefore, scientists are investigating complementary alternative medicine that utilises medicinal plants.

Medicinal plants have served as a primary source of treatment to rural communities in South Africa (Mahlangu, 2019). Traditional healers use them for the treatment of common ailments such as toothache, erectile dysfunction, libido and chronic skin disease, among others. Plants were used alone or in combination with other plants (Megersa *et al.*, 2019). Compounds derived from medicinal herbs are becoming more widely acknowledged as beneficial and supplemental treatments for cancer (Dietz and Dekker, 2017). Numerous clinical studies have documented the positive effects of herbal medicine on cancer patients' quality of life, immune system function, and survival when combined with traditional therapies (chemotherapy, radiation therapy, and surgery) (Thompson and Hawkins, 2025;Youn *et al.*, 2023;Gaobotse *et al.*, 2023). The chemopreventative and chemotherapeutic

activities of natural phenolic compounds in the treatment and management of cancer have made them one of the most intriguing secondary metabolites (Dietz and Dekker, 2017).

Tetradenia riparia belongs to the Lamiaceae family, and grows up to a height of three meters tall along riverbanks, forest margins and hillsides in many parts of South Africa (Shimira, 2022). It is locally known as "iboza" and is popularly referred to as “ginger bush". Inhaling the aroma of crushed leaves is used to treat malaria, stomachaches, chest pains, and headaches (Shimira, 2022). In addition, *T. riparia* extracts have medicinal properties for alleviating headaches, dropsy, toothache, diarrhoea, fever, and cough. The essential oil from *T. riparia* leaves has proven to have repellent potential and at the molecular level, demonstrates cytotoxicity and anti-cancer potential (Shimira, 2022;Milato *et al.*, 2018). In addition, studies on essential oils of *T. riparia* have reported some antioxidant activity of the isolated compounds (Milato *et al.*, 2018).

Antioxidants are molecules that prevent oxidative stress, a condition defined as an imbalance between oxidants in the form of reactive oxygen species (ROS) and reactive nitrogen species (RNS), and antioxidants in favour of the oxidants (Sies and Jones, 2020). The nucleophilic antioxidants react with electrophilic oxidising agents, donating electrons to them, thereby inhibiting oxidative stress and associated diseases, including cancer (Sies and Jones, 2020). The ROS are very reactive chemical molecules that include a variety of different chemical species, including hydrogen peroxide (H_2O_2), hydroxyl radical ($^{\bullet}OH$), and superoxide anion radical ($O_2^{\bullet-}$). The most prevalent RNS are peroxynitrite ($^{\bullet}ONOO$) and nitric oxide ($NO^{\bullet}$) (Aranda-Rivera *et al.*, 2022). These molecules are essential in cell signalling, but disruption of redox homeostasis results in molecular damage to lipids, protein and DNA (Kurashova *et al.*, 2020). Lipid peroxidation results in the formation of aldehyde products such as malondialdehyde (MDA), a marker for oxidative stress. Heatshock protein 70 (HSP70) is essential for proteostasis during oxidative stress, while oxidised DNA bases are repaired by base excision repair and lipid hydroperoxides are neutralised by glutathione (Rosenzweig *et al.*, 2019;Kurashova *et al.*, 2020).

The nuclear factor erythroid 2–related factor 2 (Nrf2) antioxidant mechanism activates the production of the enzymes glutathione peroxidase (Gpx), catalase, and superoxide dismutase 2 (SOD2), which guard against oxidative stress (Aranda-Rivera *et al.*, 2022). An inverse relationship exists between Nrf2 and nuclear factor kappa B (NFκ-B), signifying an important relationship between oxidative stress, inflammation and cell death (Liu *et al.*, 2022). To protect the cell, SOD2 catalyses the dismutation of two $O_2^{\bullet-}$ (plus two protons) into H_2O_2 and molecular oxygen (O_2), which can be

expelled as water in reactions catalysed by catalase and Gpx; it is essential to note that Gpx requires reduced glutathione (GSH) to reduce H_2O_2 to water (Ndlovu *et al.*, 2021). During oxidative and nitrosative stress, oxidation of cellular macromolecules results in damage that predisposes to cell death.

The physiologically-regulated and methodically-planned process of programmed cell death, also known as apoptosis, occurs to preserve the ideal ratio of cell division to death (Prasad, 2022). The extrinsic pathway uses extracellular signals to induce apoptosis by binding death ligands to tumour necrosis factor (TNF) family death receptors, including the TNF receptor and the first apoptosis signal (Fas) receptor (Soond *et al.*, 2021; Prasad, 2022). These death ligands include TNF-related apoptosis-inducing ligand (TRAIL), Fas ligand (Fas-L), and TNF-α, which bind to their cognate receptors and form a death-inducing signalling complex (DISC) (Prasad, 2022). The proximity of pro-caspase-8 to DISC results in activated caspase-8, which will then cleave and activate downstream executioner caspase-3 and -7 (Prasad, 2022; Singh and Lim, 2022). Executioner caspases can also be activated via the intrinsic apoptosis pathway.

The B cell lymphoma-2 (BCL-2) family of proteins regulates the activation of the intrinsic (mitochondrial) pathway in response to cellular stress like degradation of deoxyribonucleic acid (DNA), nutrient shortage and hypoxia (Cavalcante *et al.*, 2019). Pro-apoptotic (Bax, BAK, BOK, and Bid) or anti-apoptotic (Bcl-2, MCL-1, BFL-1/A1, BCL-w, Bcl-x, and Bcl-xL) BCL-2 family members regulate mitochondrial outer membrane permeabilisation (MOMP) to facilitate the extrusion of intermembrane space proteins (Cavalcante *et al.*, 2019). Cytochrome c, apoptosis-inducing factor, endonuclease G and second mitochondria-derived activator of caspases/direct inhibitor of apoptosis-binding protein with low pI (SMAC/DIABLO) are among the pro-apoptotic molecules released into the cytoplasm when MOMP is induced by oligomerisation of pro-apoptotic BCL-2 proteins (Prasad, 2022). When cytochrome c binds with the adaptor protein apoptotic protease activating factor-1 (APAF-1) and pro-caspase 9, the resultant apoptosome activates caspase-9 (Cavalcante *et al.*, 2019). The cells can execute apoptosis when caspase-3/7 is subsequently activated (Cavalcante *et al.*, 2019). The binding of SMAC to an inhibitor of apoptosis proteins (IAPs) prevents the inhibition of caspase-9, caspase-3 and caspase-7, thus, ensuring completion of the intrinsic apoptotic pathway (Cavalcante *et al.*, 2019). Execution of apoptosis by caspase-3/7 ensures the programmed dismantling of the cell by activating the cleavage of nuclear and cytoplasmic proteins and externalising phosphatidylserine for apoptotic cell recognition by phagocytes (Cavalcante *et al.*, 2019).

1.2 PROBLEM STATEMENT / RATIONALE

Liver cancer is rated 6th and 3rd in cancer–related incidence and mortality, respectively (Bray *et al.*, 2024). In South Africa, the burden is compounded by a low 5-year survival rate, with many patients succumbing to the disease within one year of diagnosis (Sykes, 2021). Although treatment is available, it is evident that they are ineffective. In addition, harsh side effects are associated with the treatments. Thus, new strategies are required to halt this growing burden. Many people are now choosing traditional methods to treat diseases as these treatments are cheap and contain no known adverse side effects. Traditional healers have used medicinal plants to cure cancer or minimize the debilitating side effects (Ghuman *et al.*, 2019). However, the efficacy and mechanisms require further investigation. This study, therefore, aimed to provide evidence on the cytotoxic mechanisms induced by *T. riparia* aqueous leaf extract (*TRALE*) in liver cancer (HepG2) cells.

1.3 SIGNIFICANCE AND IMPLICATIONS

The world sits in balance observing the war between drug discovery and new variants in diseases, making it difficult to penetrate these diseases and illnesses; thus, making therapeutic agents of clinical importance. Cancer has increased in eminence and, along that path, has killed millions of people and has destroyed family trees across the globe (Sung *et al.*, 2021). Such a finding would benefit patients' families and reduce the burden on frail healthcare systems since the plants are easily accessible and may be grown in the backyard.

1.4 RESEARCH QUESTION

Does *TRALE* induce cytotoxicity via free radical production and apoptosis in HepG2 cells?

1.5 ALTERNATIVE HYPOTHESIS

TRALE will induce oxidative stress and cell death as cytotoxic manifestations in the HepG2 cells.

1.6 NULL HYPOTHESIS

TRALE will not induce oxidative stress and cell death as cytotoxic manifestations in the HepG2 cells.

1.7 AIM

This study aimed to determine the cytotoxic effect of *TRALE* in hepatocellular carcinoma (HepG2) cancer cells.

1.8 OBJECTIVES

- To evaluate the cytotoxicity of *TRALE* on HepG2 cells by:
  - assessing cell viability using the MTT assay to determine the inhibitory concentration (IC_{50}) for subsequent assays, and
  - using JC-10 and ATP luminometric tests to evaluate mitochondrial integrity.
- To evaluate how oxidative stress is affected by:
  - the TBARS assay was used to measure lipid peroxidation by quantifying MDA levels;
  - quantifying RNS using the nitrite/nitrate assay and probing for *iNOS* gene expression using qPCR;
  - quantifying GSH using luminometry;
  - determining gene expression of antioxidant genes (*Gpx1*, *SOD2*, *Nrf2*, and *Catalase*) using qPCR; and
  - detecting *NF-κB* (qPCR) and HSP70 (Western blot) to evaluate the stress response.
- To identify the process by which cells die by:
  - using the caspase luminometry assay to determine the initiator and executioner caspases involved;
  - using the annexin V assay to detect the externalised phosphatidylserine and necrosis;
  - detecting anti-apoptotic proteins (cIAP and *BCL-2*) for inhibition of apoptosis; and
  - analysing end-stage cell death by employing the LDH assay to detect damage to the cell membrane.

CHAPTER 2 : LITERATURE REVIEW

2.1 CANCER

Cancer is a genetic disease that transpires when bodily cells proliferate uncontrollably and may potentially spread to different body sections (Sung *et al.*, 2021). When cells multiply rapidly, they can form tumours and disrupt normal body functions. Ten enabling hallmarks associated with cancer may be inherited or acquired when environmental factors cause accumulating mutations (Ferlay *et al.*, 2021). Unfortunately, cancer is a significant global health concern, with an estimated 10 million deaths reported worldwide in 2020 and 2022 (Figure 2.1) (Bray *et al.*, 2024;Sung *et al.*, 2021). The numbers are anticipated to rise by 45% from 2008 levels to over 13 million deaths in 2030, with most deaths occurring in low- to medium-income countries such as South Africa (Bray *et al.*, 2018). Lung cancer was the most frequently diagnosed cancer in 2022 (Figure 2.1), responsible for almost 2.5 million new cases world-wide (12.4% of all cancers globally), followed by female breast cancer (11.6%), colorectal cancer (9.6%), prostate cancer (7.3%) and stomach cancer (4.9%) (Bray *et al.*, 2024). Lung cancer was also the leading cause of cancer death globally (Figure 2.1), with an estimated 1.8 million deaths (18.7%), followed by colorectal (9.3%), liver (7.8%), female breast (6.9%), and stomach (6.8%) cancers (Bray *et al.*, 2024). Breast cancer and lung cancer were the most frequent cancers in women and men, respectively (both cases and deaths). In 2022, primary liver cancer was ranked the sixth most common cancer and the third leading cause of cancer death worldwide (Figure 2.1). In South Africa, the highest incidence recorded was for breast cancer at 13.2%, followed by prostate cancer at 11.4% and cervix uteri at 10.3%. While lung cancer was 4th with 8.1% incidence, it was the first leading cause of mortality (12.7%) (Bray *et al.*, 2024).

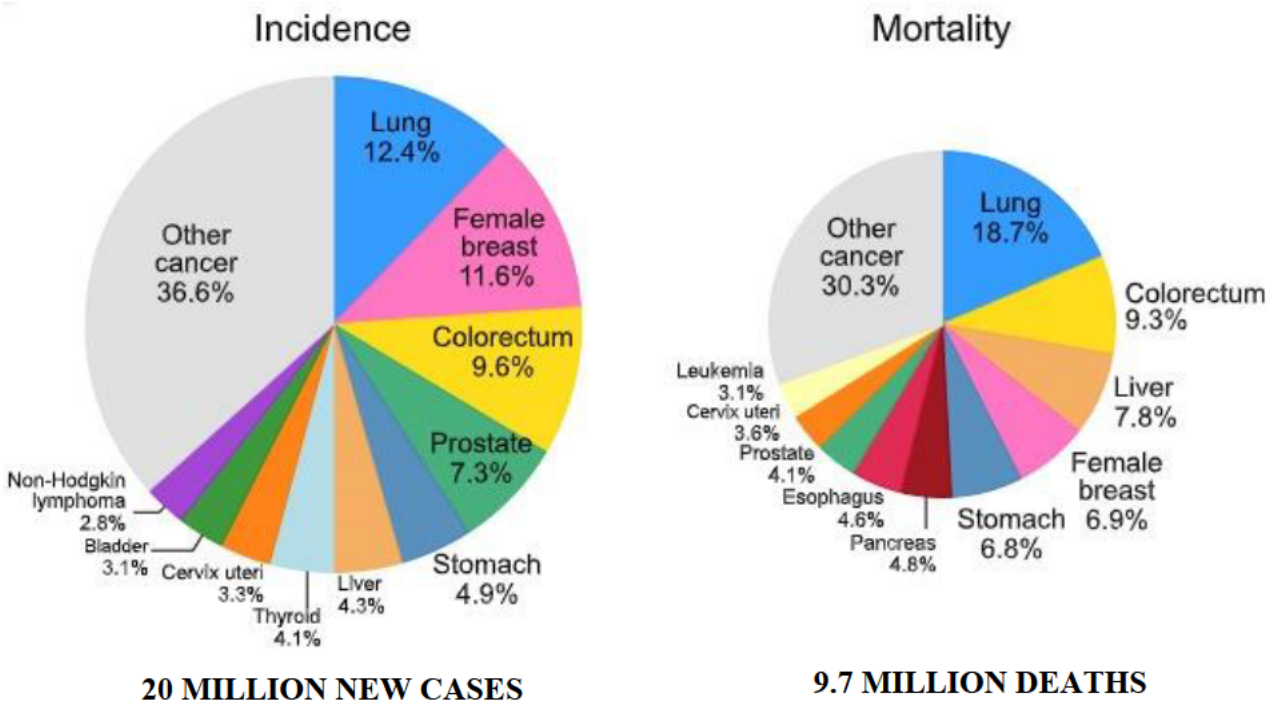

Figure 2.1: The incidence and mortality of liver cancer worldwide compared to other types of cancers worldwide. Lung cancer is the most frequently diagnosed cancer, responsible for almost 2.5 million new cases and liver cancer ranked the sixth most distinguished cancer and the third leading cause of cancer death worldwide (Bray *et al.*, 2024).

2.2 LIVER CANCER

2.2.1 Incidence and mortality

Liver cancer, also known as hepatic cancer, is a type of cancer that originates from the hepatocytes. Unfortunately, liver cancer remains a significant issue that is associated with 4.3% of new cancer cases and 7.8% of cancer-related deaths globally in 2022 (Bray *et al.*, 2024). The incidence of liver cancer is higher in males (Figure 2.2), accounting for 5.8% of new male cancer cases and 9.6% of male cancer deaths in 2022. On the other hand, females accounted for 2.7% of new cases and 5.5% of deaths due to liver cancer. Furthermore, among men, liver cancer ranks as the second most frequent cause of cancer-related death (Bray *et al.*, 2018). The highest incidence rate of liver cancer was recorded in Eastern Asia, with 22.4% of cases in males and 7.2% in females (Figure 2.2). In contrast, Southern Africa had a lower incidence rate, 6.1% for males and 3.7% for females (Figure 2.2). Black African men and women had recorded mortality-to-incidence ratios of 4.0 and 3.4, respectively (Mak *et al.*, 2018). In South Africa, liver cancer was ranked in the 10th position for incidence and the 7th in mortality (Bray *et al.*, 2024).

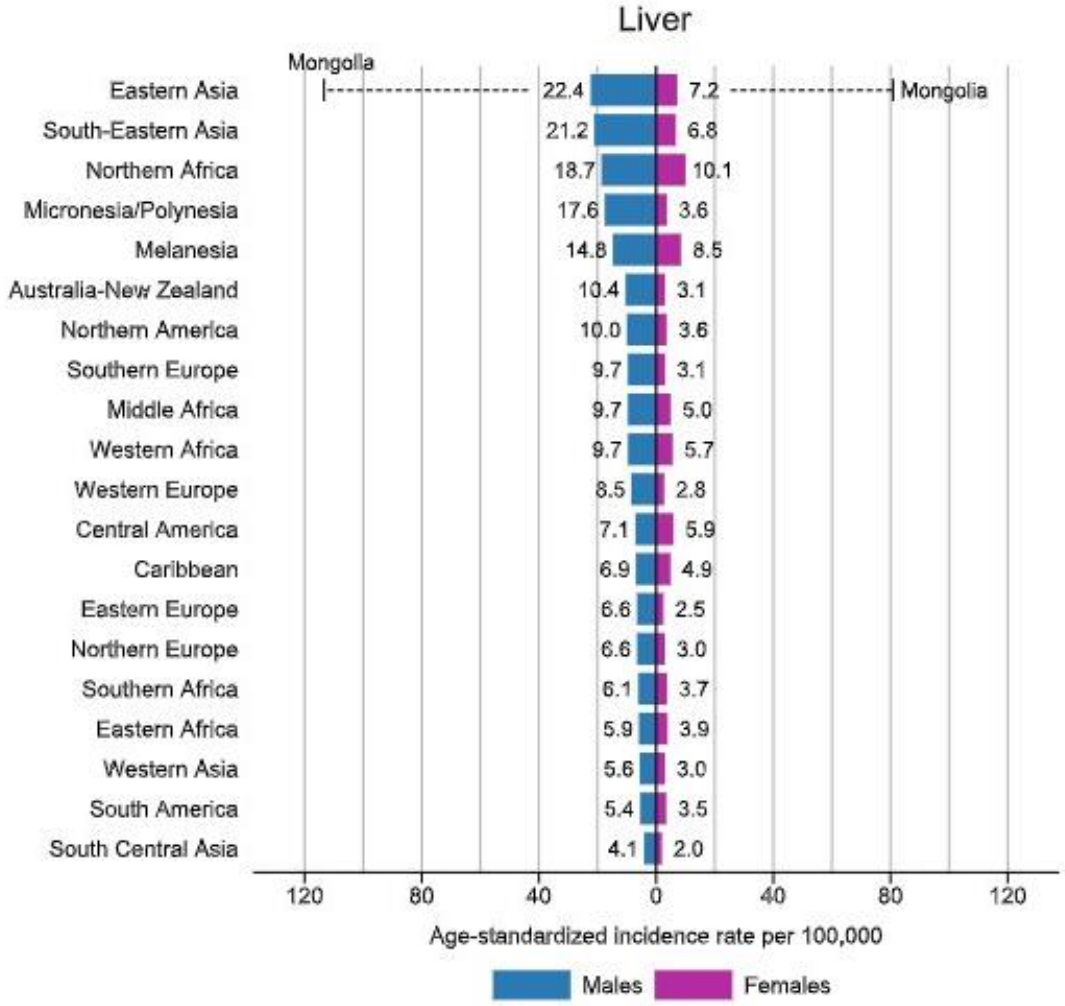

Figure 2.2: Region-specific incidence age-standardised rates by sex for liver cancer in 2022. South Central Asia had the lowest recorded incident rate of liver cancer for both male and females with 4.1% in males and females sitting at 2.0% incidences whereas the highest incidence rate of liver cancer in males was recorded in Eastern Asia, with 22.4% of cases and the highest incident in females was recorded in Northern Africa with 10.1% cases (Bray *et al.*, 2024).

2.2.2 The liver structure and function

The liver is the largest solid organ in the body (Figure 2.3A). In the anomalous hollow, it is in the upper right-hand area, just below the diaphragm and above the stomach, right kidney, and intestines (Nyahada, 2021). There are two sections to the liver; a larger right lobe and a smaller left lobe (lobes). Both are divided into eight segments. The segments comprise thousands of lobules (Figure 2.3B) (Petrick and McGlynn, 2019). The common hepatic duct comprises larger ducts that connect to smaller ducts that connect to the lobules. Bile produced by the liver is transported to the gallbladder via the hepatic duct and the first segment of the small intestine (the duodenum). The portal veins supply the liver with about 75% of its blood straight from the spleen and gastrointestinal system (Licata, 2016). The liver is particularly vulnerable to harm from the almost undiluted toxic medicines

and xenobiotics it receives because of its intimate relationship with the gastrointestinal tract and distinct metabolic function (Ortega-Alonso and Andrade, 2018).

The liver performs many essential functions, such as regulating blood clotting and filtering toxins from the blood. It supports the body in over 500 ways (Nyahada, 2021). Additionally, the liver plays a crucial role in regulating blood sugar levels, removing toxins and waste materials from the bloodstream, and producing essential nutrients. Bile, a transparent yellow or orange fluid that helps in the digestion and absorption of fats by solubilising them, is secreted by the liver (Calderaro *et al.*, 2019).

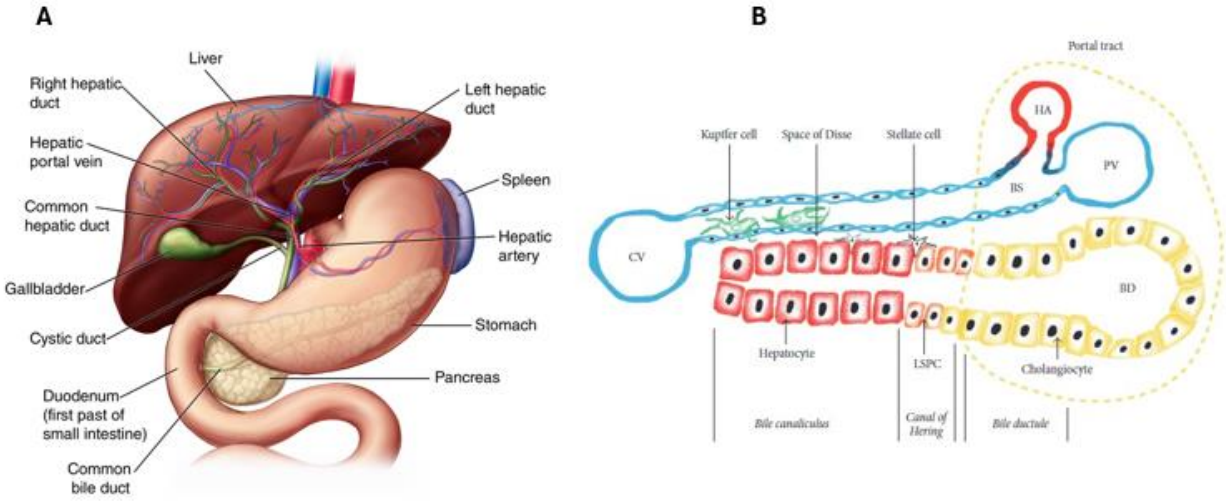

Figure 2.3: Structure and the essential parts of the lung. (A) The liver is the largest internal organ in the body and is responsible for many functions, such as metabolism and detoxification. **(B)** The liver lobule and location of essential cells for optimal liver function (Nyahada, 2021).

2.2.3 Cellular anatomy of the liver

Hepatocytes are parenchymal cells that makeup about 80% of all liver cells (Figure 2.3B) (Calderaro *et al.*, 2019). Hepatic stellate cells (HSC) (Figure 2.3B) retain fat and vitamin A. These cells contribute to the onset and progression of hepatic fibrosis because of liver injury, which may facilitate the development of hepatic carcinogenesis (Nyahada, 2021). Gastrointestinal endotoxins activate hepatic macrophages known as Kupffer cells (Figure 2.3B), which have high levels of phagocytic, endocytic, and secretory activity. Communication between the hepatocytes and the inner sinusoidal region is mediated by non-parenchymal cells known as sinusoidal endothelial cells (Figure 2.3B) (Nyahada, 2021). Furthermore, endothelial cells prevent infections from entering the hepatic parenchyma, and hepatocytes are essential for protein synthesis, metabolism, and detoxification (Calderaro *et al.*, 2019).

2.2.4 Role of hepatocytes

Hepatocytes play an active role in the hepatic production of bile and the metabolism of proteins, lipids, glycides, vitamins, and metals. Additionally, these cells support excretion, detoxification, and energy storage (Calderaro *et al.*, 2019). Hepatocytes release various proteins into the bloodstream, such as albumin, transferrin, plasminogen, fibrinogen, fetoprotein, and clotting factors (Schrödl *et al.*, 2016). Serum albumin, which is only produced by hepatocytes, is the most abundant protein released by any cell (Dao Thi *et al.*, 2020). In the Golgi, proteins are packaged in secretory vesicles for transport to the basolateral membrane for exocytosis (Ortega-Alonso and Andrade, 2018). Filtered and altered blood can flow into the hepatic vein and the inferior vena cava because hepatocytes have cords arranged into hexagonal lobules (Figure 2.3B) constructed around a central vein (Dao Thi *et al.*, 2020). This configuration assures that hepatocytes are some of the first cells to encounter everything taken orally and subsequently taken up by the digestive tract, regardless of its potential benefits or drawbacks (Ortega-Alonso and Andrade, 2018).

2.2.5 Xenobiotic metabolism

Chemicals not typically metabolised by an organism, such as antibiotics and analgesics, are known as xenobiotics (Đanić and Mikov, 2020). Xenobiotic metabolism refers to the metabolic processes that change the chemical structure of xenobiotics (Đanić and Mikov, 2020). Many xenobiotics may accumulate to toxic levels if not broken down by proper cellular metabolism. Most of the metabolic activity within the cell requires energy, cofactors and enzymes (Đanić and Mikov, 2020). Cytochrome P450 (CYP) enzymes are among hepatocytes' most essential drug-metabolising enzymes (Guo *et al.*, 2021). Metabolism, also known as biotransformation, is typically carried out by a series of CYP-dependent enzymatic processes (Chen *et al.*, 2019). Among the CYP isoforms, CYP1, CYP2, and CYP3 are known to play critical roles in most drug metabolism (Chen *et al.*, 2019). The CYP enzymes catalyse hydroxylation, dealkylation, and oxygenation reactions but can also catalyse reductive reactions, resulting in CYP inactivation due to the metabolites produced (Guo *et al.*, 2021). CYP isozymes have been identified in the kidney, skin, lungs, and gastrointestinal system, even though the liver is where most of these reactions occur. The CYP3A enzyme subfamily, which comprises the isoforms CYP3A7, CYP3A5 and CYP3A4, is the most prevalent CYP in the liver. With 50% of the total CYP content and a significant function in drug and xenobiotic metabolism, CYP3A4 is the most highly expressed CYP in the liver and small intestine (Li and Lampe, 2019).

Biotransformation is divided into two stages, each aiding in drug elimination from the body (Li and Lampe, 2019). Phase I enzymes are the first to metabolise lipophilic xenobiotics because they make them more polar and create sites for conjugation processes (Zhao *et al.*, 2021b). One of the most

common modifications is hydroxylation, catalysed by a CYP-dependent mixed-function oxidase system. A highly reactive oxyferryl species is formed, and cytochrome-bound oxygen is reduced as part of the reaction mechanism of CYP oxidases (Pan *et al.*, 2020). Oxidation, reduction, hydrolysis, cyclisation, decyclisation, and the addition or removal of hydrogen or oxygen are examples of phase I reactions carried out by mixed-function oxidases. These oxidative reactions typically involve a CYP monooxygenase, nicotinamide adenine dinucleotide phosphate hydrogen (NADPH) and oxygen (Pan *et al.*, 2020). When phase I metabolites are sufficiently polar, they can be easily eliminated at this stage. Certain phase I products undergo a phase II reaction, where an endogenous substrate combines with the newly added functional group to create a highly polar conjugate, and these products are hard to eliminate (Zhao *et al.*, 2021a). In subsequent phase II processes, charged species like glutathione (GSH), sulphate, and glycine are conjugated with the activated xenobiotic metabolites. Conjugation reactions on medications take place at the amino (NH_2), thiol (-SH), carboxyl (-COOH), and hydroxyl (-OH) groups ((Pan *et al.*, 2020). In contrast to phase I reactions, which often yield active metabolites, conjugation reaction products are less active and have a larger molecular weight than their substrates (Pan *et al.*, 2020). When large anionic groups detoxify reactive electrophiles, more polar metabolites are produced that need to be actively transported since they cannot traverse membranes (Pan *et al.*, 2020).

Many pathways are involved in the hepatic injury, either causing or exacerbating it. Many chemicals harm mitochondria, which produce energy within the cell (Bischoff *et al.*, 2018). Their malfunction generates an excess of oxidants, causing hepatic cell damage. Activating certain enzymes in the CYP family, such as CYP2E1, can also cause oxidative stress (Ortega-Alonso and Andrade, 2018). When hepatocytes and bile duct cells are damaged, bile acid builds up in the liver (Bischoff *et al.*, 2018). This accelerates the liver's destruction. The last stage of all chronic liver illnesses is cirrhosis, which limits the effectiveness of anti-cancer treatments for both liver and non-hepatic cancers in addition to being a significant risk factor for the development of liver cancer (Bischoff *et al.*, 2018).

2.2.6 Types of liver cancer

The most common types of heterogeneous malignant liver tumours in South Africa include hepatocellular carcinoma (HCC) and intrahepatic cholangiocarcinoma (iCCA) (Petrick and McGlynn, 2019). Other examples include mixed hepatocellular cholangiocarcinoma (HCCCCA), fibrolamellar HCC (FLC) and paediatric neoplasm hepatoblastoma. Hepatocellular carcinoma originates from epithelial cells called hepatocytes, the most frequent histological type of primary liver cancer (Petrick and McGlynn, 2019). Alone, HCC accounts for 90% of all cases of primary liver cancer. Intrahepatic cholangiocarcinoma is the second most frequent type of liver cancer, with the

highest incidence in Southeast Asia and the lowest incidence in Western countries (Sia *et al.*, 2017). Nonetheless, there has been a consistent increase in incidence (Sia *et al.*, 2017). Primary sclerosing cholangitis is a risk factor for the development of iCCA. Although HCC and iCCA are separate cancers that arise from discrete cell populations, several have lately been identified as tumour subtypes of a continuous spectrum of disorders (Sia *et al.*, 2017).

2.2.7 Risk factors and molecular mechanisms of carcinogenesis

Chronic inflammation, viral infections, occupational or environmental exposure, excessive alcohol consumption, tobacco use, inherited metabolic diseases, genetic predisposition, physical inactivity, unhealthy diet rich in fat and red meat products, fibrosis and cirrhosis are all risk factors for the development of HCC (Stockdale *et al.*, 2020). Exposure to risk factors causes inflammation, which can lead to fibrosis and cirrhosis before developing cancer, or it can lead straight to HCC (Stockdale *et al.*, 2020). The most notable risk factors are chronic hepatitis B virus (HBV) infection, aflatoxin B_1 (AFB_1) exposure and excessive alcohol intake (Figure 2.4) (Stockdale *et al.*, 2020).

The molecular mechanisms underlying the aetiology of HCC are still poorly understood despite extensive research into its pathogenesis, especially the role and impact of xenobiotics in initiating hepatic carcinogenesis (Mhlanga *et al.*, 2019). Numerous pathways, such as the deregulation of key cell survival (p53), differentiation (E-cadherin), and proliferation (activator protein-1, nuclear factor kappa B (NF-κB), and Wnt/-catenin) genes, are connected to the formation of HCC by chronic HBV infection (Taylor *et al.*, 2020). Additionally, it can activate or deactivate cyclin A and retinoic acid receptors. Provirus insertion or deletion or the direct effects of viral HBx proteins promote chromosomal instability and epigenetic alterations in HBV (Taylor *et al.*, 2020). Exposure to the dietary fungal toxin over time in Sub-Saharan Black Africans, AFB_1 is a significant risk factor for HCC; it induces carcinogenesis via deactivating p53 protein gene expression and cell cycle regulation, as well as by directly interacting with DNA molecules to create DNA adducts and initiate tumours (Taylor *et al.*, 2020).

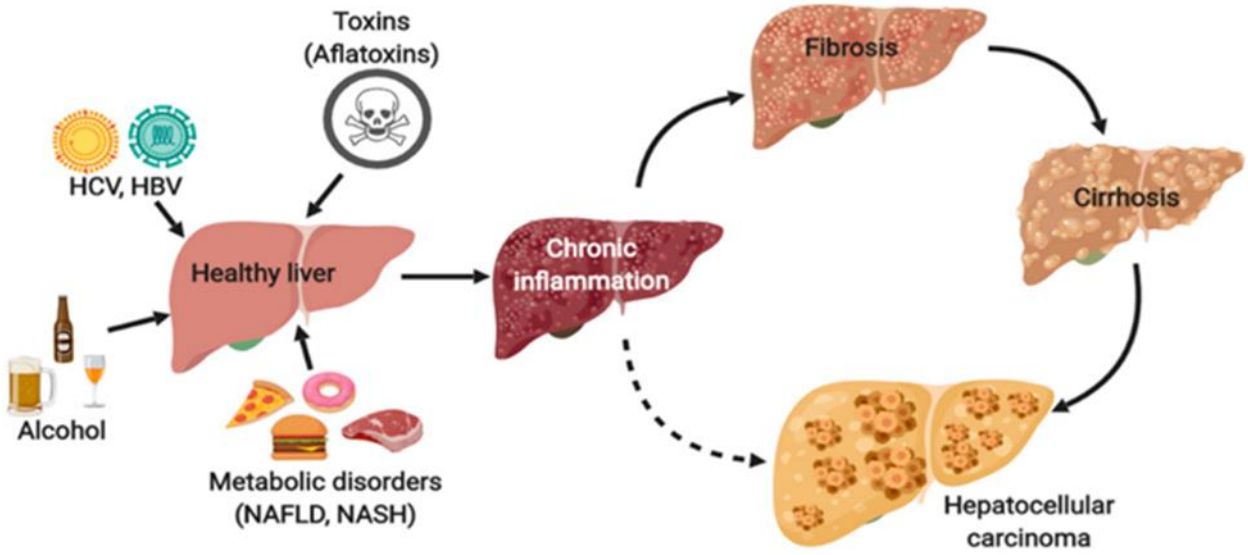

Figure 2.4: Risk factors of hepatocellular carcinogenesis and the accompanying sequence of changes in the development of HCC. Exposure to risk factors causes inflammation, which can lead to fibrosis and cirrhosis before developing cancer, or it can lead straight to HCC (Mhlanga *et al.*, 2019).

Exposure to risk factors can cause inflammation, which may result in fibrosis and cirrhosis (Figure 2.4). This can then progress to cancer or directly lead to HCC (Stockdale *et al.*, 2020). Chronic inflammation is linked with increased cell proliferation due to the growth factors in inflammatory cells, activated stroma, and DNA-damage-promoting agents. This significantly increases the risk of neoplastic development in a microenvironment of cell proliferation (Greten and Grivennikov, 2019). Liver fibrosis occurs due to the accumulation of excess extracellular matrix (ECM) rich in fibril-forming collagens. This condition is associated with a disruption of the normal architecture of the liver, leading to pathophysiological damage that results in liver cirrhosis (Suk and Kim, 2015). Liver cirrhosis is characterised by a vascularised fibrosis septum that allows for interaction between portal tracts and central veins, resulting in liver nodules surrounded by a fibrotic band devoid of a central vein.

2.2.8 Diagnosis and treatment of HCC

Detecting alpha-fetoprotein (AFP) levels through a blood test is one way to diagnose HCC (Liu *et al.*, 2017). The AFP tumour marker is elevated in 60-70% of patients with HCC (Sauzay *et al.*, 2016). Biomarkers such as Glypican-3, Dickkopf-1 and circulating miRNAs can also detect early HCC (Kuwabara *et al.*, 2018). Radiographic techniques such as magnetic resonance imaging, computed tomography scan and ultrasound are also commonly used for HCC diagnosis (Cerny *et al.*, 2018). Treatment options for HCC include radiotherapy, chemotherapy, cryosurgery, percutaneous ethanol injection, liver transplantation, radiofrequency ablation, surgical resection, and cisplatin-gel injection

(Yamashita and Kaneko, 2016). However, these therapies are costly and demand costly equipment. Alternatively, numerous plants have been used for cancer treatment in Africa (Youn *et al.*, 2023;Gaobotse *et al.*, 2023). Although much research is undertaken for complementary medicine that makes use of medicinal plants, clinical trials for anti-cancer phytochemicals are relatively new (Süntar, 2020;Youn *et al.*, 2023).

2.3 *TETRADENIA RIPARIA*

A medical plant is any plant that includes compounds that can be utilised for therapeutic purposes, as well as substances that can be employed as precursors to produce effective pharmaceuticals (Süntar, 2020). Several studies have demonstrated that medicinal plants can help with a variety of conditions, including degenerative diseases, diabetes and cancer. Plants have secondary metabolites with biological effects on human health; thus, research is critical (Mahlangu, 2019). Medicinal plants contain phytochemicals such as flavonoids, alkaloids, terpenoids and organosulfur compounds (Figure 2.6) (Van Wyk and Prinsloo, 2018). Flavonoids have been shown to have anticancer, cardiovascular disease, and viral and bacterial infection protective effects (Shimira, 2022). Meanwhile, products of alkaloids have antimicrobial effects through intercalation with the DNA of microorganisms (Dietz and Dekker, 2017). The terpenoids have been shown to have cytotoxicity against a range of tumour cells and cancer prevention and anticancer properties (Dietz and Dekker, 2017). Organosulfur compounds have been shown to have biological effects such as carcinogen detoxification, antimicrobial effect, free radical scavenging, cell cycle arrest, apoptosis induction, and inhibition of tumour cell proliferation and DNA adduct formation (Dietz and Dekker, 2017).

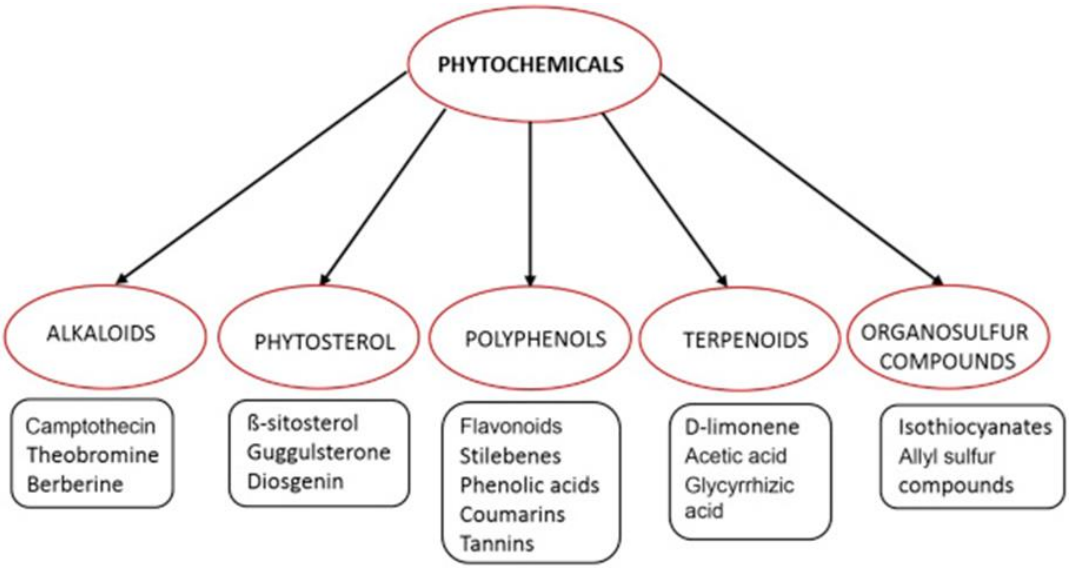

Figure 2.5: Different types of phytochemicals in plants. Medicinal plants contain phytochemicals such as flavonoids, alkaloids, terpenoids and organosulfur compounds for reproduction, protection, colour, odour and for growth signalling (Van Wyk and Prinsloo, 2018).

2.3.1 Description

Tetradenia riparia belongs to the *Lamiaceae* family and the genus *Tetradenia*, which has 20 species (Milato *et al.*, 2018). *Tetradenia riparia (Hochst.) Codd (Lamiaceae*) (Figure 2.6) is generally known as ginger bush and locally known in South Africa as "iIboza or ibozane" (Milato *et al.*, 2018). It is an herbaceous, deciduous, aromatic shrub with intensely perfumed leaves that grow to 1-3 meters tall (Figure 2.6A, Figure 2.6C) (Luanda and Ripanda, 2022). The stem is smooth and covered in light grey-brown bark (Figure 2.6A, Figure 2.6B). Its leaves are hairy, oval, sticky, crenate-dentate and semi-succulent, with scattered to dense glandular pubescence (Figure 2.6A, Figure 2.6B). Touching the leaves of *T. riparia* reveals a strong sticky aroma that stays on the tips of the fingers due to the high concentration of essential oil (Milato *et al.*, 2018). It flowers generally from May to September in South Africa, with bunches of inflorescence at the branch terminals (Figure 2.6B, Figure 2.6C) (Luanda and Ripanda, 2022).

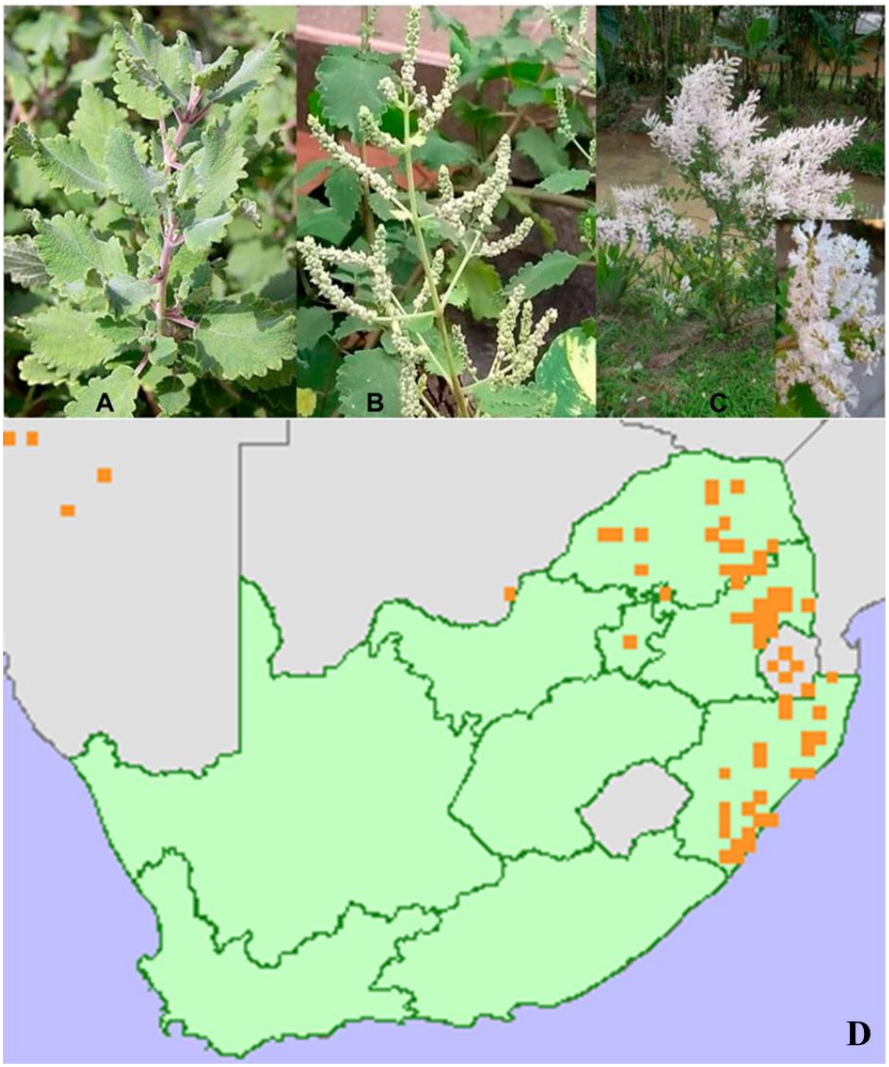

Figure 2.6: *T. riparia* is an indigenous plant to Africa's central regions. **(A)** The perfumed leaves and smooth brownish stem of *T. riparia*. **(B)** The leaves, smooth stem and flower buds of *T. riparia*. **(C)** Open flowers on a *T. riparia* shrub. **(D)** Distribution of *T. riparia* in South Africa (Panda *et al.*, 2022; van Staden, 2016).

2.3.2 Geographical distribution of *T. riparia*

Tetradenia riparia is indigenous to Africa's central, eastern and southern regions, including South Africa, Angola, Swaziland, Mozambique, Malawi, Namibia and Zimbabwe, where it is mostly used as a medicinal plant (Luanda and Ripanda, 2022;von Staden, 2016). It is also distributed through Tropical East Africa, Kenya, Uganda and Tanzania to Ethiopia (Njau and Ndakidemi, 2017). Within Soth Africa, the plant grows in Gauteng, KwaZulu-Natal, Limpopo and Mpumalanga (Figure 2.6D) (von Staden, 2016). The shrub grows well along damp, warm and sometimes dry areas such as forest edges, valleys and hills (Panda *et al.*, 2022;von Staden, 2016;Njau and Ndakidemi, 2017).

2.3.3 Uses of *T. riparia*

T. riparia is present in practically every rural home, and its dried leaves are used as an infusion or decoction to treat several illnesses (Shimira, 2022). *Tetradenia riparia*, like other medicinal plants, has traditionally been used to treat various medical diseases, including respiratory ailments, fever, stomach infections, snake bites, malaria, gonorrhoea, and dental difficulties (Shimira, 2022). Moreover, it is used to treat dental abscesses, dropsy, fevers and pains, mouth ulcers, angina, cough, colds and flu, malaria, stomach disturbances, yaws, gonorrhoea, gastroenteritis, toothache, flatulence, diarrhoea, headache, and anthelmintic-induced disorders in South Africa (Milato *et al.*, 2018;Panda *et al.*, 2022). Aside from medical purposes, bioactive chemicals in its essential oil are employed as insect repellents. The concentration of bioactive chemicals discovered in *T. riparia* varied seasonally (Luanda and Ripanda, 2022). This is attributed to environmental conditions that often impact the synthesis of secondary metabolites in plants, such as essential oils, which operate as the chemical shield of the plant. *T. riparia's* major components are fenchone (15%), which acts as a plant metabolite, delta-cadinene (11%), 14-hydroxy—caryophyllene (8%), and tau-cadinol (7%).

2.3.4 Essential oils of *T. riparia*

Tetradenia riparia essential oil possesses significant medicinal qualities such as pest management, attractants, repellents and toxicants (Luanda and Ripanda, 2022). Genetic and environmental factors influence the essential oil content of medicinal plants (de Oliveira *et al.*, 2022). One of the most popular techniques for protecting plant materials from germs and making them easier to handle is drying. Sample drying techniques significantly impact compositions, especially essential oil components (de Oliveira *et al.*, 2022). Investigation of essential oil from aerial parts of *T. riparia* revealed the presence of tau-cadinol, δ-cadinene, 14-hydroxy-β-caryophyllene, and fenchone as significant compounds. Flower buds have caryophyllene oxide and 14-hidroxy-9-epi-caryophyllene (de Oliveira *et al.*, 2022). Leaves contain fenchone, α-cadinol, aromadendrene oxide, dronabinol ,

6,7-dehydroroyleanone, and caryophyllene oxide, calyculone viridiflorol, abietadiene, (E,E)-farnesol, α-fenchyl acetate, verbenone, *cis*-muurolol-5-en-4α-ol, 14-hydroxy-9-epi-caryophyllene, α-terpineol, β-fenchyl alcohol, perillyl (Luanda and Ripanda, 2022). Furthermore, farnesol, α-fenchyl acetate, caryophyllene oxide, and guaiol are the main constituents of the essential oil that was extracted from the stem of *T. riparia*.

2.3.5 Phytochemicals found in *T. riparia*

Phytochemicals are non-nutrient bioactive components that are primarily responsible for scavenging toxic radicals after oxidative stress by generating antioxidants, the main cause of most chronic diseases (Van Wyk and Prinsloo, 2018). Fruit phytochemicals displayed high antioxidant capacities linked to a lower incidence of degenerative diseases and a lower mortality average in humans (Van Wyk and Prinsloo, 2018). Table 2.1 shows phenolic acids, flavonoids, tannins, saponins, alkaloids, and cardiac glycosides are some of the phytochemicals in *T. riparia* (Shimira, 2022).

Table 2.1: Phytochemical examinations of *T. riparia* (Panda *et al.*, 2022).

Phytochemical	**Inference**
Tannins	Present
Flavonoids	Present
Alkaloids	Present
Saponins	Present
Cardiac glycoside	Present
Phenols	Present

Secondary metabolites known as alkaloids are cyclic compounds with nitrogen in a state of negative oxidation (Van Wyk and Prinsloo, 2018). They impact the nervous system's chemical transmitter's function. Other pharmacological properties include antimicrobial, antihypertensive, antispasmodic, analgesic, and antiarrhythmic effects. Tannins such as gallic or protocatechuic acid glycosides in plants are also classified as secondary metabolites (Van Wyk and Prinsloo, 2018). Since they are astringent, they can help avoid diarrhoea and controlling haemorrhage due to their ability to precipitate proteins, mucus, and constrict blood vessels. The anti-carcinogenic and anti-mutagenic potentials of tannins may be related to their antioxidative property which is important in protecting against cellular oxidative damage including lipid peroxidation (Shimira, 2022). Tannins have also been shown to have physiological effects, including raising blood pressure, lowering serum

cholesterol, causing liver necrosis, and triggering immunological responses (Van Wyk and Prinsloo, 2018).

Flavonoids are secondary metabolites with polyphenolic structures and are synthesised in plants through the polypropanoid pathway (Shimira, 2022). They contain antioxidants that shield cells in plants, animals, and humans from the harm caused by free radicals (Shimira, 2022). Flavonoids have been classified into six sub-groups: flavones, flavanol, flavanone, flava-3-ols, isoflavone, and anthocyanidin. Two notable flavonoids in *T. riparia* is astragalin (Figure 2.7A) and luteolin (Figure 2.7B).

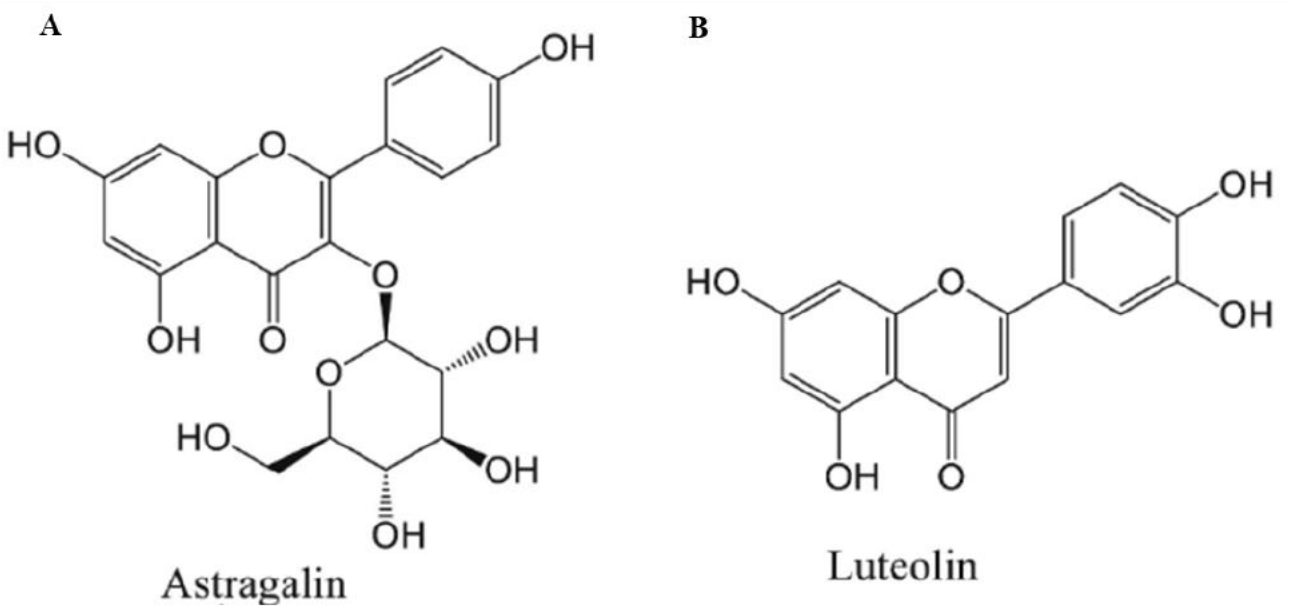

Figure 2.7: Flavonoids present in *T.riparia* essential oil. Chemical structures of astragalin and luteolin, two flavonoids identified in *Tetradenia riparia* essential oil (Luanda and Ripanda, 2023).

2.3.5.1 Astragalin

Astragalin (kaempferol-3-O-β-D-glucoside) is a naturally occurring bioactive flavonoid that has long been recognized for its therapeutic value. According to reports, it possesses various pharmacological qualities, such as cardioprotective, neuroprotective, anti-inflammatory, anticancer, and antioxidant qualities (Riaz *et al.*, 2018;Chen *et al.*, 2023). Astragalin actively contributes to reducing the degradation of IκBα and limiting the nuclear translocation of NF-κB, which in turn inhibits the activation of NF-κB caused by lipopolysaccharide (LPS) (Riaz *et al.*, 2018). Apoptosis and eosinophilia can result from oxidative stress caused by endotoxins, which astragalin also prevents. Additionally, altering the lipopolysaccharide-toll-like receptor (LPSTLR) signalling network can counteract endotoxin-induced oxidative stress (Riaz *et al.*, 2018;Ruan *et al.*, 2024). Astragalin suppressed cell growth *in vitro* in hepatocellular carcinoma (HepG2) cells. Astragalin reduces

oxidative stress and modifies apoptosis-related pathways to prevent 6-hydroxydopamine-stimulated neurotoxicity in *Caenorhabditis elegans*. (Riaz *et al.*, 2018). Astragalin can improve neural function in rats' ischemia brain injury model by blocking the apoptosis in the hippocampus region by enhancing the expression of neural cell adhesion molecule (Riaz *et al.*, 2018).

2.3.5.2 Luteolin

Luteolin is a flavone compound in many medicinal plants (Aziz *et al.*, 2018). Luteolin is present in vegetables, fruits, and medicinal herbs, including broccoli, onion leaves, carrots, peppers, cabbages, apple skins etc. Numerous studies have documented luteolin's anti-inflammatory, anti-microbial, antioxidant, chemo-preventive, chemotherapeutic, cardioprotective, anti-diabetic, neuroprotective, and anti-allergic qualities. A thorough evaluation of luteolin's anti-inflammatory properties was conducted in 2008 (Aziz *et al.*, 2018). According to the report, luteolin's anti-inflammatory properties include: scavenging of reactive oxygen species (ROS); inhibiting ROS production and activating antioxidant enzymes; inhibiting leukotriene production and release; suppressing pro-inflammatory cytokine expression; inhibiting the NF-κB pathway, protein kinase B (AKT), and the mitogen-activated protein kinase (MAPK) pathway; blocking adhesion molecule membrane binding, hyaluronidase activity, and elastase activity; preserving mast cells; lowering vascular permeability; and controlling cell membrane fluidity (Aziz *et al.*, 2018).

Luteolin has been demonstrated to regulate a variety of cytokines in both in vitro and in vivo models, and it partially reduces inflammation by controlling inflammatory mediators (Imran *et al.*, 2019). Because cytokines are important modulators of both acute and chronic inflammation, cytokine control is essential (Aziz *et al.*, 2018). Luteolin can raise the level of IL-10, an anti-inflammatory cytokine, while inhibiting pro-inflammatory cytokines such as interleukin (IL)−1β, IL-2, IL-6, IL-8, IL-12, IL-17, TNF-α, interferon (IFN)-β, and granulocyte-macrophage colony-stimulating factor. Some of these effects have been noted on the mRNA level (Aziz *et al.*, 2018). Luteolin works in part by preventing NO synthesis, *iNOS* expression, and *iNOS* function. Since NO is a labile radical, this suppression has been linked to luteolin's capacity to control ROS (Imran *et al.*, 2019). According to reports, luteolin functions as an antioxidant enzyme activator, a ROS scavenger, and an inhibitor of ROS formation.

2.4 OXIDATIVE STRESS

The term oxidative stress describes an imbalance favouring oxidants over antioxidants, leading to a disruption in redox signalling and possible molecular damage (Figure 2.8) (Sies and Jones, 2020). Despite a strong antioxidant response, this situation causes free radicals to build up and is frequently

linked to reduced antioxidant capacity (Ndlovu *et al.*, 2021). Oxidative stress has been linked to a number of conditions, including inflammation, autoimmune illnesses, cataracts, cancer, Parkinson's disease, aging and atherosclerosis (Luanda and Ripanda, 2022). Several illnesses, including cancer, asthma, liver disease, cataracts, diabetes, gastrointestinal inflammatory diseases, cardiovascular disease, cataracts, periodontal disease, and other inflammatory processes, have been linked to free radicals (Shimira, 2022).

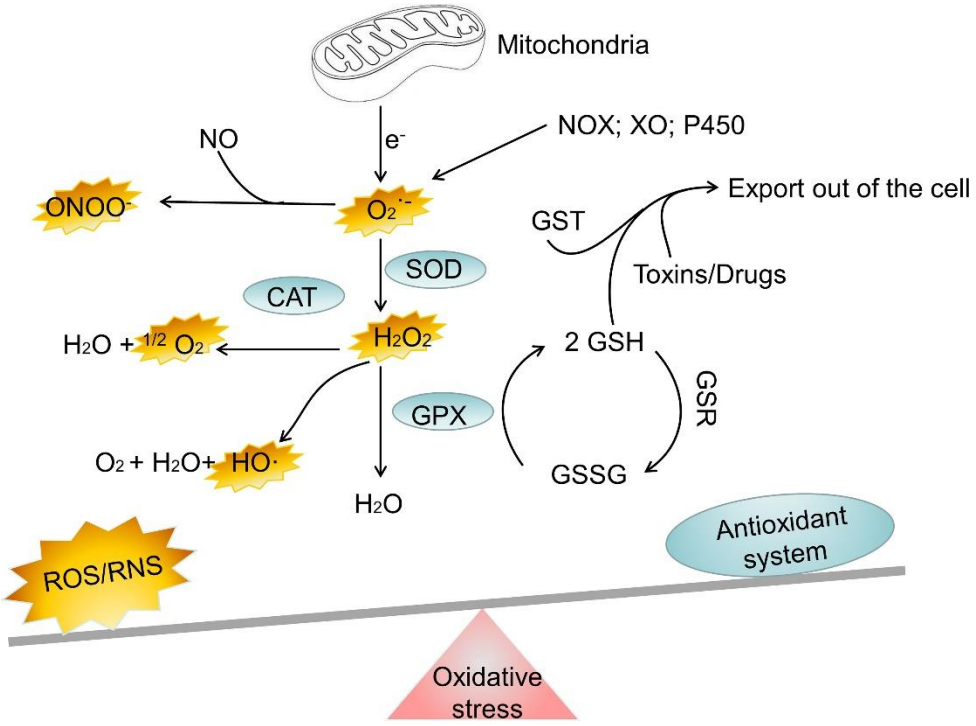

Figure 2.8: A depiction of reactive oxygen species against antioxidant activity. An imbalance between oxidants and antioxidants, which disrupts redox signalling and can cause molecular damage results in oxidative stress (Liu *et al.*, 2023).

Normal bodily chemical processes produce these oxidants and may sustain damage from free radicals (Luanda and Ripanda, 2022). Common ROS and RNS include superoxide anion radical ($O_2^{\bullet-}$), hydrogen peroxide (H_2O_2), hydroxyl radical ($^{\bullet}OH$), nitric oxide ($NO^{\bullet}$) and peroxynitrite ($ONOO^-$) (Figure 2.9); these electrophiles are highly reactive chemical compounds (Ndlovu *et al.*, 2021). The metabolism of the amino acid L-arginine produces the $NO^{\bullet}$. Nitric oxide synthases (NOS) are the enzymes that catalyse this process. They oxidise guanidine nitrogen of L-arginine by five electrons, converting it into L-citrulline and $NO^{\bullet}$ (Di Meo *et al.*, 2016). While the free radical produced by iNOS in macrophages and smooth muscle cells aids in their killing mechanism, the $NO^{\bullet}$ produced by nNOS in neurons facilitates communication between nerve cells, while the $NO^{\bullet}$ produced by eNOS in the

brain, heart, and endothelium relaxes blood vessels and maintains normal blood pressure (Di Meo *et al.*, 2016).

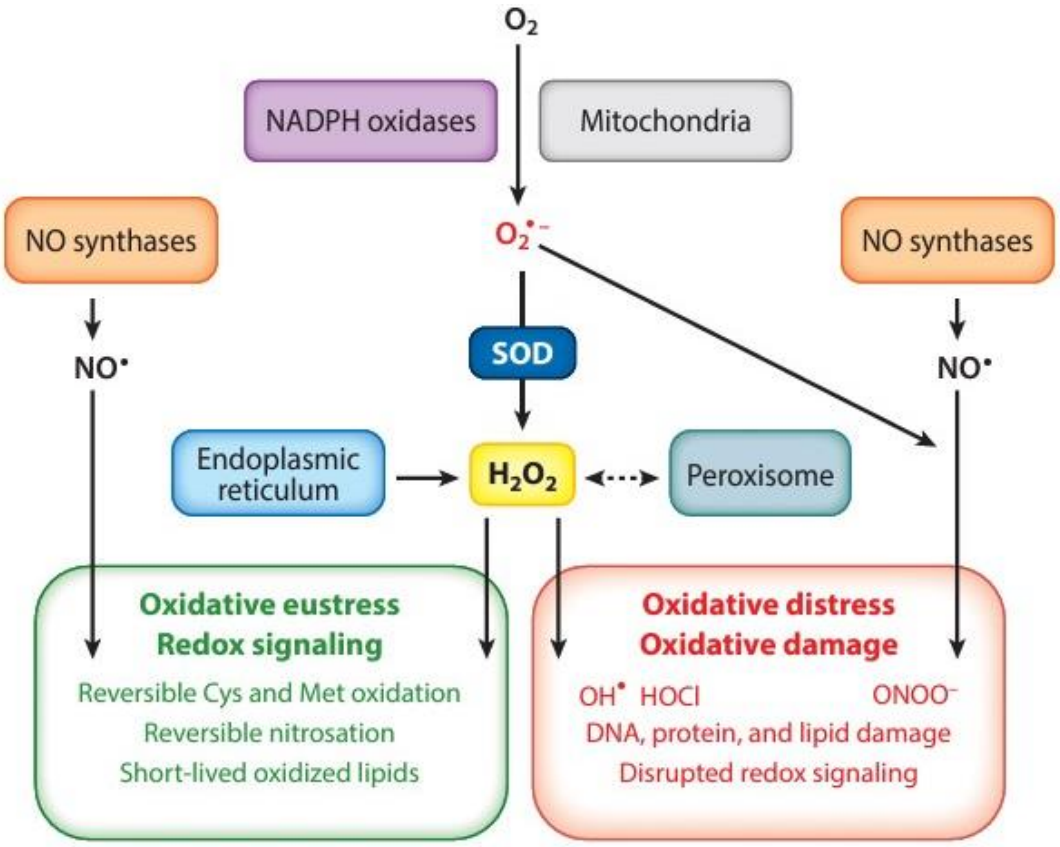

Figure 2.9: The intracellular sources of reactive oxygen species (ROS) and reactive nitrogen species (RNS) indicating potential damage induced. The production of ROS and RNS is associated with oxidative damage to cellular macromolecules (Sies, 2018).

Chemicals known as antioxidants help lessen the damage that free radicals do to our cells (Ghuman *et al.*, 2019). Antioxidant enzymes and their substrates and coenzymes make up most of the antioxidants that operate in cellular defence against oxidants (Sies, 2018). Exogenous low-molecular-mass chemicals also have a role, although it is more restricted (Sies and Jones, 2020). Antioxidants are nucleophilic compounds that can donate one or two electrons to oxidizing agents, which are typically electrophiles (Sies and Jones, 2020). Pro-oxidants are detoxified and the potential harm they can cause is limited by enzymatic antioxidants such as superoxide dismutase 2 (SOD2), glutathione peroxidase (Gpx1) and catalase (Figure 2.8, Figure 2.9) (Dosunmu-Ogunbi *et al.*, 2022). While Gpx1 requires reduced glutathione (GSH) as a co-factor, the antioxidant response is thought to be primarily regulated by nuclear factor erythroid 2-related factor 2 (Nrf2) (Klaunig, 2018). The $O_2^{\bullet-}$ is broken down by SOD into H_2O_2, which is subsequently detoxified by catalase or Gpx1 (Figure 2.8, Figure 2.9) (Klaunig, 2018). Water and molecular oxygen are produced when catalase eliminates cellular H_2O_2 (Klaunig, 2018). On the other hand, Gpx1 reduces various hydroperoxides (including H_2O_2) to

H_2O by oxidising reduced GSH into its disulphide form (GSSG). It also controls autoxidation by interrupting the propagation of free radicals or inhibiting their formation (Klaunig, 2018). This cytoprotective mechanism is regulated by the transcription factor Nrf2 in cooperation with a zinc thiol protein known as Kelch-like ECH-associated protein 1 (Keap1), referred to as Nrf2- Keap1 (Ndlovu *et al.*, 2021). Following ROS activation, Nrf2 moves into the nucleus, where it attaches to the antioxidant response element (ARE) and stimulates the transcription of cytoprotective proteins, including glutathione S-transferase A2 (GSTA2), SOD2, Gpx and catalase (Ndlovu *et al.*, 2021).

Damage to cellular macromolecules occurs when ROS or RNS outnumber antioxidants during oxidative stress (Figure 2.9) (Sies, 2018). Adding -OH to double bonds is a common step in DNA base oxidation. The removal of hydrogen from deoxyribose is the cause of the base deficiency. The purine and pyrimidine bases in the deoxyribose backbone make it highly reactive with hydroxyl radicals (Babbar *et al.*, 2020). ROS typically target the ester bond between glycerol and fatty acid as well as the unstable connection between two carbon atoms. Lipid peroxidation produces malondialdehyde (MDA), which is linked to cell membrane rupture (Babbar *et al.*, 2020). Downregulation of mitochondrial functions may arise from ROS production and lipid peroxidation initiation within the mitochondria.

2.5 MECHANISM OF CELL DEATH

Resistance to cancer therapy is a major challenge due to abnormal growth and death patterns in cancer cells caused by mutations in key regulatory genes (Wu *et al.*, 2023). On the other hand, healthy cells have mechanisms like autophagy, ferroptosis, necrosis, necroptosis and apoptosis that help remove unnecessary or abnormal cells (Figure 2.10). Autophagy is an important process within cells that involves autophagosomes' absorption of cellular components and their subsequent breakdown upon merging with lysosomes (Jung *et al.*, 2020;Wu *et al.*, 2023). This helps to maintain a healthy balance within the cell and allows for the recycling of cytoplasmic contents, making it a key protective mechanism. Autophagy can be triggered by adverse environmental conditions like starvation, growth factor deprivation, and pathogen infection, while extracellular signals like hormones and cytokines can also regulate the process (Figure 2.10). Ferroptosis is a form of cell death due to iron overload, excess ROS production, and depletion of antioxidant systems, leading to oxidative stress (Wu *et al.*, 2023). Stressors like radiation, toxins, restricted blood supply, heat, and lack of oxygen can cause cell necrosis. Necrosis causes energy loss, swelling, and harm to the plasma membrane. This leads to the release of cytosol components into the extracellular space, which can trigger inflammation and cause damage to nearby tissue (Galluzzi *et al.*, 2018).

Necroptosis is a programmed form of cell death that combines features of necrosis and apoptosis. Necroptosis can occur without the involvement of caspase proteins but requires specific proteins like mixed lineage kinase domain-like (MLKL), and receptor-interacting protein kinase (RIPK) 1 and 3 (Wu *et al.*, 2023). Apoptosis is a type of programmed cell death usually evaded in cancer cells, and therefore a viable target for compounds with anti-cancer potential (Prasad, 2022).

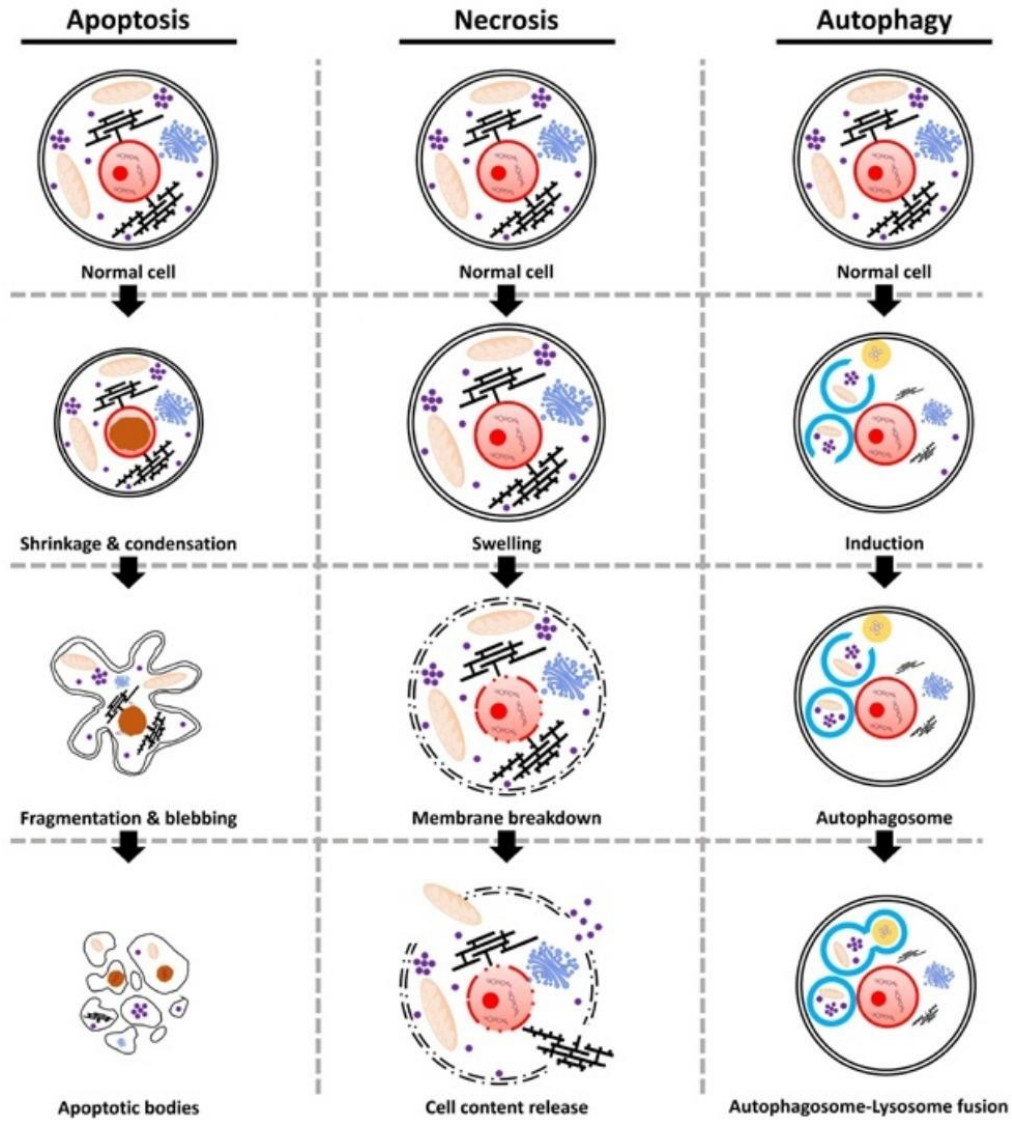

Figure 2.10: Different types of cell death. Apoptosis is a type of cell death in which a series of molecular steps in a cell lead to its death. During autophagy, the cell breaks down and destroys old, damaged, or abnormal proteins and other substances in its cytoplasm, and necrotic cell death refers to unregulated dismantling of body tissue (Patil *et al.*, 2020).

2.5.1 Apoptosis

The term apoptosis was first used by Kerr *et al.* in 1972 to describe cell death that resembles leaves falling from a tree (Patil *et al.*, 2020). Apoptosis is generally known as programmed cell death mediated by caspases (Krüger and Richter, 2022), and these cells exhibit unique morphological features such as cell shrinkage, cell blebbing, loss of surface microvilli, nuclear and chromosomal condensation, mitochondrial depolarization, cellular acidification, and nuclear fragmentation and apoptotic body formation in the late stages (Patil *et al.*, 2020). Apoptotic cells also undergo biochemical changes, such as the exposure of phosphatidylserine on the outer plasma membrane in the early stages. The molecular level of the apoptosis process is regulated by various cellular signals that originate from either the extracellular (extrinsic inducer pathway) or intracellular (intrinsic inducer pathway) sources (Figure 2.11) (Pfeffer and Singh, 2018;Patil *et al.*, 2020). Different stimuli, such as the extrinsic or death receptor pathway, can activate one of these pathways.

The attachment of a death signal to a death receptor initiates the extrinsic apoptosis pathway. TNF ligand (TNFL) and Fas ligand (Fas-L) are the ligands for the two recognized death receptors, TNF receptor (TNFR1) and first apoptotic signal (Fas / CD95) (Pfeffer and Singh, 2018;Soond *et al.*, 2021). Intracellular death domains found in death receptors draw adaptor proteins such as procaspase 8, TNF-associated death domain (TRADD), a cysteine aspartate protease, and Fas-associated death domain (FADD) (Soond *et al.*, 2021). The death domains are activated upon ligand binding, and adaptor proteins come together to form a death-inducing signalling index complex (DISC). The DISC complex then activates pro-caspase 8 to caspase-8, an initiator caspase responsible for initiating apoptosis by cleaving other downstream executioner caspases (Figure 2.11) (Singh and Lim, 2022, (Pfeffer and Singh, 2018).

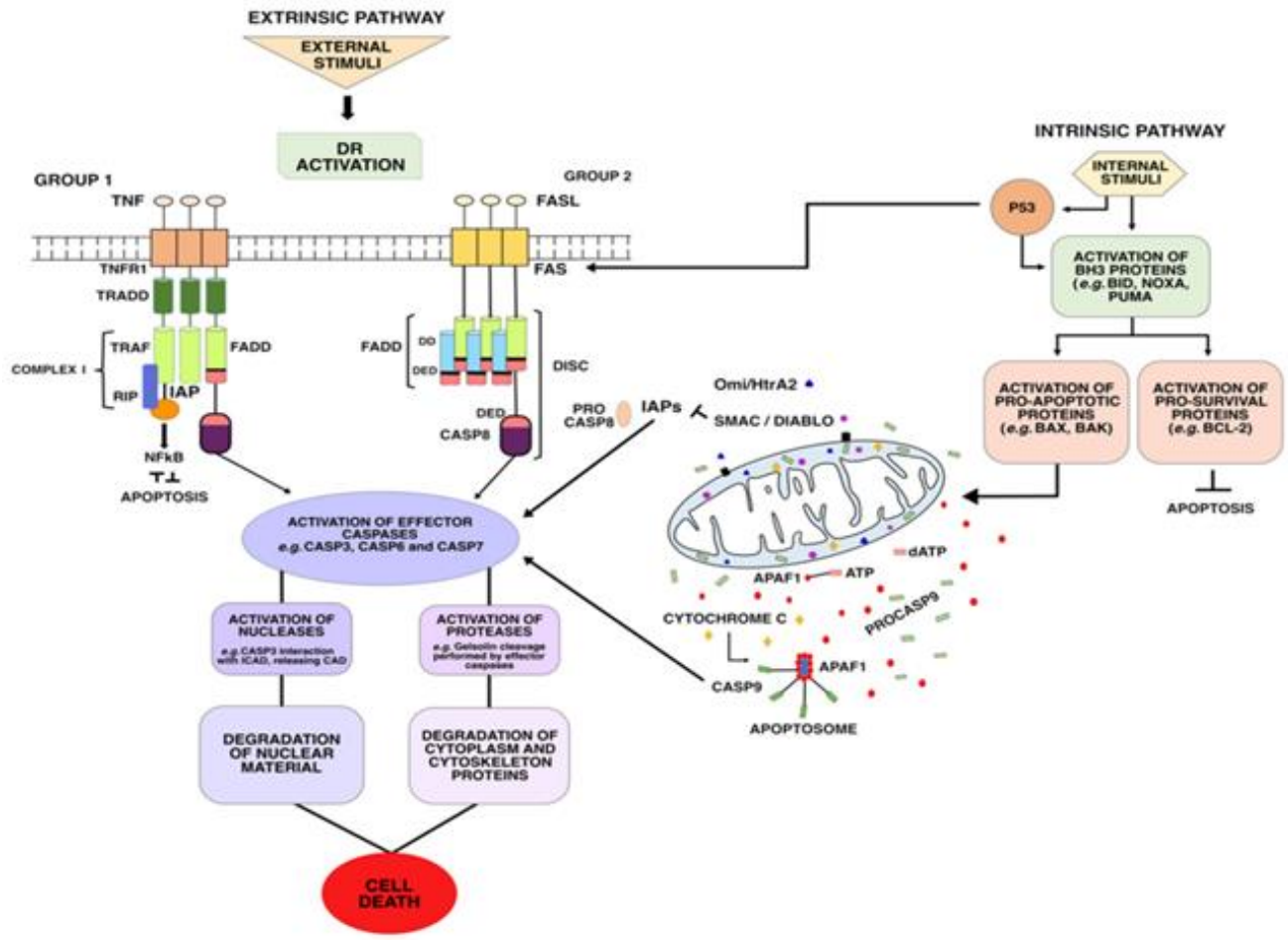

Figure 2.11: The intrinsic and extrinsic pathways of cell death. The extrinsic apoptosis pathway is triggered when a death signal attaches to a death receptor and certain proteins in the BCL-2 family regulate the intrinsic route, inhibiting or stimulating apoptosis (Pfeffer and Singh, 2018).

The intrinsic pathway is controlled by certain proteins within the BCL-2 family that promote or inhibit apoptosis (Patil *et al.*, 2020). In contrast to pro-apoptotic proteins, which have three or one of the BCL-2 Homology (BH) domains (BH1-3), or BH3, anti-apoptotic proteins have four BH domains (BH1-4) (Obeng, 2021). The intrinsic route is activated when the BH3-only protein is stimulated (Downey, 2019). The BH3-only proteins activate multi-BH proteins through direct binding or blocking of anti-apoptotic (Bcl-2) proteins (Cavalcante *et al.*, 2019). When intracellular stress occurs, such as DNA damage or ER stress, proapoptotic proteins such as BIM, NOXA, BIK, PUMA, and BID are activated by signalling molecules like ATM and CHK (Moujalled *et al.*, 2021). This leads to the activation of the p53 gene, which causes BH3-only proteins to bind to anti-apoptotic BCL-2 proteins, freeing BAK and BAX (Zhao *et al.*, 2022;Wu *et al.*, 2023). The liberated BAX/BAK increases mitochondrial permeability, releasing pro-apoptotic molecules like cytochrome c into the cytosol. Caspase-8 can also initiate the intrinsic pathway by cleaving Bid to t-Bid, activating BAX. Cytochrome c binds to Apaf-1, forming a heptamer that activates procaspase 9 into caspase -9. Both

caspase-8 and caspase-9 can activate pro-caspase 3 to caspase-3, an effector caspase (Patil *et al.*, 2020;Zhao *et al.*, 2022;Wu *et al.*, 2023).

Caspase-3 is the most well-studied executioner caspase-activated by both the intrinsic and extrinsic pathways. It functions in the cleavage of several substrates to induce changes in cell morphology, such as cell shrinkage, membrane blebbing, DNA fragmentation and condensation and formation of apoptotic bodies (Cavalcante *et al.*, 2019;Patil *et al.*, 2020;Pfeffer and Singh, 2018). Phagocytes remove these apoptotic bodies. Cleavage of poly (ADP-ribose) polymerase (PARP) to cPARP halts DNA repair, while removal of the inhibitor from caspase-activated DNase is associated with DNA fragmentation (Cavalcante *et al.*, 2019;Pfeffer and Singh, 2018). The externalisation of phosphatidylserine from the inner to the outer plasma membrane is a marker of apoptotic cells that is essential for phagocytes' recognition and clearance of apoptotic bodies (Cavalcante *et al.*, 2019).

CHAPTER 3 : METHODOLOGY

3.1 MATERIALS

The HepG2 cells were purchased from Cellonex (Johannesburg, South Africa (SA)). Cell culture reagents were acquired from Thermo Fisher Scientific (Waltham, Massachusetts, United States of America (USA)) and plasticware was bought from Lasec (Johannesburg, SA). The western blot reagents were obtained from Bio-Rad (Hercules, California, USA), whilst the Cell Signalling Technology (CST, Danvers, Massachusetts, USA) antibodies and Promega (Madison, Wisconsin, USA) products were purchased from Anatech (Johannesburg, SA). Unless stated otherwise, all other reagents were purchased from Merck (Darmstadt, Germany).

3.2 CELL CULTURE

HepG2 cells are a human hepatoma cell line derived from and excised liver cancer of a 15-year-old, White male. These cells are valuable in research of drug metabolism and hepatotoxicity because of their epithelial-like shape, rapid rate of proliferation and capacity to carry out a variety of distinct liver activities (Donato *et al.*, 2015). The form and structure of HepG2 cells are comparable to those of cells found in epithelial tissues, a phenomenon known as epithelial-like morphology. With a diameter of roughly 10–20 µm, they are usually polygonal in shape, feature big nuclei, 3–7 nucleoli, and a comparatively low mitochondrial content (Donato *et al.*, 2015). They secrete a variety of plasma proteins, such as albumin, transferrin, fibrinogen, and alpha-2 macroglobulin, among other specialized liver functions. HepG2 cells are frequently employed in drug metabolism and hepatotoxicity investigations because of their capacity to carry out liver functions.

The HepG2 cells were thawed and reconstituted in 25 cm^2 flasks containing 5 ml complete culture medium (CCM) that comprised of Dulbecco's Modified Eagle Medium (DMEM), supplemented with 10% foetal bovine serum, 1% L-glutamine and 1% penicillin streptomycin-fungizone. The cells were placed in an incubator (37°C, 5% CO_2) to attach and grow under physiological conditions. Cell development was regularly tracked, and CCM changed as necessary. For cell maintenance, the HepG2 cells were washed thrice with 5 ml of 0.1 molar (M) phosphate-buffered saline (PBS) and replenished with 5 ml CCM. At approximately 80% confluence, the HepG2 cells were washed thrice with 5 ml PBS, then trypsinised with 1 ml trypsin. The resulting cell suspension was counted using the trypan blue exclusion method, and cell number/volume was adjusted for subculturing as required for the various assays.

3.3 PREPARATION OF TREATMENT

The dried powdered *T. riparia* leaves were obtained from a previous study. A 5% (w/v) concoction was prepared with distilled water (dH_2O) and extracted for 12 hours at room temperature (RT) with continuous stirring. The concoction was centrifuged (2000xg, 10 minutes, RT) to obtain a liquid extract that was freeze-dried [VirTis Sentry 2.0 (SP Scientific, Warminster, Pennsylvania)] to obtain a lyophilised *T. ripari*a aqueous leaf extract (*TRALE*). A stock solution was prepared by dissolving 5 mg in 1 ml of CCM and diluted with CCM to obtain the treatment concentrations used in this study.

3.4 3-(4,5-DIMETHYLTHIAZOL-2-YL)-2,5-DIPHENYLTETRAZOLIUM BROMIDE (MTT) ASSAY

3.4.1 Principle

The MTT assay is a commonly used assay to determine cell viability and cytotoxicity (Figure 3.1). The assay relies on mitochondrial dehydrogenases, such as succinate dehydrogenase, reducing MTT, a yellow water-soluble tetrazolium dye, to purple-coloured formazan crystals (Bahuguna *et al.*, 2017;Kumar *et al.*, 2018a). These NAD(P)H-dependent mitochondrial dehydrogenase enzymes convert NAD(P)H to NAD^+/$NADP^+$ in living cells, while the reduction reaction is inhibited in dying cells (Bahuguna *et al.*, 2017). An organic solvent such as dimethylsulfoxide (DMSO) is used to dissolve the generated formazan. Cell viability is correlated with the intensity of formazan colour, which is measured by measuring the optical density (OD) using a plate reader at wavelengths of 570 and 690 nanometers (nm). This intensity is directly proportional to the number of living cells (Kumar *et al.*, 2018b).

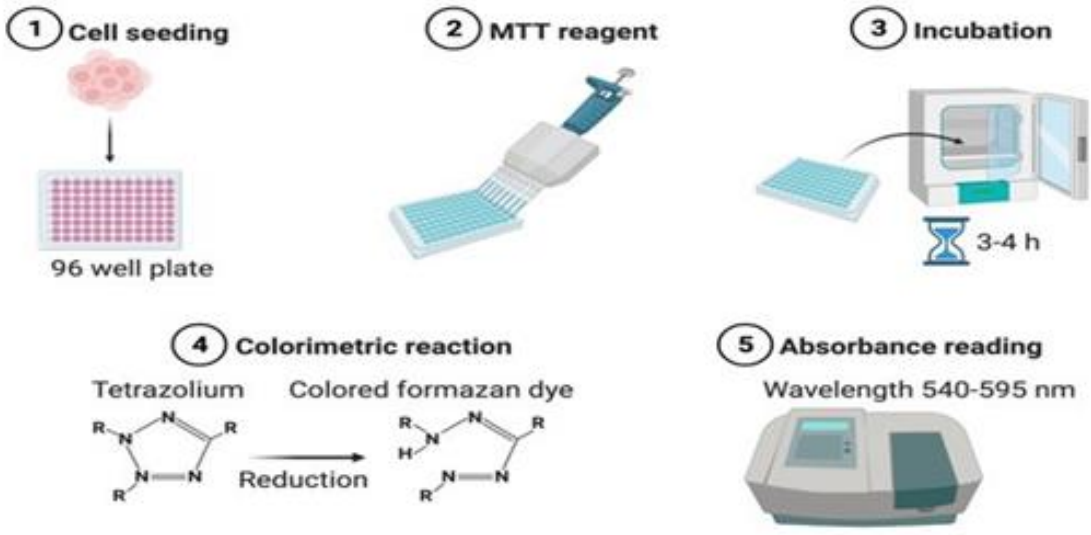

Figure 3.1: Principle and procedure of the MTT assay. The MTT assay principle showing the mitochondrial reduction of MTT to a formazan product which absorbs at a wavelength of 540-595nm. The intensity of the formazan product is directly proportional to cell viability (Kumar *et al.*, 2018b).

3.4.2 Protocol

The half-maximal inhibitory concentration (IC_{50}) and cytotoxicity of TRALE in HepG2 cells were assessed using the MTT assay. The suspension of HepG2 cells obtained by trypsinisation were seeded into a 96-well microtiter plate at a concentration of 20,000 cells/well (200 µl CCM per well), and cells were allowed to attach overnight in an incubator (37°C, 5% CO_2). After that, cells were incubated for 48 hours at 37°C with 5% CO_2 after being treated in triplicate with 300 µl of the *TRALE* concentration (0–3000 µg/ml). Following incubation, sample treatments were taken out and substituted with 100 µl of CCM and 20 µl of a 5 mg/ml MTT salt solution (in PBS). The mixture was then incubated for four hours at 37°C with 5% CO_2. Following incubation, the MTT salt solution was disposed of, and 100 µl of DMSO was added to each well. The mixture was then incubated for one hour at 37°C with 5% CO_2 to dissolve the formazan crystals. The absorbance at 570 nm was measured using a SPECTROstar® Nano microplate reader (BMG LABTECH, Ortenberg, Germany) with a reference wavelength of 690 nm. Utilising the absorbance readings, the percentage of cell viability in comparison to the control was computed [% cell viability = $\frac{\text{absorbance of sample}}{\text{absorbance of control}}$ x 100].

Using non-linear regression analysis (GraphPad Prism v5.0, GraphPad Software Inc., La Jolla, California, USA), a normalised and transformed concentration-response curve was produced to determine the IC_{50} of *TRALE*. The IC_{50} was then used to treat cells at 80% confluency in subsequent assays (48 hours, 37°C, 5% CO_2), while untreated cells were immersed only in CCM to serve as the control.

3.5 ATP QUANTIFICATION ASSAY

3.5.1 Principle

Metabolically active cells need ATP as functional energy to survive. It is synthesised at the substrate level by the Krebs cycle or the tricarboxylic acid cycle (TCA) and via the electron transport chain (ETC) during oxidative phosphorylation (Kamiloglu *et al.*, 2020). The ATP assay is employed as a viable cell biomarker because injured cells lose their ability to synthesise ATP and their membrane integrity (Figure 3.2) (Kamiloglu *et al.*, 2020). Because ATPases rapidly deplete the cytoplasm's ATP storage, ATPase inhibitors are utilized to stabilise the ATP generated from lysed cells. The stable form of the firefly luciferase enzyme is utilized to catalyse the process that generates light photons, with luciferin serving as the substrate (Zhao *et al.*, 2021b). The ATP detection reagent contains each of these elements (Kamiloglu *et al.*, 2020). The amount of ATP in the cell directly correlates with the luminous signal that is generated (Zhao *et al.*, 2021b).

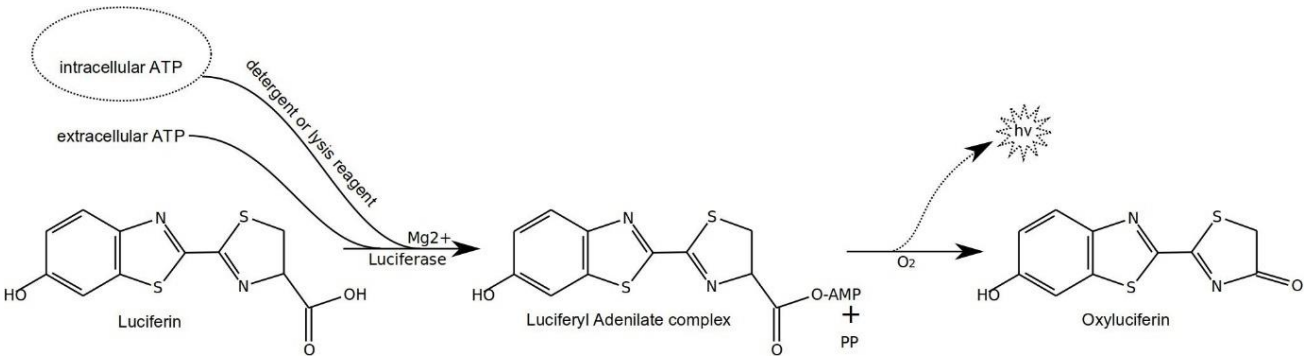

Figure 3.2: Schematic representation of ATP quantification assay. Using luciferin as a substrate, the reaction that generates light photons is catalysed by the stable form of the firefly luciferase enzyme (Braissant *et al.*, 2020).

3.5.2 Protocol

To measure intracellular ATP levels, the Promega CellTiter-Glo® assay (#G757) was utilised. The reagents were made in compliance with the guidelines provided by the manufacturer. A white opaque 96-well luminometer plate was seeded with a cell suspension of HepG2 cells at a concentration of 20,000 cells in 200 µl CCM per well, and the plate was incubated at 37˚C with 5% CO_2 overnight. The cell culture medium was withdrawn, and 300 µl/well CCM only (control) or the *TRALE* IC_{50} treatment solution was dispensed into the wells in triplicate, then the plate was incubated for 48 hours at 37˚C with 5% CO_2. After removing the treatment medium, 50 µl of PBS and 25 µl of the ATP reagent were added to each well. The luciferin-luciferase reaction was able to take place after 30 minutes of dark incubation at RT, resulting in a luminous signal that was proportionate to the intracellular ATP levels. The Modulus^{TM} microplate luminometer (Turner BioSystems Inc., Sunnyvale, California, USA) was used to quantify the luminescence, and the resulting data was reported in relative light units (RLU).

3.6 JC-10 MITOCHONDRIAL MEMBRANE POTENTIAL ASSAY

3.6.1 Principle

Cellular energy in the form of ATP is generated by the ETC in the mitochondrion, which is known as the cell's powerhouse (Sakamuru *et al.*, 2016). The mitochondrial membrane potential (ΔΨM), defined as the difference in electrical potential between the cytosol and the mitochondrial matrix, and the proton gradient provides the transmembrane potential necessary for ATP production (Younes *et al.*, 2022). As a result, the ΔΨM is utilised to identify cells that are healthy and functional. The basis for the ΔΨM assay is the cationic, lipophilic JC-10/JC-1 dye, which forms red fluorescent aggregates (Figure 3.3) at 540/590 nm after concentrating in the mitochondrial matrix of cells with polarized mitochondrial membranes (Miyai *et al.*, 2018). Nevertheless, in necrotic and apoptotic cells, JC-

10/JC-1 diffuses out of mitochondria due to ΔΨM collapse and reverts to its green-fluorescent monomeric state (Figure 3.3); monomers are visible at 490/525 nm. The ratio of red to green fluorescence intensity shows ΔΨM (Miyai *et al.*, 2018).

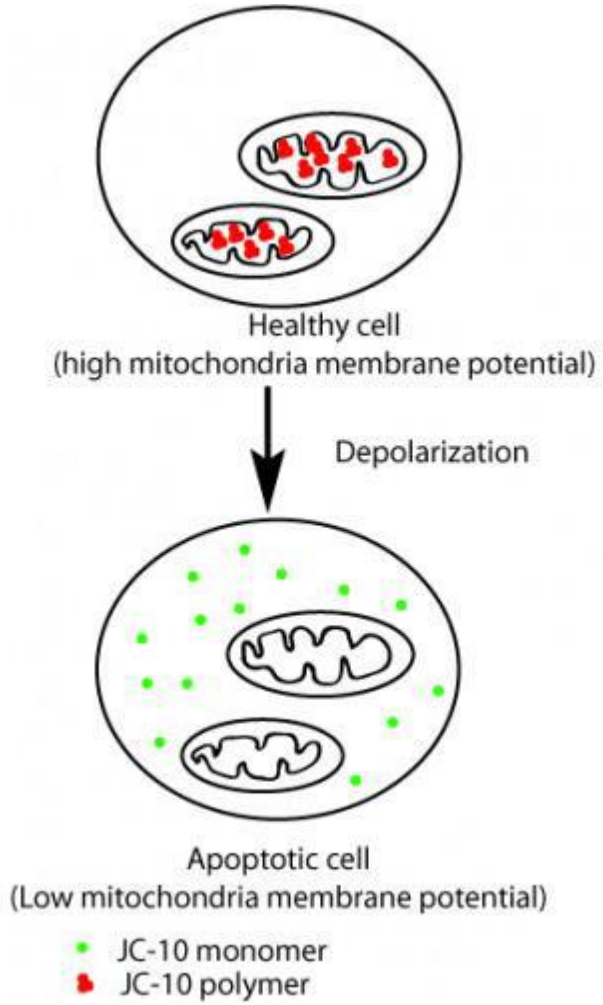

Figure 3.3: The principle of the JC-10 assay. The conversion of red to green fluorescence as an indication mitochondrial membrane potential [G Bio Sciences, 2023].

3.6.2 Protocol

The ΔΨM was quantified using JC-10 dye (MAK159, Sigma, Johannesburg, SA). The HepG2 cell suspension was dispensed into a white opaque 96-well luminometer plate (20,000 cells/well in 200 µl/well CCM). After overnight incubation (37˚C, 5% CO_2) for cell adherence, the medium was removed and cells were treated in triplicate (300 µl/well) with CCM only (control) or the *TRALE* IC_{50} treatment solution, then incubated for 48 hours (37˚C, 5% CO_2). Afterwards, sample treatments were removed and 50 µl of PBS was added to each well. Additionally, 25 µl of JC-10 reagent was added to each well after it had been prepared in accordance with the manufacturer's instructions. The plate was incubated in the dark for 30 minutes at RT. A Modulus^{TM} microplate luminometer (Turner

BioSystems Inc., Sunnyvale, California, USA) was used to measure the fluorescence at 540/590 nm and 490/525 nm, respectively. Red/green fluorescence intensity was used to express the data, which was acquired as relative fluorescence units (RFU).

3.7 THIOBARBITURIC ACID REACTIVE SUBSTANCES (TBARS) ASSAY

3.7.1 Principle

The TBARS assay measures malondialdehyde (MDA), an end-product of lipid peroxidation, and is used as an indication of oxidative stress (Ghani *et al.*, 2017). In the beginning step, lipid peroxidation occurs when free radicals attack lipids with carbon-carbon double bonds, particularly polyunsaturated fatty acids, removing hydrogen to create a lipid radical (de Dios Alché, 2019). Antioxidants give their electrons to the lipid radicals to stop the process and create non-radical molecules. MDA is an indirect indicator of oxidative stress that is created as a byproduct of lipid peroxidation (Alché Ramírez, 2019). When heat and acid are present, the MDA combines with thiobarbituric acid-butylated hydroxytoluene (TBA-BHT) to form a coloured MDA-2TBA end product that absorbs light at 530–540 nm (Figure 3.4); BHT stops lipids from oxidizing throughout the reaction (De Leon and Borges, 2020). The degree of lipid peroxidation in the sample is indicated by the color's intensity at 532 nm (Jesús, 2020).

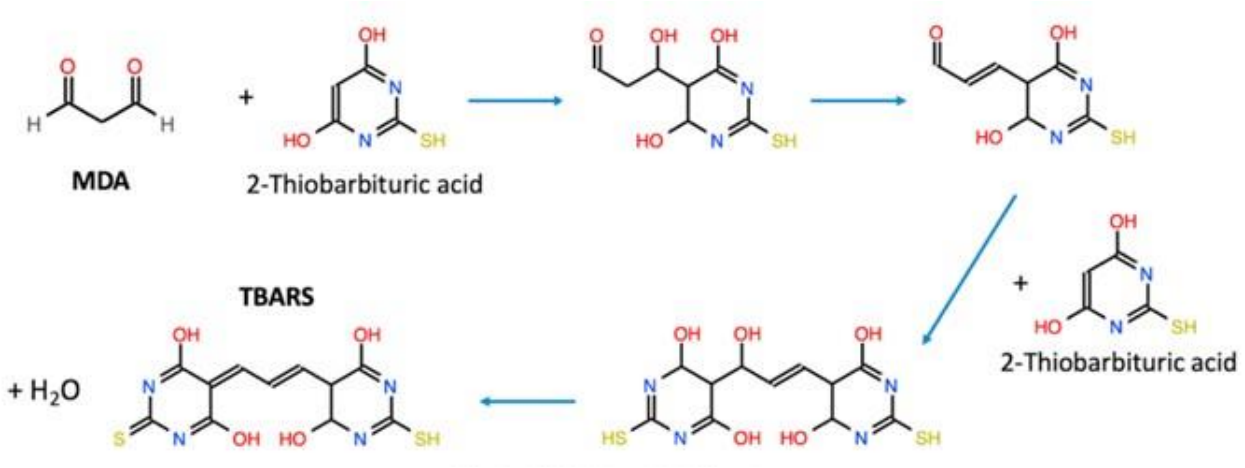

Figure 3.4: The reactions of TBARS assay that forms a quantifiable pink chromagen. The lipid peroxidation end-product, malondialdehyde (MDA) reacts with thiobarbituric acid (TBA) to produce a MDA-TBA adduct used as an indirect measure of reactive oxygen species production (Mas-Bargues *et al.*, 2021).

3.7.2 Protocol

The TBARS assay was used to indirectly quantify free radical production in treated cells. The 80% confluent HepG2 cells were treated for 48 hours (control, *TRALE* IC_{50}), and the treatment medium was retained to quantify MDA. Four labelled test tubes were prepared (control, *TRALE* IC_{50}, positive

and negative control). Each sample was mixed with 200 µl of 7% phosphoric acid (H_3PO_4), and the treated and untreated samples (200 µl), along with the positive (199 µl of CCM and 1 µl of MDA) and negative (200 µl of CCM) controls, were then put in their respective test tubes labelled accordingly. Following that, 400 µl of TBA/BHT solution was added to each sample tube, with the exception of the negative control test tube. The negative control, which also served as the blank, was given 400 µl of 3 mM HCl. The pH of each test tube was acidified by adding 200 µl of 1 M HCl after they had been vortexed. A hot water bath was used to boil each test tube for 15 minutes at 100˚C. The tubes were then taken out and allowed to cool at RT. Butanol (1500 µl) was poured into to each tube and vortexed for 30 seconds. The samples were put aside to give the mixture time to separate into two different layers. Following that, 100 µl of the samples (in triplicate) were pipetted into a 96-well plate, and 500 µl of the upper butanol layer was pipetted into a microcentrifuge tube. A SPECTROstar® Nano microplate reader (BMG LABTECH, Ortenberg, Germany) was used to measure the absorbance at 532 nm with a reference wavelength of 600 nm. In order to get the mean MDA concentration (µM), the absorbance data were divided by the absorption coefficient [156 per millimolar (mM^{-1})] [$\frac{\text{sample absorbance}}{156\ mM^{-1}}$ x 1000].

3.8 NITRATE/NITRITE ASSAY

3.8.1 Principle

Nitric oxide (NO) reacts with superoxide to form peroxynitrite, a potent reactive nitrogen species (RNS).The nitric oxide synthase (NOS) assay measures nitrate (NO_3^-) and nitrite (NO_2^-) because NO has a short lifespan and cannot be measured directly (Dong *et al.,* 2018). Nitrate is reduced to nitrite by vanadium chloride (VCl_3) (Figure 3.5). Subsequently, a two-step Griess reaction (Figure 3.5) is employed where sulphanilamide reacts with acidified nitrite to form the diazonium cation, a substrate for N-(1-naphthyl) ethylenediamine (NEDD). The azo dye product is a chromogen that can be measured with a spectrophotometer at 540 nm (Dong *et al.*, 2018).

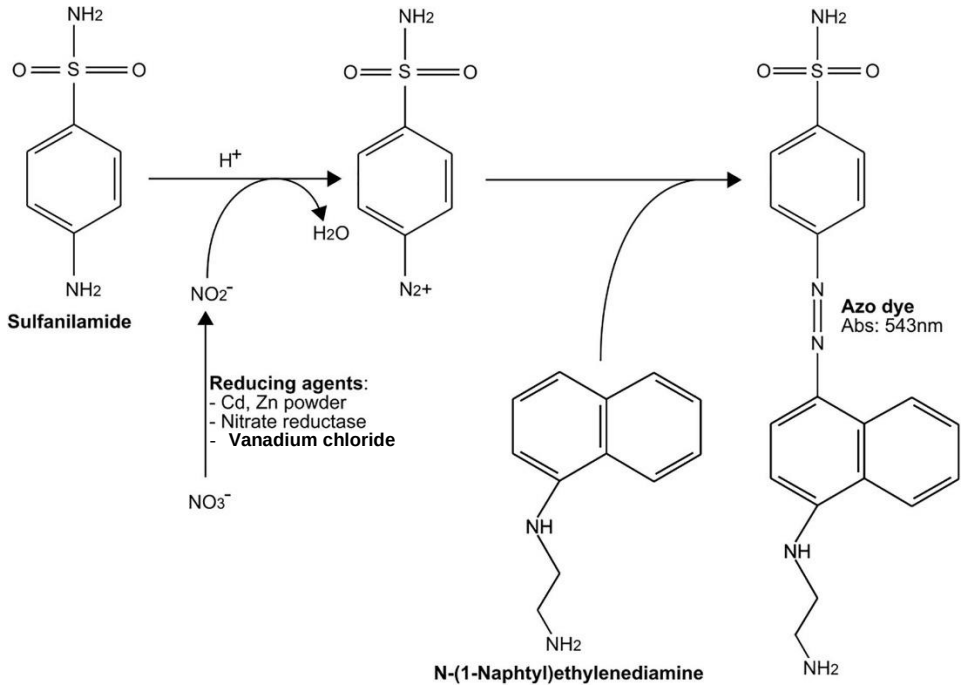

Figure 3.5: The nitrate/nitrate assay for the quantification of reactive nitrogen species. The conversion of nitrate to nitrite by VCl_3, and Griess reaction (sulfanilimide and NEDD) to generate a quantifiable azo dye product (Braissant *et al.*, 2020).

3.8.2 Protocol

The RNS produced following *TRALE* treatment was quantified using the nitrate/nitrite assay. Sodium nitrate standards (0-200 µM) were prepared and 50 µl of each concentration was aliquoted into a 96-well microtiter plate in triplicate. In triplicate, 50 µl of the treatment media from 48-hour TRALE-treated and control HepG2 cells was also applied to each well of the 96-well plate. The plate was then incubated for 45 minutes at 37˚C after 50 µl of VCl_3, 25 µl of sulfanilimide, and 50 µl of NEDD were added successively to each well. After incubation, a SPECTROstar® Nano microplate reader (BMG LABTECH, Ortenberg, Germany) was used to measure the absorbance at 540 nm with a reference wavelength of 690 nm. The nitrate/nitrite concentrations (µM) of treated and untreated samples were calculated using the extrapolated equation and a standard curve created from the average absorbances of sodium nitrate standards.

3.9 GLUTATHIONE ASSAY

3.9.1 Principle

Reduced glutathione (GSH) is a three-amino-acid peptide that functions as an antioxidant in eukaryotic cells (Sun *et al.*, 2019). Free radicals in the form of ROS and RNS can cause a drop in GSH levels either by oxidation or reaction with the thiol group. A change in GSH levels is important for assessing toxicological responses and can promote oxidative stress, potentially leading to

apoptosis and cell death (Salbitani *et al.*, 2017). The GSH assay detects and quantifies test based on luminescence produced (Sun *et al.*, 2019). The assay is based on glutathione S-transferase (GST) catalysing the conversion of a luciferin derivative to luciferin in the presence of GSH (Figure 3.6), which is a co-factor that provides reducing power in the reaction. The amount of GSH present in the sample is proportional to the signal generated in a coupled reaction with firefly luciferase (Salbitani *et al.*, 2017).

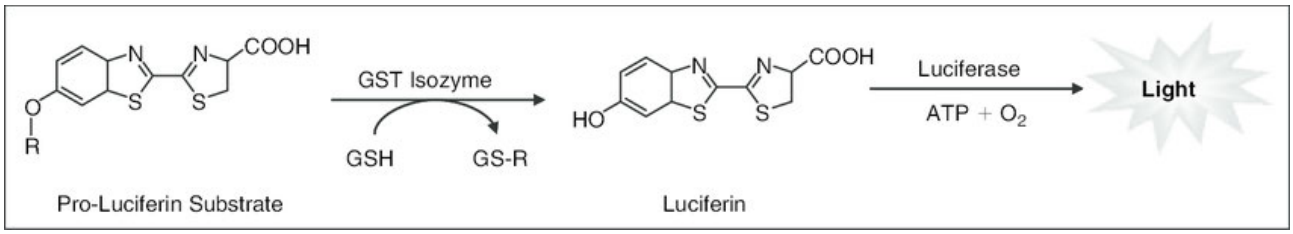

Figure 3.6: Detection and quantification test based on luminescence. Bioluminescent reaction catalysed by luciferase in the presence of GSH and GST to quantify GSH in the cells (Yasgar *et al.*, 2010).

3.9.2 Protocol

Intracellular GSH levels were determined using the Promega GSH-Glo™ assay (Cat. #V6911/2). After seeding 20,000 HepG2 cells each well in 200µl CCM per well into a 96-well white opaque luminometer plate, the cells were cultured for the whole night at 37˚C with 5% CO_2. The media was removed and cells were treated in triplicate with the *TRALE* IC_{50} dose and the control received CCM only (300 µl) for 48 hours of incubation at 37˚C with 5% CO_2. After the treatment media was withdrawn, 50 µl of PBS was added to each well. Following preparation in accordance with the manufacturer's instructions, 25 µl of GSH-Glo^{TM} reagent was applied to each well. After 30 minutes of incubation at RT in the dark, the plate was treated with 12.5 µl of luminometric detection reagent. A Modulus™ microplate luminometer (Turner BioSystems Inc., Sunnyvale, California, USA) was used to detect luminescence after 15 minutes. The mean RLU was used to express the collected data.

3.10 LACTATE DEHYDROGENASE (LDH) ASSAY

3.10.1 Principle

The LDH enzyme is in the cytoplasm and is employed as a cellular toxicity indicator. The LDH is released into the surrounding cell culture medium when the plasma membrane is damaged (Kumar *et al.*, 2018a). A linked enzymatic LDH process, in which LDH catalyses the conversion of lactate to pyruvate via NAD^+ reduction to nicotinamide adenine dinucleotide (NADH), can be used to measure extracellular LDH (Kumar *et al.*, 2018a). The NADH is then used to convert the tetrazolium salt to a red formazan product with a 490 nm wavelength (Figure 3.7). The extracellular LDH is a marker of

cellular cytotoxicity, the assay can be used to track cytotoxicity over time using the same material (Kamiloglu *et al.*, 2020).

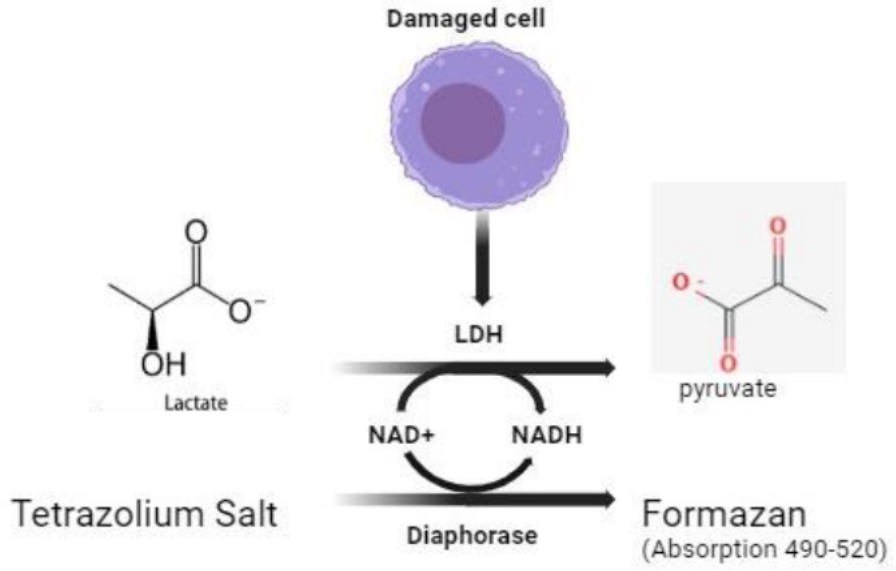

Figure 3.7: Schematic presentation of LDH Assay in damaged cells. The conversion of lactate to pyruvate by LDH and diaphorase to form pink/purple formazan [created by Author].

3.10.2 Protocol

A Cytotoxicity Detection Kit (#0474926001, Roche, Mannheim, Germany) was used to measure the extracellular LDH levels in order to evaluate the degree of cell membrane damage. In triplicate, 50 µl of the treated and untreated supernatant samples were added to a 96-well microtiter plate. The substrate combination (25 µl) containing the dye solution (INT/sodium lactate) and catalyst (diaphorase/NADP) was added to each well containing the sample, and the plate was incubated at RT in the dark for 30 minutes. Stop solution (12.5 µl/well) was added to each well containing samples, then a SPECTROstar® Nano microplate reader (BMG LABTECH, Ortenberg, Germany) was used to measure the absorbance at 490 nm with a reference wavelength of 600 nm. Data was captured as mean optical density (OD).

3.11 CASPASES LUMINOMETRIC ASSAY

3.11.1 Principle

A family of cysteine proteases known as caspases is crucial for the proteolytic disassembly of the majority of cellular components, including the cytoskeleton and cell junctions, during apoptosis (Mposula *et al.*, 2021). Cell lysis reagent and an amino-luciferin-DEVD substrate, which is cleaved by the corresponding caspase to release amino-luciferin (Figure 3.8), are components of the caspase activity tests (Scabini *et al.*, 2011). In the presence of ATP, magnesium ions (Mg^{2+}), and oxygen, the released amino-luciferin combines with luciferase to produce light, which the luminometer measures

(Mposula *et al.*, 2021). The amount of caspase that is active in the sample determines how much light is produced (figure 3.8).

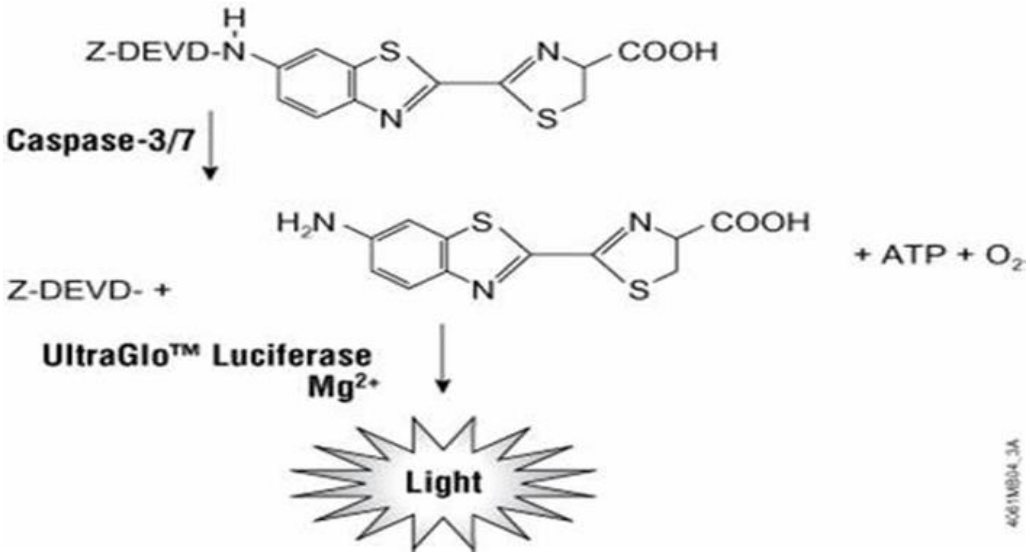

Figure 3.8: Schematic Diagram of the caspase-Glo® 3/7 assay technology. amino-luciferin reacts with luciferase in the presence of ATP, magnesium ions (Mg^{2+}) and O_2 to generate light that is quantified by the luminometer (Procházková *et al.*, 2022).

3.11.2 Protocol

The Promega Caspase-Glo® assay was used to measure the activity of caspases-8, -9, and -3/7. A white opaque 96-well luminometer plate was seeded with the HepG2 cell suspension in triplicate at a density of 20,000 cells/well (200 µl/well CCM) and incubated for the entire night at 37˚C with 5% CO_2. The CCM was removed, and 200 µl of CCM (control) and *TRALE* IC_{50} treatment solution was applied in triplicate. After an incubation period of 48 hours at 37˚C with 5% CO_2, the treatment was removed and each well received 50 µl of PBS. After preparing the Caspase-Glo®-3/7 (#G8090), Caspase-Glo®-8 (#G8200) and Caspase-Glo®-9 reagents (#G8210) in accordance with the manufacturer's instructions, 25 µl of the caspase reagent was applied to the appropriate treatment wells. The plate was then incubated (dark, 30 minutes, RT). Luminescence was detected using the Modulus™ microplate luminometer (Turner BioSystems Inc, Sunnyvale, California, USA) in RLU.

3.12 ANNEXIN V ASSAY

3.12.1 Principle

Healthy cells have lipids on their surface that are asymmetrically distributed throughout the inner and outer leaflets of the plasma membrane. Usually found only in the cytoplasm of cells, phosphatidylserine is restricted to the inner leaflet of the plasma membrane (Kupcho *et al.*, 2019). It is possible to detect phosphatidylserine on the surface of apoptotic cells by using fluorescently tagged

Annexin V, a 36-kDa calcium-binding protein that binds to phosphatidylserine (Kupcho *et al.*, 2019). Because the membranes of necrotic cells have burst, the DNA-binding probe in the Annexin V kit can enter the cell and stain it (Kupcho *et al.*, 2019). This method describes how to use Annexin V binding and PI uptake, followed by flow cytometry, to identify and measure necrotic and apoptotic cells. A simple luminescence signal is used to detect Annexin V binding (Figure 3.9) (Kabakov and Gabai, 2018).

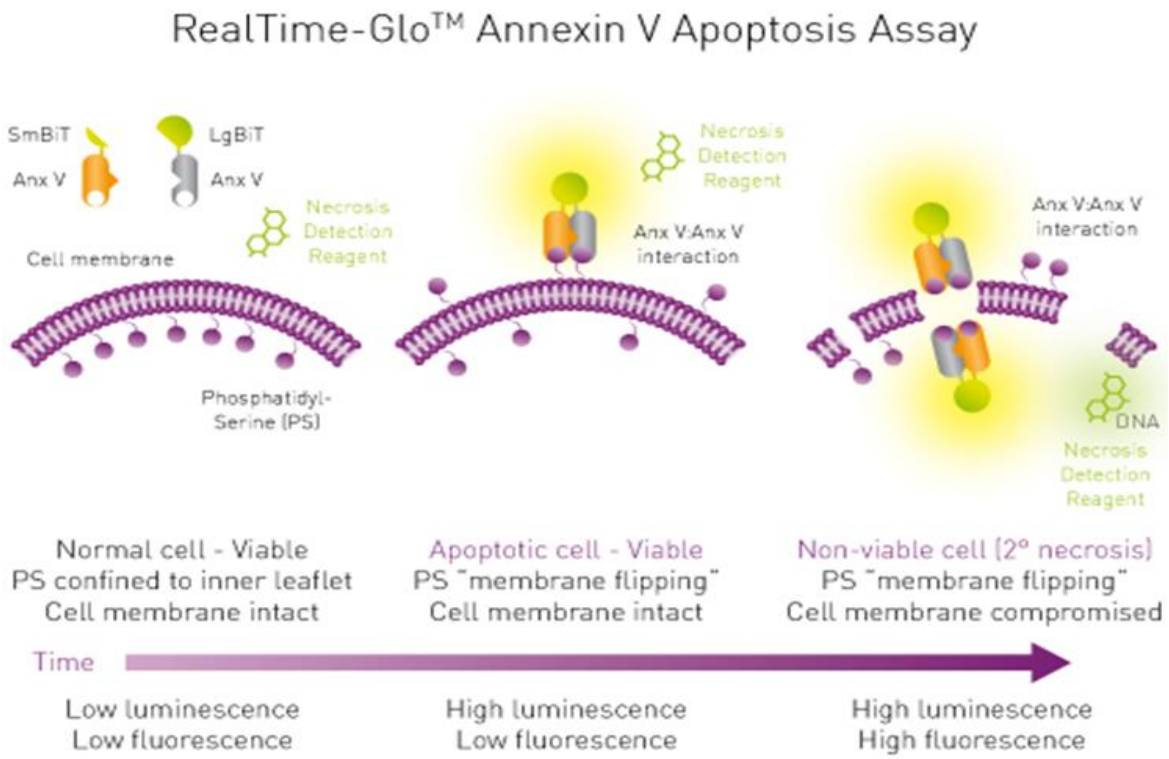

Figure 3.9: **Schematic representation of changes in the plasma membrane during early events of apoptosis.** The luminometric detection and quantification of necrotic and apoptotic cells using annexin V and a DNA binding dye (BMGlabtech, 2024).

3.12.2 Protocol

The Annexin V apoptosis and necrosis assay were used to identify the presence of apoptosis. At a concentration of 20,000 cells/well (200 µl CCM each well), in a white opaque 96-well luminometer plate, the HepG2 cell suspensions were sown in triplicate and incubated overnight at 37˚C with 5% CO_2. Following the removal of the culture medium, control cells were given CCM alone (300 µl), and each well received 300 µl of *TRALE* solution (IC_{50}). After 48 hours of incubation at 37˚C with 5% CO_2, the plate was cleared of the treatment medium. 50 µl of PBS was added to each well. Following the manufacturer's instructions, 25 µl of the RealTime-Glo™ Apoptosis, Necrosis and Annexin V Assay reagent (Cat. #JA1011) was produced and added to the sample wells. After 30 minutes incubation (dark, RT), the luminescent and fluorescent signal were detected using the

Modulus™ microplate luminometer (Turner BioSystems Inc, Sunnyvale, California, USA) and data was presented in RLU and RFU.

3.13 WESTERN BLOTTING

3.13.1 Principle

Western blotting, commonly known as protein blotting or immunoblotting, is based on the immunochromatography principle for a sensitive and quick detection and characterisation of proteins (Figure 3.10) (Bass *et al.*, 2017). Proteins are isolated, quantified and standardised from the samples as needed, then separated in polyacrylamide gels based on their molecular weight (Bass *et al.*, 2017). The proteins are subsequently transferred or electro-transferred onto nitrocellulose membranes, where they are detected using a primary antibody and a enzyme-labelled secondary antibody and substrate (Bass *et al.*, 2017). The GelDoc XRS equipment (Bio-Rad) is used to detect captured chemiluminescence. A housekeeping protein, such as β-actin or GAPDH, is used to normalise the concentration of the protein of interest.

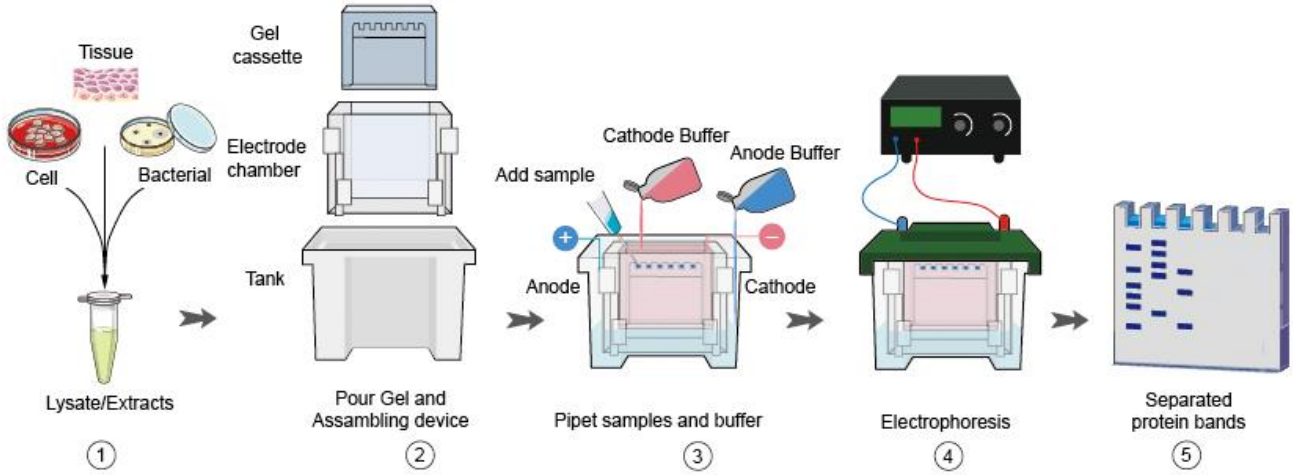

Figure 3.10: Schematic representation of western blotting assay. The principle of western blotting, which involves sorting proteins onto polyacrylamide gels according to their molecular weight, transferring to a solid support, then immumoprobing for a protein of interest (Kurien and Scofield, 2015), (CD diagnostic creatives®, 2024).

3.13.2 Protocol

The western blotting was used to determine the protein expression of inducible nitric oxide synthase (iNOS), cellular inhibitor of apoptosis protein (cIAP) and heatshock protein 70 (HSP70) on HepG2 cells. After 48 hours treatment at 37°C (5% CO_2) with the *TRALE* IC_{50} and CCM (control), the cells were rinsed with PBS. Using the Cytobuster™ reagent (Novagen, San Diego, California, USA) in conjunction with protease and phosphatase inhibitors [(Roche (Germany), 05892791001 and

04906837001, respectively], crude protein was extracted from both treated and untreated cells. After adding 400 µl of the cytobuster reagent, the flasks were left on ice for 15 minutes. After being scraped and collected into microcentrifuge tubes, samples were left on ice for a further ten minutes, then the cell lysate was centrifuged for five minutes at 10000×g and 4°C. After removing the supernatants that contained the crude protein, the bicinchoninic acid (BCA) assay was used to quantify the results.

Bovine serum albumin (BSA) standards were produced and pipetted (12.5 µl) into triplicate wells of a 96-well plate at concentrations of 0, 0.2, 0.4, 0.6, 0.8, and 1 mg/ml. Following the addition of the samples in triplicate, each well received 100 µl of BCA solution, which was made up of 2 µl $CuSO_4$ and 99 µl BCA. After the plate had been incubated for 30 minutes at 37˚C, a SPECTROstar Nano spectrophotometer (BMG Labtech, Ortenberg, Germany) was used to detect absorbance at 562 nm. A standard curve was created from the average absorbances of the standards, and the extrapolated equation was used to determine each sample's crude protein concentration. Following standardisation to 1 mg/ml, each protein sample was mixed in a 1:4 ratio of Laemmli buffer [dH_2O, 0.5 M Tris-HCl (pH 6.8), glycerol, 10% of sodium dodecyl sulfate (SDS), β-mercaptoethanol, and 1% bromophenol blue]. The samples were boiled at 100˚C for five minutes, cooled to ambient temperature and stored at -80˚C until they were needed.

The standardised samples (25 µl) were dispensed into individual wells of prepared polyacrylamide gels. The gels were made up of two different layers, including a 4% stacking gel layer [dH_2O, 0.5 M Tris-HCl (pH 6.8), 10% (w/v) SDS, 30% Acrylamide/Bis, 10% APS, and TEMED] and a 10% resolving gel layer [dH_2O, 1.5 M Tris-HCl (pH 8.8), 10% (w/v) SDS, 30% Acrylamide/Bis, 10% APS, and TEMED]. The gels were immersed in 1x running (electrode) buffer (dH_2O, Tris, glycine, pH 8.3, 4°C) and used a Bio-Rad small power source to apply an electric field for 90 minutes at 150 V. Following electrophoresis, the gels were immersed for 10 minutes in a cold transfer buffer (dH_2O, Tris, glycine, methanol, pH 8.3). Using the fibre pads, nitrocellulose membrane and electrophoresed polyacrylamide gel in a cassette, the gel sandwich was assembled using the transfer method. Air bubbles were then removed, excess buffer was drained and the Transblot®Turbo™ Transfer system (Bio-Rad, California, USA) was used to electrotransfer proteins onto the nitrocellulose membrane (25 V, 2.5 mA, 30 minutes). Following transfer, 2% BSA in Tris-buffered saline (TTBS; 150 mM sodium chloride (NaCl), potassium chloride (KCl), 25 mM Tris; pH7.5) with 0.05% Tween20 was used to block the nitrocellulose membranes for 2 hours (RT). After removing the blocking solution, primary antibodies (1:1000 dilution in 2% BSA/TTBS) were used to probe the membrane for an hour on the shaker (RT). To enable the primary antibody to bind to the particular targeted protein, the membranes were thereafter incubated for an entire night at 4˚C.

The membranes were equilibrated to RT for an hour, then primary antibody was discarded and the membrane was washed five times with TTBS (10 minutes each). After removing the final wash, 5 ml of secondary antibody conjugated to horse-radish peroxidase (HRP) [anti-rabbit IgG (#7074) or anti-mouse IgG (#7076), 1:2500 dilution in 2% BSA/TTBS] was added to the membranes after washing, and they were shaken for 2 hours at RT and then incubated for 24 hours at 4˚C. After removing the secondary antibody, the membranes underwent five TTBS washes, each lasting ten minutes. After adding the Clarity Western ECL Substrate (catalogue no. 1705061, Bio-Rad), images of the nitrocellulose membranes were taken with the ChemidocTM Imaging System and Bio-Rad imaging system (Bio-Rad, California, USA).

Subsequently, the membranes were quenched with 5% hydrogen peroxide (H_2O_2) at 37˚C for 30 minutes, rinsed twice with TTBS, and blocked in 2% BSA in TTBS for an hour. After that, they were probed for beta (β)-actin (A0bD12141, Sigma), a house-keeping protein used to normalise protein expression, for one hour at RT. After three TTBS washes (10 minutes each), an image of the nitrocellulose membranes was taken using the ChemidocTM Imaging System and the Bio-Rad Imaging System (Bio-Rad, California, USA. The band intensity of each protein and β-actin were measured during image analysis, and the protein band was normalised against the respective β-actin band. The data was displayed as the mean relative band density (RBD).

3.14 QUANTITATIVE POLYMERASE CHAIN REACTION (QPCR)

3.14.1 Principle

A technique for amplifying a particular DNA sequence from template strands is the qPCR. This method uses primers, which are single-stranded DNA molecules that surround the targeted gene (Hsieh *et al.*, 2021). The attachment of deoxynucleotide triphosphates (dNTP) to the 3'end of primers is made possible by the subsequent extension of strands by DNA polymerase (Taq polymerase) (Nagura-Ikeda *et al.*, 2020). In order to make precise copies of the target DNA exponentially, samples are subjected to recurrent cycling (30–40 times) of three incubation phases at varying temperatures using a thermocycler (Nagura-Ikeda *et al.*, 2020). Amplification is achieved by denaturation (95˚C), annealing (at the primer-specific temperature) and extension (72˚C). The following components (Figure 3.11) are required for the PCR to occur:

- A specific DNA sequence of interest is included in the DNA template, together with forward and reverse primers that attach to the 3' ends of the target sequence's forward and reverse strands (Nagura-Ikeda *et al.*, 2020).

- When nucleotides are added to the ends of the annealed primers, Taq DNA polymerase, which catalyses the production of new strands of DNA complementary to the sequence of interest, is activated. This cofactor magnesium chloride speeds up the amplification of DNA.
- Taq DNA polymerase is used to lengthen the growing DNA strand after deoxynucleotide triphosphates (dNTPs) form a hydrogen bond with the complementary DNA strand. Finally, a buffer system is used to maintain the ideal pH for the PCR process to take place (Nagura-Ikeda *et al.*, 2020).

qPCR can be used to measure the PCR amplicons produced during each PCR cycle. A dsDNA binding dye called SYBR green is used to measure the amount of amplicon during PCR by detecting overall fluorescence emission. The dye attaches itself to the minor groove of dsDNA but not to ssDNA (Nagura-Ikeda *et al.*, 2020). To normalize target DNA expression levels and concentrations in relation to the quantity of a housekeeping gene, a housekeeping gene is employed.

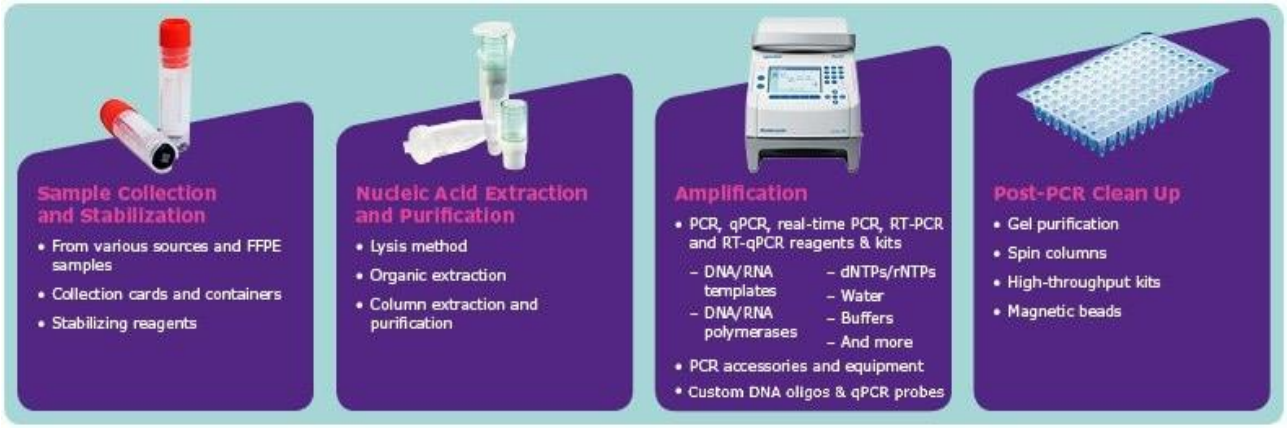

Figure 3.11: RNA isolation and standardisation, cDNA synthesis and qPCR. amplification of specific DNA sequence from template strands [Merck KGaA, 2024].

3.14.2 Protocol

The qPCR technique was used to quantify gene expression of antioxidant and apoptosis-related molecules. After removing the CCM from the treated HepG2 cells and the untreated (control) flasks, the flasks were given a PBS rinse once. Each flask then received 500 µl of Trizol and 500 µl of PBS. After that, the suspension was put into 1.5 ml RNAse/DNA-free microcentrifuge tube and left overnight at -80˚C. Following the samples thawing to RT, 100 µl of chloroform was added and tube contents were mixed and centrifuged (12000xg, 15 minutes, 4°C). After transferring the crude mRNA-containing aqueous layer into fresh 1.5 ml microcentrifuge tubes, 250 µl of isopropanol was added, and the tubes were incubated for the entire night at -80˚C. Samples were thawed and centrifuged (12000xg, 15 minutes, 4˚C). The resultant mRNA pellets were rinsed with cold 75% ethanol (500 µl) and samples were centrifuged again (12000xg, 20 minutes, 4˚C). After removing the

ethanol, the mRNA pellets were air-dried for roughly 2 hours, then resuspended in 15 µl of nuclease-free water. Using the Nanodrop2000 spectrophotometer (Thermo Scientific, Waltham, Massachusetts, USA), the amount of RNA was measured and standardised to 1000 ng/µl. cDNA was synthesised using an iScript™ cDNA Synthesis kit (Bio-Rad; catalogue no 107-8890) comprised of 4 µl RNA template, 2 µl 5X iScript™ reaction mix, 0.5 µl iScript reverse transcriptase, and nuclease-free water. Conditions for the thermocycler were 25˚C for 5 minutes, 42˚C for 30 minutes, 85˚C for 5 minutes, and then a hold at 4˚C. Each tube was filled with 80 µl of nuclease-free water once the procedure was finished, and the samples were kept at -80˚C until they were needed.

As directed by the manufacturer, SsoAdvanced™ Universal SYBR® Green Supermix (catalog no. #172-5271, Bio-Rad) was utilised to analyse gene expression. The mRNA expressions of *catalase, NF-κB, GPx1*, *BCL-2*, *iNOS, Nrf2* and *SOD2 (*Table 3.1), were analysed using specific forward and reverse primers. Reaction volumes consisting of the following were prepared: Nuclease-free water (3.75 µl), forward primer (0.5 µl), reverse primer (0.5 µl), and SYBR green (6.25 µl). The cDNA template (1 µl) was then added in triplicate after the 11 µl reaction mix had been added to each well. Using a Bio-Rad CFX96 Touch™ Real-Time PCR Detection System, the samples were amplified. To ascertain the relative variations in mRNA expression, the 2(-Delta Delta C(T) method, where 2-ΔΔCT represents the fold change observed in mRNA expression (Livak and Schmittgen, 2001). The expression of the gene of interest was normalised against the house-keeping gene.

Table 3.1: The gene of interest, annealing temperatures, and primer sequences used for qPCR.

Gene	**Annealing Temperature**	**Primer**	**Sequence**
GPx1	58	Forward Reverse	5’-GACTACACCCAGATGAACGAGC-3’ 5’-CCCACCAGGAACTTCTCAAAG-3’
Nrf2	60	Forward Reverse	5’-AGTGGATCTGCCAACTACTC-3’ 5’-CATCTACAAACGGGAATGTCTG-3’
NF-κB	60	Forward Reverse	5’-GACCTGAATGCTGTGCGGC-3’ 5’-ATCTTGAGCTCGGCAGTGTT-3’
SOD2	59	Forward Reverse	5’-GAGATGTTACACGCCCAGATAGC-3’ 5’-AATCCCCAGCAGTGGAATAAGG-3’

iNOS	55	Forward Reverse	5’-CGCTACAACATCCTGGAG-3’ 5’- ACATTCTGCTTCTGGAAACTA-3’
BCL-2	50	Forward Reverse	5’- ATTGATGGGATCGTTGCCTTATGCA-3’ 5’- CCCTTGGCATGAGATGCAGGAAA-3’
Catalase	55	Forward Reverse	5’-TAAGACTGACCAGGGCATC-3’ 5’-CAACCTTGGTGAGATCGAA-3’
GAPDH	62	Forward Reverse	5’-TCCCTGAGCTGAACGGGAAG-3’ 5’-GGAGGAGTGGGTGTCGCTGT-3’

3.15 STATISTICAL ANALYSIS

The GraphPad Prism v 5.0 program (GraphPad Software Inc., La Jolla, CA, USA) was used for all statistical analyses. To determine the IC_{50} for the MTT experiment, a non-linear regression was used to produce a log inhibition versus normalised response-variable slope. Welch's correction was applied to the unpaired student *t*-test in order to ascertain statistical significance for the ensuing tests. The mean±standard deviation was used to express the data. With a 95% confidence interval and a p value of less than 0.05, the data was deemed statistically significant.

CHAPTER 4 : RESULTS

4.1 CELL VIABILITY (MTT) ASSAY

The MTT assay was used to measure the cytotoxicity of *TRALE* using the HepG2 cells and to derive the half maximum inhibitory concentration (IC_{50}) used in this study [Figure 4.1]. The dose-response curve showed a decrease in cell viability with increased the concentration of *TRALE* (0-3000 µM) in HepG2 cells. The HepG2 cell viability was not markedly affected at the 500 µg/ml *TRALE* treatment (105.0 %), but decreased to 59.5% for the 1000 µg/ml treatment and induced the lowest cell viability of 9.5% at 2500 µg/ml and 3000 µg/ml. The 1240 µg/ml IC_{50} was used in all subsequent assays.

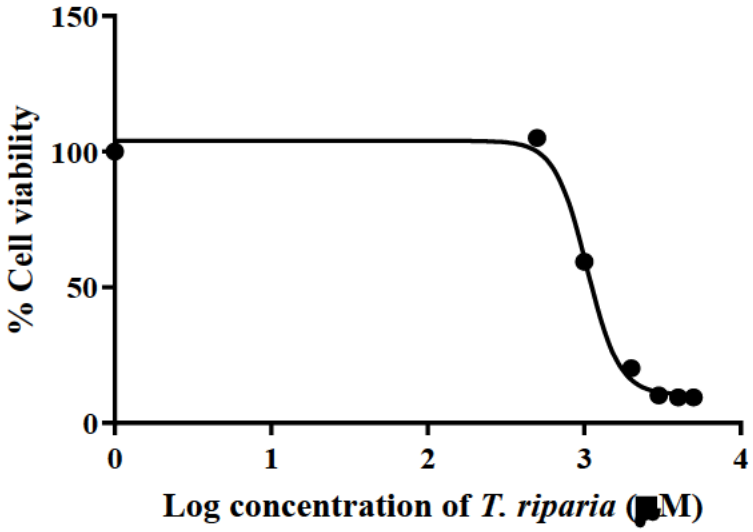

Figure 4.1: A dose-response declining cell viability in HepG2 cells after 48 hours treatment with varying concentrations of *T. riparia*. Cell viability initially increased to 105%, then decreased with subsequent increases in *TRALE* treatment concentration.

4.2 MITOCHONDRIAL INTEGRITY

The study used the ATP assay to measure the cell viability and mitochondrial integrity of HepG2 cells treated with *TRALE*. Additionally, the ratio of JC-10 red and green was used to determine the changes in mitochondrial membrane potential (ΔΨm). The results showed that the *TRALE* treatment significantly reduced ATP levels in HepG2 cells [Figure 4.2**A**] to 0.41-fold at the IC_{50} (7176000±64120 RLU; p = 0.0128) compared to the control (17380000±1165000 RLU). Furthermore, there was a significant 1.19-fold increase in ΔΨM in *TRALE*-treated HepG2 cells (1.550±0.005773 RLU) compared to the control (1.300±0.03215 RLU; p = 0.0166) [Figure 4.2**B**].

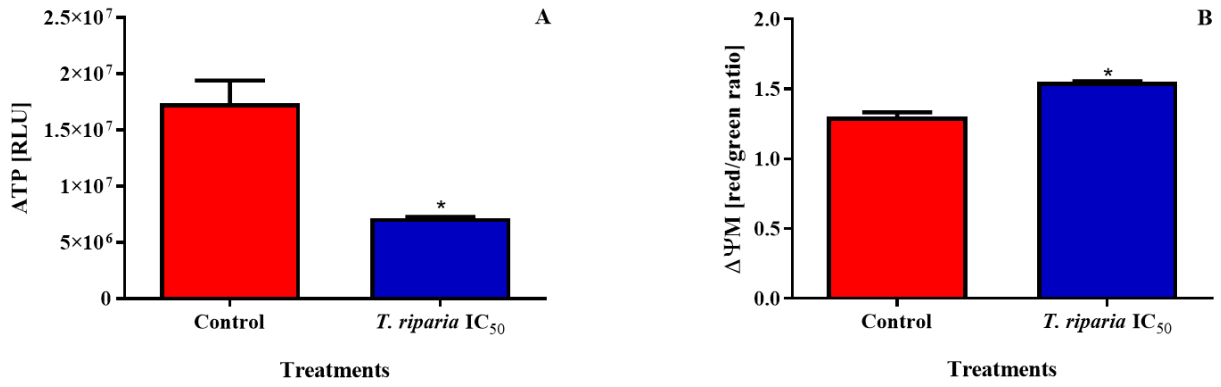

Figure 4.2: The *TRALE* treatment modulated mitochondrial function as indicated by the altered ATP and mitochondrial membrane potential (ΔΨM). (A) A significant decrease in ATP concentration in HepG2 cells treated with IC_{50} of *T. riparia*. **(B)** The ΔΨM was significantly increased in HepG2 cells. [*$p \leq 0.05$ using the unpaired students *t*-test with Welch's correction].

4.3 FREE RADICAL PRODUCTION

Lipid peroxidation was used to assess ROS production by quantifying MDA using the TBARS assay, while the presence of RNS was detected through indirect measurement of nitrate and nitrite levels using the NOS assay to quantify nitric oxide. The *TRALE* treatment induced a significant 1.17-fold increase in MDA concentration (0.2757±0.003756 µM; $p = 0.0024$) when compared to the control (0.2350±0.002000 µM) [Figure 4.3**A**]. A 1.25-fold increase in nitrate and nitrate concentration [Figure 4.3**B**] was observed in IC_{50}-treated HepG2 cells (3.557±0.03868 µM; $p = 0.0020$) in comparison to the control (2.841±0.05909 µM).

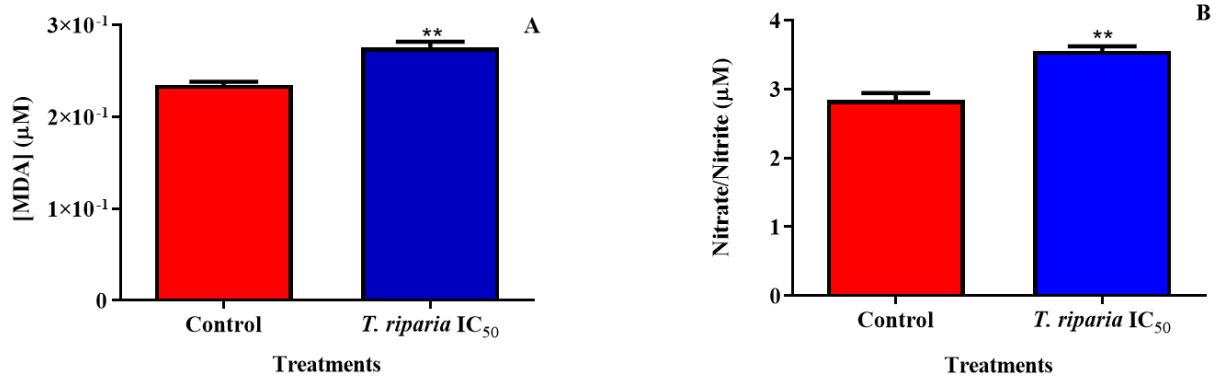

Figure 4.3: Increased oxidant production in TRALE-treated HepG2 cells. (A) The MDA concentration was significantly increased in HepG2 cells at IC_{50} after 24h treatment with *TRALE* compared to the control. **(B)** Nitrite/nitrate concentrations were significantly increased in HepG2 cells at the IC_{50} treatment compared to the control. [*$p \leq 0.05$ using the unpaired students *t*-test with Welch's correction].

4.4 ANTIOXIDANTS

To evaluate the antioxidant response to oxidative stress, the gene expression of SOD2, catalase and GPx1 were measured using qPCR, and GSH and GSSG were quantified using luminometry. The

SOD2 gene expression was significantly increased to 1.660±0.1323 RFC ($p = 0.0379$) in IC_{50}-treated HepG2 cells when compared to the control [Figure 4.4**A**]. Both *catalase* [Figure 4.4**B**] and *Gpx1* [Figure 4.4**C**] gene expression increased to 19.11±0.4900 RFC ($p = 0.0172$) and 10.31±4.998 RFC ($p = 0.2035$) after *TRALE* treatment, when compared to the respective controls. However, treatment with *TRALE* decreased both GSH and GSSG, with a decreased GSH/GSSG ratio observed for the treated cells. The GSH [Figure 4.4**D**] decreased by 0.74-folds compared to the control (7711000±83780 RLU), to 5701000±348600 RLU ($p = 0.0304$) in the IC_{50}-treated cells. Similarly, GSSG levels [Figure 4.4**E**] also significantly decreased to 0.21-fold in *TRALE*-treated HepG2 cells (696900±22470 RLU; $p < 0.0001$) compared to the control (3374000±33530 RLU). Consequently, the GSH/GSSG ratio was significantly decreased at the IC_{50} to 0.64-fold (5.224±0.3286 RLU; $p = 0.0084$) when compared to the control (8.147±0.3359 RLU) [Figure 4.4**F**).

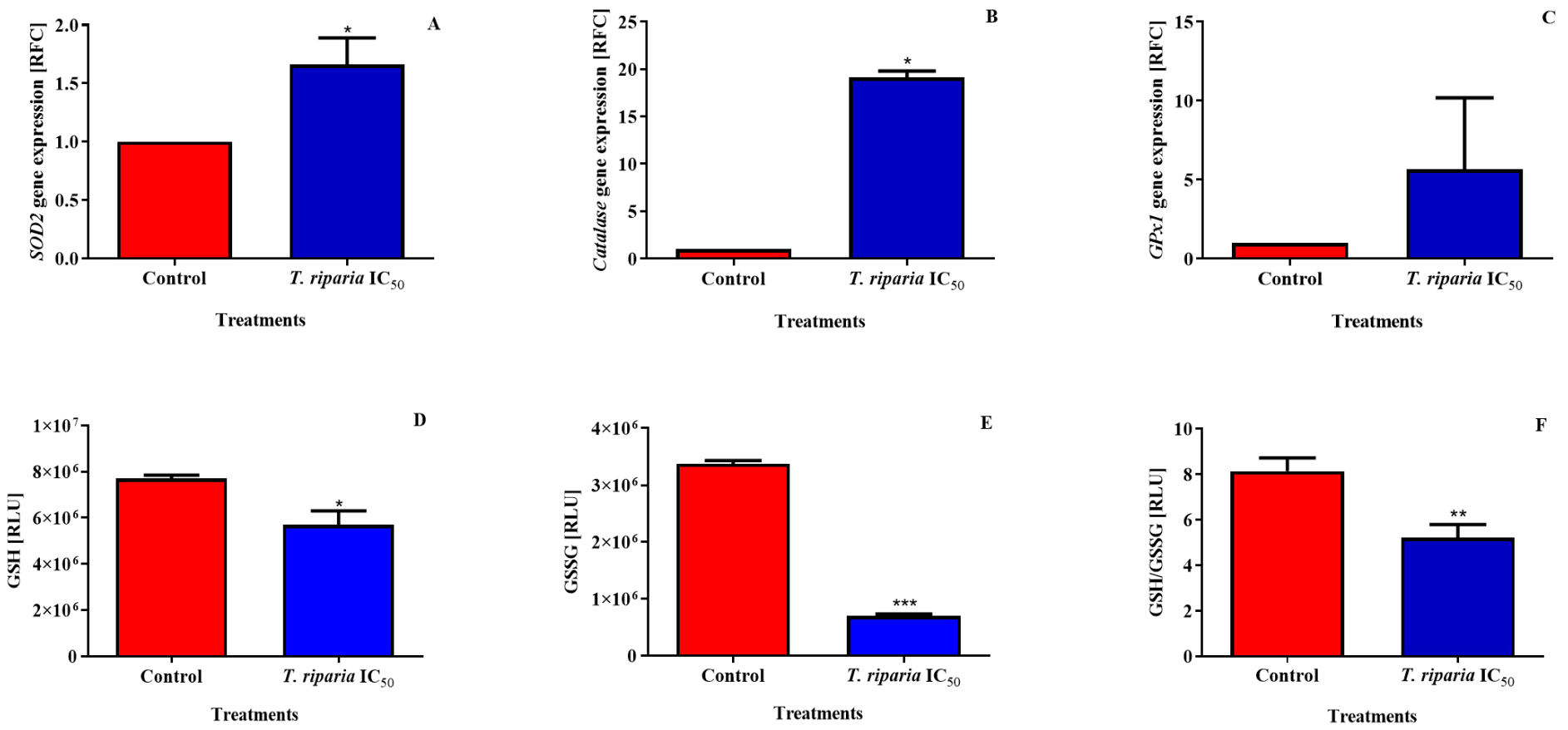

Figure 4.4: The antioxidant reponse in TRALE-treated HepG2 cells. (A) A significant increase in *SOD2* gene expression was observed at the IC_{50} compared to the control. **(B)** The gene expression of *catalase* was significantly increased in the IC_{50}-treated cells. **(C)** A non-significant increase in *GPx1* level after *TRALE* treatment. **(D)** The levels of GSH were decreased in HepG2 cells at the IC_{50} after 24h treatment with *TRALE*. **(E)** A significant decrease in the GSSG levels was observed for IC_{50}-treated HepG2 cells when compared to the control. **(F)** A significant decrease in GSH/GSSG ratio at the IC_{50} when compared to the control. [*$p \leq 0.05$ using the unpaired students *t*-test with Welch's correction].

4.5 RESPONSE TO OXIDATIVE STRESS

The effectiveness of the antioxidant response was further assessed by evaluating the NRF2 and Hsp70 response to *TRALE* treatment. A significant decrease in *NRF2* gene expression to 0.4967±0.08647 RFC (p = 0.0283) when compared to the control (1.000±0.0000005860 RFC) [Figure 4.5**A**], and HSP70 protein expression [Figure 4.5**B**] was similar in the control and IC_{50}-treated HepG2 cells; (3.429±0.2484 RBD; p = 0.8860) relative to the control (3.485±0.2545 RBD).

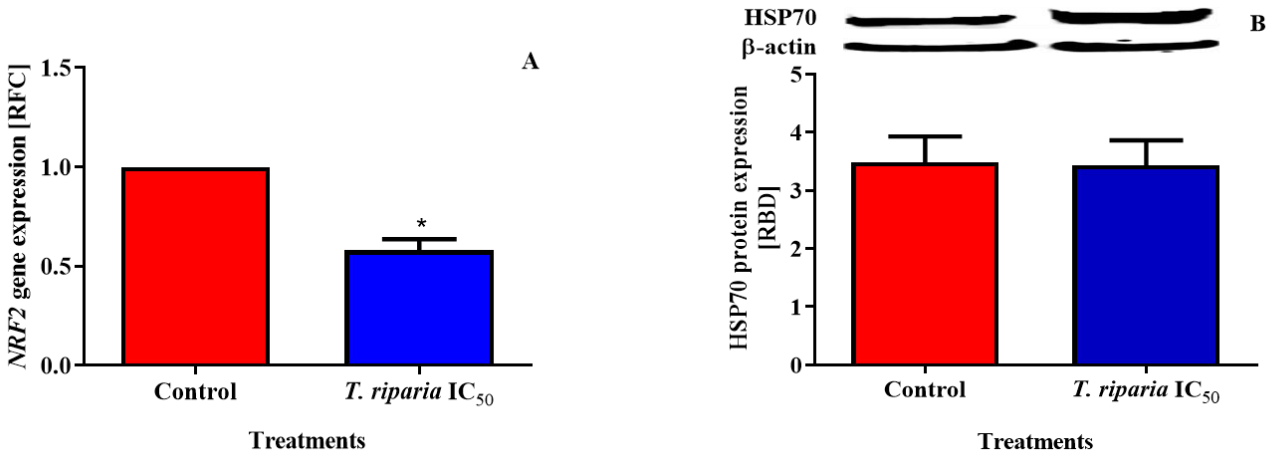

Figure 4.5: Oxidative stress markers were decreased in *TRALE*-treated HepG2 cells. (A) A significant decrease in NRF2 levels at IC_{50} when compared to the control. **(B)** The HSP70 was slightly decreased in the IC_{50}-treated cells. [*$p \leq 0.05$ using the unpaired students t-test with Welch's correction].

The *NF-κB* pathway is activated by oxidative stress, and levels correlate with NRF2. Therefore, *NF-κB* and *iNOS*, a marker activated by *NF-κB* was evaluated by qPCR. The *TRALE* treatment increased the gene expression of *NF-κB* to 1.837±0.2826 RFC (p = 0.0977) relative to the control (1.000±0.0000005860 RFC) [Figure 4.6**A**]. The gene expression of *iNOS* showed a significant decrease to 0.1733±0.08570 RFC; p = 0.0106) when compared to the control (1.000±0.0000005860 RFC) [Figure 4.6**B**].

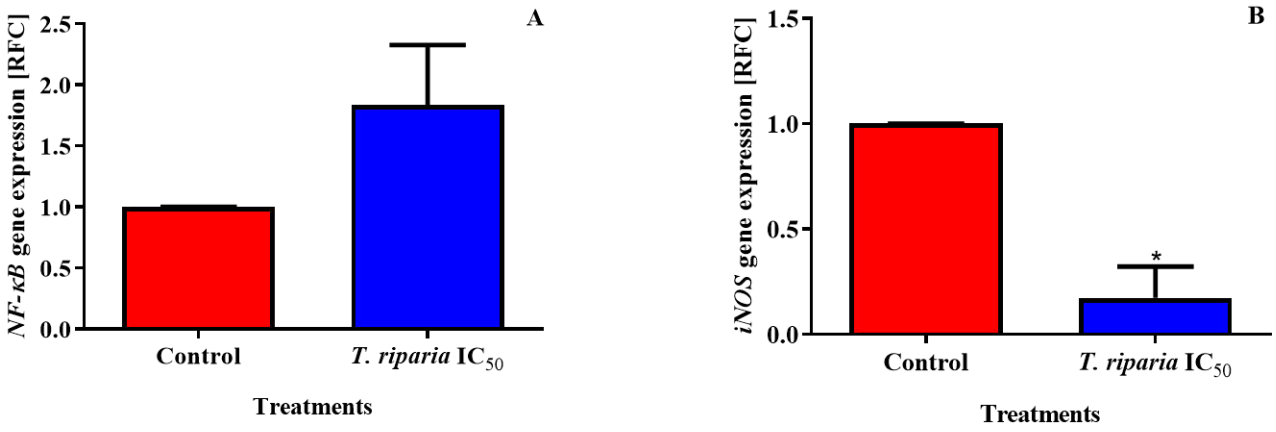

Figure 4.6: The NF-κB response to oxidative stress in *TRALE*-treated HepG2 cells. (A) Increased NF-κB gene expression in the IC_{50}-treated cells compared to the control. **(B)** The nitric oxide gene expression was significantly decreased in HepG2 cells at the IC_{50} treatment compared to the control. [*$p \leq 0.05$ using the unpaired students *t*-test with Welch's correction].

4.6 ACTIVATION AND EXECUTION OF APOPTOSIS

The initiation and execution of apoptosis through the extrinsic (caspase-8 activity), intrinsic (caspase-9 activity) pathways, as well as execution (caspase-3 activity) was assessed using a luminometric assay. In addition, markers of apoptosis were assessed using western blot or qPCR. A 1.06-fold increase in caspase-8 was observed in IC_{50}-treated HepG2 cells (173100±28270 RLU; $p = 0.7834$) when compared to the control (163800±9029 RLU) [Figure 4.7**A**]. The cIAP protein expression [Figure 4.7**B**] to 0.48-fold for the IC_{50} treatment (0.5516±0.05894 RBD; $p = 0.0134$) when compared to the control (1.141±0.09543 RBD).

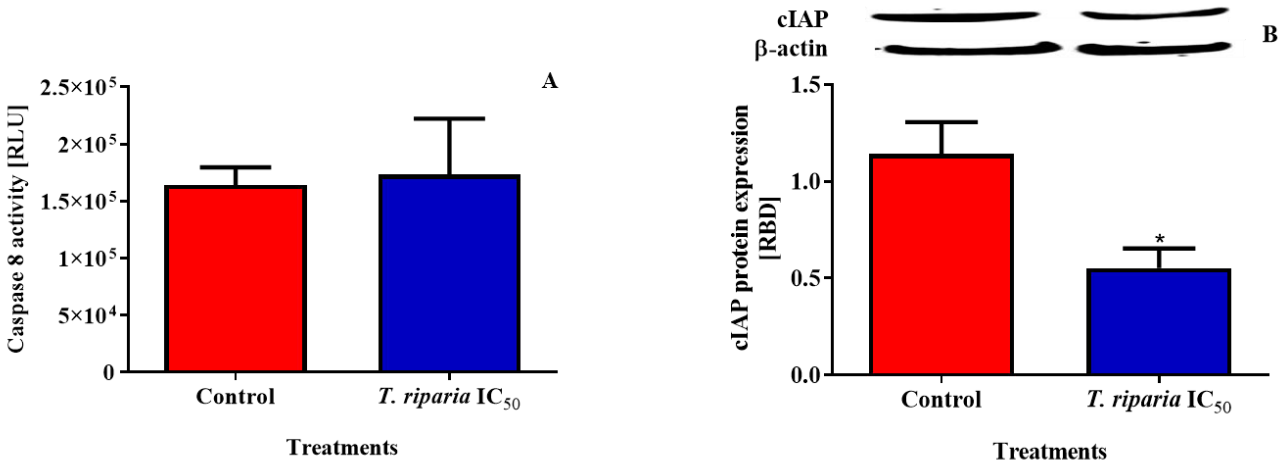

Figure 4.7: Intrinsic apoptosis in *TRALE*-treated HepG2 cells. (A) A non-significant increase in caspase-8 was observed at IC_{50} (when compared to the control, **(B)** The cIAP protein expression was significantly decreased at the IC_{50}. [*$p \leq 0.05$ using the unpaired students *t*-test with Welch's correction].

The effects of *TRALE* treatment on intrinsic apoptosis was evaluated. A significant increase in caspase-9 activity to 3.54-fold was observed in the IC_{50}-treated HepG2 cells (1502000±37140 RLU; p = 0.0003) when compared to the control (424800±40400 RLU) [Figure 4.8**A**]. The *BCL2* gene expression [Figure 4.8**B**] was decreased by the IC_{50} treatment to 0.3300±0.0900 RFC (p = 0.0850) when compared to the control (1.000±0.000005781 RFC).

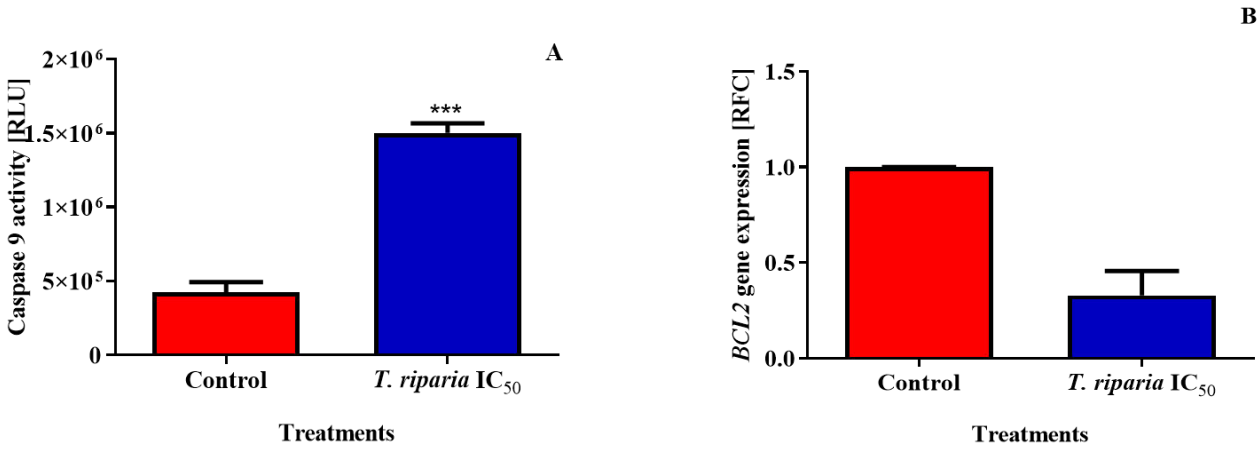

Figure 4.8: The HepG2 cells responded to *TRALE* treatment by activating intrinsic apoptosis. (A) The significant increase in caspase-9 activity was observed at IC_{50}. **(B)** Gene expression of *BCL2* was downregulated in IC_{50}.-treated HepG2 cells. [*$p \leq 0.05$ using the unpaired students *t*-test with Welch's correction].

Execution of apoptosis was assessed after *TRALE* treatment. A significant increase in caspase-3 activity to 24.88-fold was observed at the IC_{50} (778500±29450 RLU; p = 0.0016) when compared to the control (31280±1528 RLU) [Figure 4.9**A**]. Annexin V, a marker of apoptosis quantified using luminometry [Figure 4.9**B**], was similar in the IC_{50} (73660±12910 RLU; p = 0.9123) and the control (72050±1360 RLU) HepG2 cells.

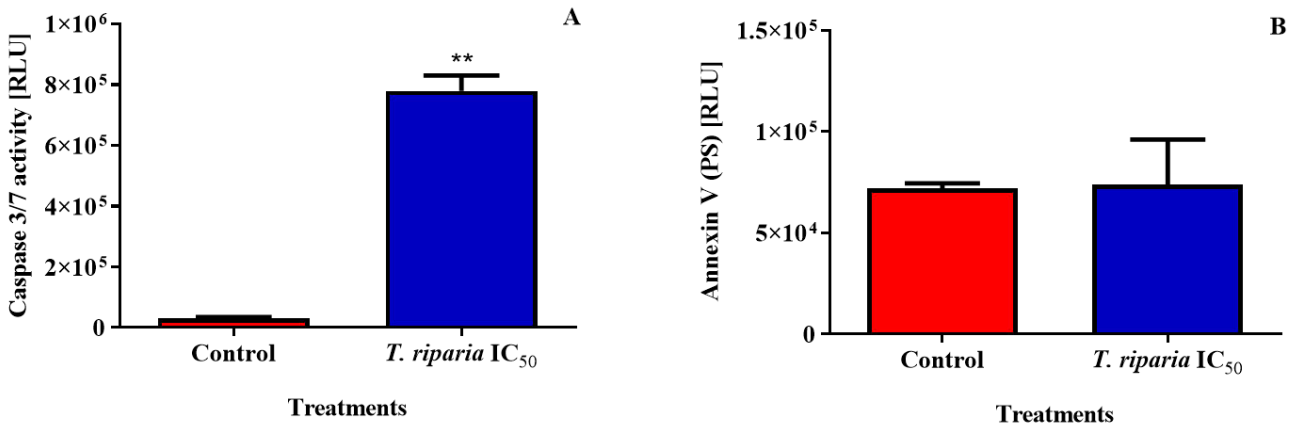

Figure 4.9: Execution of apoptosis in TRALE-treated HepG2 cells. (A) A significant increase in caspase-3 and -9 and a slight increase to caspase-8 at IC_{50} when the HepG2 cells were treated for 24 hours with *TRALE*. RLU: relative light units. **(D)** A slight increase in the early marker of apoptosis was observed at the IC_{50}. [*$p \leq 0.05$ using the unpaired students *t*-test with Welch's correction].

4.7 NECROSIS AND LDH

Necrosis is the death of body cells that is not programmed and can result in inflammation. When the HepG2 cells were treated with *TRALE* for 24 hours, a significant 0.31-fold decrease in necrotic cells was observed at the IC_{50} (190200±7329 RLU*;* $p < 0.0001$) when compared to the control (617500±8935 RLU) [Figure 4.10**A**]. The extracellular LDH leakage was decreased to 0.94-fold at the *TRALE* IC_{50} (351500±6952 OD; $p = 0.0751$) compared to the control (374200±4848 OD) [Figure 4.10**B**].

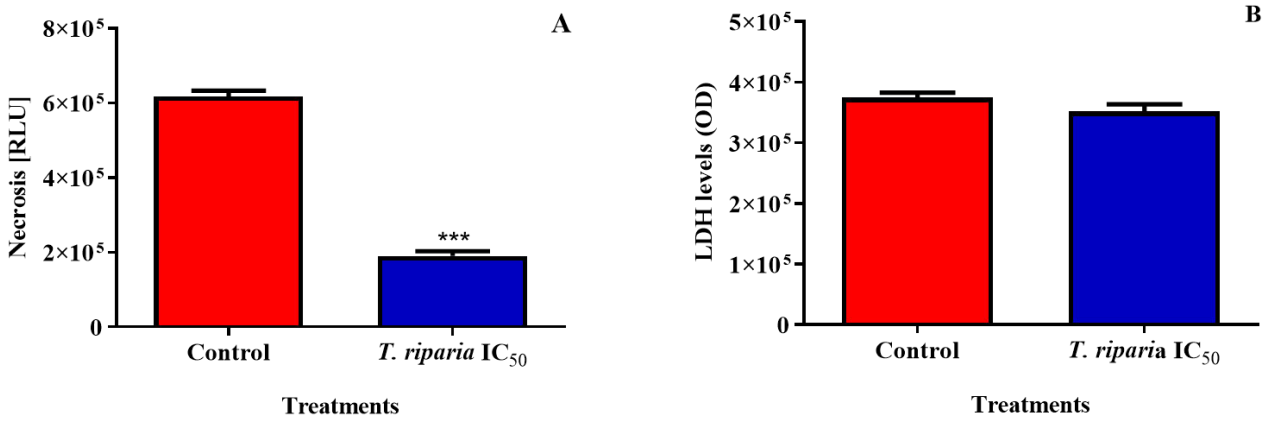

Figure 4.10: Necrosis was not activated in *TRALE*-treated HepG2 cells. (A) The necrotic levels in the HepG2 cells significantly decreased by the IC_{50}. **(B)** The extracellular levels of LDH were not significantly decreased by the IC_{50}. [*$p \leq 0.05$ using the unpaired students *t*-test with Welch's correction].

CHAPTER 5 : DISCUSSION

The escalation in cancer incidence and mortality is a global concern. Liver cancer is currently the third leading cause of cancer-related deaths in the world, accounting for 7.8% of cancer-related deaths in 2022 (Bray *et al.*, 2024). In addition, most liver cancer patients die within a year of being diagnosed (Sung *et al.*, 2021). Chemotherapeutic drugs, surgery and radiation therapy have a bad reputation due to their high cost, limited accessibility and/or invasiveness. Anticancer drugs have also been linked to nephrotoxicity, which accounts for approximately 60% of acute renal injuries (Małyszko *et al.*, 2017). Therefore, the current focus of anti-cancer research is to elucidate therapies that cause little or no damage to healthy cells while effectively targeting and eradicating cancer cells. Medicinal plants contain a plethora of anti-cancer phytochemicals, and traditional healers administer decoctions to treat various cancers or alleviate the side effects associated with treatment. *Tetradenia riparia* is an herbaceous and aromatic shrub commonly known as ‘ginger bush’ and is locally known in South Africa as "Iboza or Ibozane" (Shimira, 2022). The *Tetradenia riparia* dried leaves are used as an infusion or decoction remedy for various diseases; this is attributed to the variety of biological activities that confer larvicidal, antispasmodic, insecticidal, antimicrobial, antimalarial, anti-inflammatory, antioxidant and anticancer properties (Shimira, 2022;Milato *et al.*, 2018). This study investigated the antioxidant and cell death mechanisms associated with the cytotoxicity of *Tetradenia riparia* aqueous leaf extract (*TRALE*) on hepatocellular carcinoma (HepG2) cells after a 24-hour exposure.

Most cytotoxicity studies evaluate cell viability, a measure of the number of cells unaffected by exposure. The methylthiazol tetrazolium (MTT) assay is a commonly employed cytotoxicity assay used to assess the cell viability, and is based on the ability of viable cells to reduce the MTT salt into a water-insoluble purple formazan crystal (Rai *et al.*, 2018). The reduction is facilitated by succinate dehydrogenase (SDH) in the mitochondria of metabolically active cells. The SDH mitochondrial enzyme forms part of complex II of the electron transport chain (ETC), transferring electrons from FADH2 to complex III, catalysing succinate to fumarate oxidation (Rai *et al.*, 2018). In this study, the MTT assay assessed the metabolic activity of HepG2 cells exposed to varying concentrations of *TRALE*. The study observed a dose-dependent decline in cell viability associated with *TRALE* exposure, with a half maximum inhibitory concentration (IC_{50}) of 1240 µg/ml (Figure 4.1). This suggests that 1240 µg/ml *TRALE* decreased the reduction of the MTT salt by 50%. This IC_{50} was significantly higher than other studies; for example, 50 µg/ml *T. riparia* essential oil caused 60% growth inhibition in MDA-MB-435 breast cancer cells, while 78% and ±85% growth inhibition was

noted for SF295 glioblastoma cells and HL60 / HCT8 colon cancer cells respectively (Gazim *et al.*, 2014). In addition, ethanol and dichloromethane extracts yielded IC_{50} values ranging from 10.83 µg/ml to 85.43 µg/ml in various cell lines (Chepng'etich *et al.*, 2018). The above studies imply different sensitivities to the *T. riparia* based on the cell type. In addition, the essential oil possibly contained different concentrations or types of phytochemicals, accounting for the differences noted. However, research suggests that polar solvents extract more phenolic phytochemicals, while polar/non-polar solvents extract both flavonoids and phenolics (Abubakar and Haque, 2020;Nawaz *et al.*, 2020). *Tetradenia riparia* flavonoids luteolin and astragalin were cytotoxic to HepG2 and HCT116 cells, respectively (Milato *et al.*, 2018;Yang *et al.*, 2021;Idowu, 2020), but higher IC_{50} values in normal colon and kidney cells suggested that these cells were less sensitive to the flavonoids. Although this study employed an aqueous extraction used routinely by traditional healers and known for its high yield of phytochemicals (Ozioma and Chinwe, 2019;Truong *et al.*, 2019), it suggested that *TRALE* interfered with SDH activity as implied by the decreased cell viability in this study.

Due to its essential role in the Krebs cycle, ETC and ATP production, inhibition of the ETC (SDH) complex II may hinder ATP synthesis. When electrons are transferred to complexes I, III and IV of the ETC, the accompanying transfer of protons from the mitochondrial matrix into the intermembrane space generates a mitochondrial membrane potential ($\Delta\Psi M$) that is essential to ATP production; the proton gradient created is used by ATP synthase at complex V to form ATP (Zhao *et al.*, 2019). Therefore, the $\Delta\Psi M$ generally correlates with ATP levels. In this study, the ATP assay was employed as a viable cell biomarker because injured cells lose membrane integrity and the ability to maintain $\Delta\Psi M$, thus compromising ATP synthesis (Kamiloglu *et al.*, 2020). Interestingly, decreased ATP corresponded to an increase in $\Delta\Psi M$ for the *TRALE* IC_{50} treatment (Figure 4.2A and B). The ATP result concurs with data from several studies that used aqueous extracts of medicinal plants, including *Momordica foetida*, *Moringa oleifera*, *Warburgia salutaris* and *Carica papaya* (Netshitangani, 2022;Shunmugam, 2016;Maruma *et al.*, 2022;Nxumalo *et al.*, 2024), but decreased $\Delta\Psi M$ was only shown in the *M. foetida* treated HepG2 cells. A rise in $\Delta\Psi M$ when ATP levels are low signifies mitochondrial damage and reduced functioning of the ETC (Feno *et al.*, 2019). To maintain $\Delta\Psi M$, ATP enters the mitochondrial matrix through the adenine nucleotide transporter and is used by ATP synthase to pump protons out of the mitochondrial matrix into the intermembrane space. Thus, $\Delta\Psi M$ is preserved, and cell death may be delayed; cell death is associated with sustained depolarisation of the mitochondrial membrane that could lead to increased levels of ROS due to electron leakage (Begum and Shen, 2023;Zorova *et al.*, 2018).

Electrons can leak from the respiratory chain to molecular oxygen from 1-electron sites within complexes I and III (Feno *et al.,* 2019). High membrane potential prolongs the length of stay of the electron at these sites and increases the probability of leakage to form superoxide ($O_2^{\bullet-}$), the first free radical or reactive oxygen species (ROS) produced in mitochondria (Zhao *et al.*, 2019). In this study, increased $O_2^{\bullet-}$ is implied by the elevated MDA (Figure 4.3A). The production of reactive nitrogen species (RNS) can also be attributed to excess $O_2^{\bullet-}$, as it can react with nitric oxide ($NO^{\bullet}$) to produce peroxynitrite ($ONOO^-$) (Satyo *et al.*, 2020). In this study, $NO^{\bullet}$ concentration was increased in HepG2 cells (Figure 4.3B). Inducible NOS *(iNOS)* produces $NO^{\bullet}$ when L-arginine, O_2, and NADPH are co-substrates (Pappas *et al.*, 2023). However, a decrease in *iNOS* was observed (Figure 4.6B), indicating a decreased inflammatory response or reduced immune activation associated with a less aggressive inflammatory response; this could be beneficial in chronic inflammatory diseases where excessive $NO^{\bullet}$ production can cause tissue damage. Inhibition of *iNOS* may be attributed to the anti-inflammatory properties of luteolin, which has been shown to scavenge ROS, inhibit *iNOS* expression and activate antioxidant enzymes (Aziz *et al.*, 2018). In this study, the downregulation of *iNOS* could also indicate a cell response to inhibit RNS production. Nevertheless, this study suggests that *TRALE* increased ROS and RNS production. This study is similar to many studies experimenting on medicinal plants such as *luteolin*, *Momordica foetida* and *Hibiscus sabdariffa,* which were found to increase ROS and RNS (Nunes *et al.*, 2017;Idris, 2021;Netshitangani, 2022).

Elevated ROS and RNS can result in DNA, protein and lipid oxidation/nitration (Juan *et al.*, 2021). The heat shock protein 70 (HSP70) expression increases in response to stress conditions such as oxidative stress and exposure to toxins, helping cells to survive these conditions by stabilising proteins and cellular structures (Kurashova *et al.*, 2020). It also assists in the proper folding of newly synthesised proteins and refolds misfolded or denatured proteins (Rosenzweig *et al.*, 2019). It also translocates proteins across cellular membranes, including endoplasmic reticulum and mitochondria (Rosenzweig *et al.*, 2019). The HSP70 also interacts with various components of the apoptotic machinery, often exhibiting anti-apoptotic effects by inhibiting key steps in the cell death pathways (Kurashova *et al.*, 2020). In this study, HSP70 expression was like the control (Figure 4.5B), indicating minimal oxidative damage to proteins. However, increased MDA attests to increased lipid peroxidation.

The hydroxyl radical ($^{\bullet}OH$) formed from H_2O_2 is an essential mediator of lipid peroxidation. First, $O_2^{\bullet-}$ is dismutated to the less radical hydrogen peroxide (H_2O_2) by superoxide dismutase (SOD) (Di Meo *et al.*, 2016). The H_2O_2 is toxic to somatic cells and leads to the formation of $^{\bullet}OH$ via the Fenton

reaction (Ighodaro and Akinloye, 2018). The $^{\bullet}OH$ is more potent than $O_2^{\bullet-}$, oxidising biomolecules and causing oxidative stress (Conde de la Rosa *et al.*, 2022). Therefore, catalase and glutathione peroxidase *(GPx1)* are crucial for converting H_2O_2 into H_2O and oxygen, thus protecting cells from oxidative damage (Adwas *et al.*, 2019). The reduction of H_2O_2 and organic hydroperoxides by *GPx1* is reliant on reduced glutathione (GSH) to act as a reducing agent and donate an electron, becoming oxidised and forming glutathione disulfide (GSSG) (Adwas *et al.*, 2019). Toxicity induced by GSSG is prevented by glutathione reductase (GR). In this study, upregulated protein expression of *SOD2* in *TRALE*-treated HepG2 cells (Figure 4.4A) may be attributed to increased $O_2^{\bullet-}$. The consequent increase in H_2O_2 mobilised *catalase* (Figure 4.4B) and *GPx1* (Figure 4.4C), which were also upregulated. It was, therefore, not surprising that *TRALE* increased GSH utilisation, with a consequent decrease in GSH (Figure 4.4D). Interestingly, GSSG was decreased (Figure 4.4E), implying downregulated GR or NADPH. In addition, the GSH/GSSG ratio was decreased (Figure 4.4D). The significant decrease in these molecules is an indication of oxidative stress. This study is backed by a study of (Ceci *et al.*, 2022), which used medicinal plant extracts of *Moringa oleifera* and *Ginkgetin*, a derivative of *Ginko Biloba* (Lou *et al.*, 2021) leaves where similar results of decreased GSH, GSSG and GSH/GSSG ratio were observed.

Both nuclear factor erythroid 2-related factor 2 (Nrf2) and nuclear factor-kappa B *(NF-κB)* are important modulators of oxidative stress and Nrf2 depletion is associated with upregulated *NF-κB* (Gao *et al.*, 2022). In response to oxidative stress, the Nrf2 protein controls the gene expression of several cytoprotective proteins, such as antioxidants, detoxification enzymes, and proteins that support repairing or removing damaged macromolecules. This enables the cells to adapt and endure under adverse circumstances. The Nrf2 protein is subjected to proteasomal degradation due to its attachment to Keap1, but Keap1 oxidation during oxidative stress releases Nrf2 to the nucleus to promote the transcription of many genes (Ulasov *et al.*, 2022). The *NF-κB* pathway possesses both pro- and anti-oxidant potential, making it an essential component of the response to oxidative stress (Yu *et al.*, 2020). Lower levels of Nrf2 in this study (Figure 4.5A) were peculiar since *SOD2*, *catalase* and *GPx1* were upregulated (Figure 4.5). Cancer cells exhibit enhanced amounts of antioxidant enzymes as a defence against the increased oxidative stress brought on by rapid cell division. In certain situations, mutations or other signalling pathways may downregulate Nrf2 or circumvent its function (Jomova *et al.*, 2023). However, its downregulation corresponds with GSH depletion and oxidative stress. The increased redox transcriptional function of *NF-κB* causes transcription and translation of pro- and anti-inflammatory proteins. The *NF-κB* also activates the transcription of iNOS (Zhang *et al.*, 2021). The activation of *iNOS* by *NF-κB* is part of a coordinated response to

stress, infection, and inflammation. During infections, pathogens such as bacteria or viruses can trigger *NF-κB* activation through pattern recognition receptors like TLRs. Activating *NF-κB* leads to the transcription of pro-inflammatory cytokines, which in turn further activate *NF-κB* and *iNOS* expression. In this study, the upregulation of *NF-κB* (Figure 4.6A) did not correspond to *iNOS* (Figure 4.6B), suggesting that luteolin exerted a more substantial effect on *iNOS* than *NF-κB* (Aziz *et al.*, 2018). This data differs from the study (Yang *et al.*, 2021), where astragalin inhibited *NF-κB* signalling. Upregulated *NF-κB* can promote apoptosis by upregulating the expression of death receptors on the cell surface, such as Fas (also known as CD95) and TRAIL (TNF-related apoptosis-inducing ligand) receptors; these death receptors are part of the extrinsic apoptosis pathway and activate a cascade leading to caspase activation and apoptosis (Guerrache and Micheau, 2024).

Apoptosis is generally known as programmed cell death mediated by caspases (Krüger and Richter, 2022). These cells exhibit unique morphological features such as cell shrinkage, cell blebbing, loss of surface microvilli, nuclear and chromosomal condensation, mitochondrial depolarisation, cellular acidification, and nuclear fragmentation and apoptotic body formation in the late stages (Patil *et al.*, 2020). Increased caspase-8 (Figure 4.7A) suggests activation of the extrinsic apoptosis pathway. This corresponds with decreased cIAP (Figure 4.7B), a substrate for caspase-8 (Mandal *et al.*, 2020). Intrinsic apoptosis is implied by decreased *BCL-2* (Figure 4.8B), which facilitates caspase-9 activation (Figure 4.8A) in HepG2 cells treated with *TRALE*. This increase in intrinsic and extrinsic initiator caspases facilitated an increase in caspase-3/7 (Figure 4.9A), an executioner of apoptosis. However, the data in Figure 4.9B shows that there was no change in Annexin V levels in the treated cells when compared to the control, indicating that externalisation of PS was minimal, and apoptosis was not executed. Several scientists reported that when luteolin acts on HepG2 cells, it increases the Bax with caspase-3 expression and reduces the anti-apoptotic protein BCL-2 level, which results in the activation of caspase-3 enzyme (Imran *et al.*, 2019). Thus, there is potential for *TRALE* to help overcome resistance to cancer treatment, making cancer cells more susceptible to treatment-induced apoptosis, and the cells are more prone to undergo apoptosis. This increased susceptibility to apoptosis can have both beneficial and detrimental effects.

Necrosis resulted in a decrease at an IC_{50} level (Figure 4.10A), and LDH (Figure 4.10B), an enzyme that can be used to detect necrosis or accidental cell death, in cells indicated that the cells did not die by necrosis. It is also said that even in the presence of oxygen, cancer cells use LDH to boost their aerobic metabolism, which includes the creation of lactate, ATP and glycolysis by the process of the Warburg effect (Koukourakis and Giatromanolaki, 2019). When the cells were treated with *TRALE* for 24 hours, it was observed that there was a slight decrease in LDH (figure 4.10B), which can

indicate a slowdown in the glycolytic activity which may lead to a reduction in ATP production. Decreased LDH activity could result in less pyruvate production, potentially shifting cellular metabolism towards pathways that depend more on mitochondrial respiration (Feng *et al.*, 2018).

CHAPTER 6: CONCLUSION

Tetradenia riparia is an aromatic shrub locally known in South Africa as "Iboza or Ibozane", with identified anticancer agents in its phytoconstituents. Astragalin and luteolin have been identified to be responsible for the antioxidant activity. However, the cytotoxicity and anti-inflammatory effects of *TRALE* in HepG2 cells have not been identified. Hence, the effects were investigated within the 24 hours.

The *TRALE* induced a dose-dependent cell viability after a 24-hour exposure, followed by a significant decrease in ATP associated with a decline of reducing equivalents because only viable cells can produce ATP. An increase in ΔΨM led to increased levels of ROS production due to proton leakage. The proton leakage played a critical role in controlling the generation of ROS. Increased in ROS production was observed with an increase in the RNS production by an increase in $NO^{\bullet}$ and increased lipid peroxidation which also signifies ROS production. An increase in SOD2 and Gpx1 enhanced the HepG2 cell's ability to convert harmful superoxide radicals into H_2O_2 and help protect mitochondrial DNA, proteins and lipids from oxidative damage, preserving mitochondrial function. Nrf2 controls the expression of genes involved in antioxidant defence and lower levels of Nrf2 lead to reduced expression of antioxidant and detoxifying enzymes such as GSH and GSSG. Lower levels of GSH/GSSG were an indicative of higher oxidative stress and cellular damage, furthermore, an increase in Catalase also signified an oxidative damage, the increased Catalase helps the HepG2 cells to cope with increased production of ROS and maintain balance. Increased *NF-κB* contributed to apoptosis with a decrease in anti-apoptotic gene expression (BCL2), anti-apoptotic protein expression of HSP70 and cIAP with an increase in caspase initiation and activation (caspase-8, caspase-9 and caspase-3/7) making the HepG2 cells more susceptible to the apoptosis enhancing the effectiveness of *TRALE*. This study suggests the potential of *T. riparia* in treating liver cancer.

There is a need for further investigation of the mechanisms that led to a decrease in antioxidants such as GSH and GSSG, as well as the role in inflammation. In addition, the effects of the antioxidant mechanisms of astragalin and luteolin need a thorough investigation in the HepG2 cells and normal kidney cells. Additional phytochemical analysis is recommended to establish the candidate phytochemicals responsible for the observed biological effects. Furthermore, studies on other cancer cell lines and normal cell lines must be done to ensure that *T. riparia* is safe to consume. The *in vivo* effects of the *T. riparia* treatment would support the *in vitro* data presented in this study.

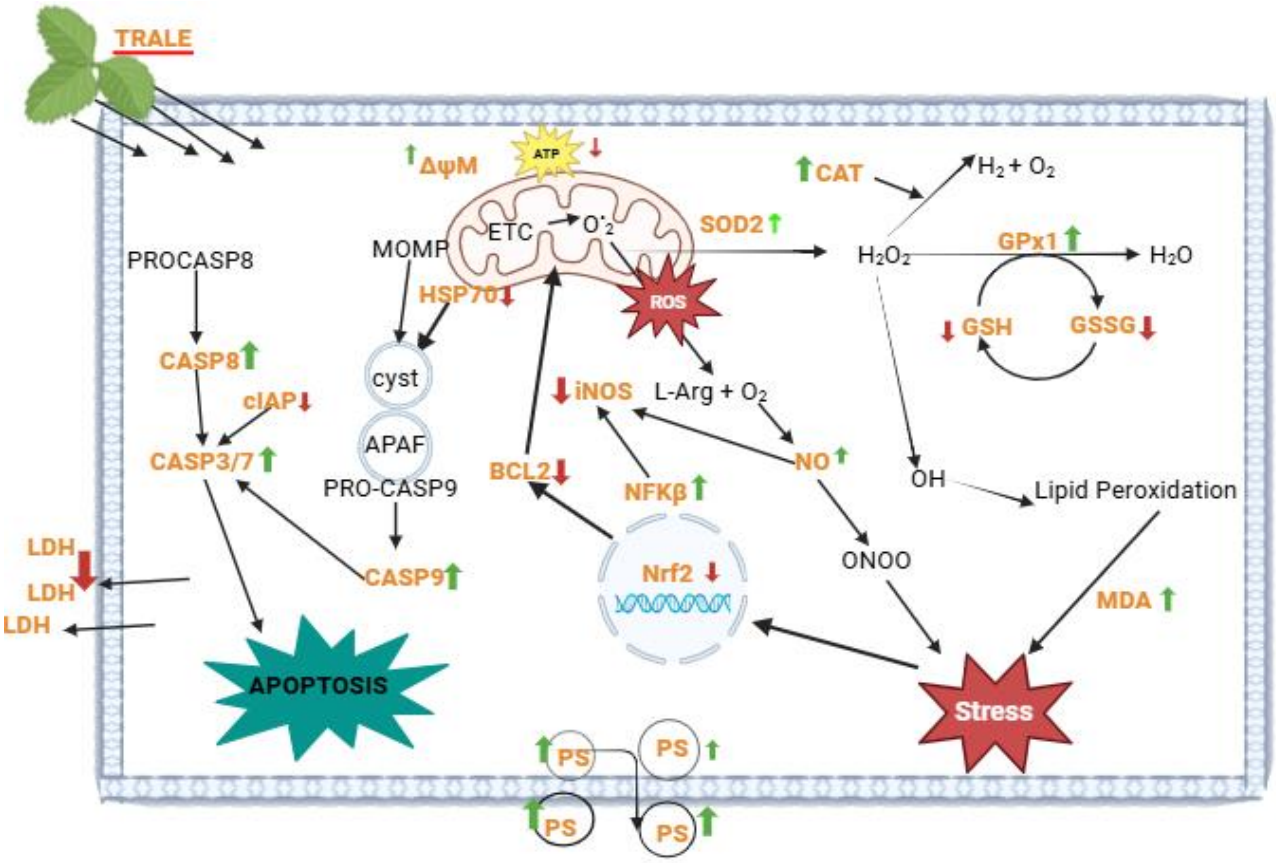

Figure 6.1: Schematic overview of the biochemical effects of *TRALE* on cell viability, metabolic activity, oxidative stress, and apoptosis in hepatocellular carcinoma (HepG2) cells over 24-hour acute exposure. (Prepared by Author).

REFERENCES

Abubakar, A. R. & Haque, M. 2020. Preparation of medicinal plants: Basic extraction and fractionation procedures for experimental purposes. *Journal of Pharmacy and Bioallied Sciences,* 12**,** 1-10.

Adwas, A. A., Elsayed, A., Azab, A. E. & Quwaydir, F. A. 2019. Oxidative stress and antioxidant mechanisms in human body. *J. Appl. Biotechnol. Bioeng,* 6**,** 43-47.

Alché Ramírez, J. D. D. 2019. A concise appraisal of lipid oxidation and lipoxidation in higher plants.

Anwanwan, D., Singh, S. K., Singh, S., Saikam, V. & Singh, R. 2020. Challenges in liver cancer and possible treatment approaches. *Biochimica et Biophysica Acta (BBA)-Reviews on Cancer,* 1873**,** 188314.

Aranda-Rivera, A. K., Cruz-Gregorio, A., Arancibia-Hernández, Y. L., Hernández-Cruz, E. Y. & Pedraza-Chaverri, J. 2022. RONS and oxidative stress: An overview of basic concepts. *Oxygen,* 2**,** 437-478.

Aziz, N., Kim, M.-Y. & Cho, J. Y. 2018. Anti-inflammatory effects of luteolin: A review of in vitro, in vivo, and in silico studies. *Journal of ethnopharmacology,* 225**,** 342-358.

Babbar, M., Basu, S., Yang, B., Croteau, D. L. & Bohr, V. A. 2020. Mitophagy and DNA damage signaling in human aging. *Mechanisms of ageing and development,* 186**,** 111207.

Bahuguna, A., Khan, I., Bajpai, V. K. & Kang, S. C. 2017. MTT assay to evaluate the cytotoxic potential of a drug. *||| Bangladesh Journal of Pharmacology,* 12**,** 115-118.

Bass, J. J., Wilkinson, D. J., Rankin, D., Phillips, B. E., Szewczyk, N. J., Smith, K. & Atherton, P. J. 2017. An overview of technical considerations for Western blotting applications to physiological research. *Scandinavian journal of medicine & science in sports,* 27**,** 4-25.

Begum, H. M. & Shen, K. 2023. Intracellular and microenvironmental regulation of mitochondrial membrane potential in cancer cells. *WIREs mechanisms of disease,* 15**,** e1595.

Bischoff, K., Mukai, M. & Ramaiah, S. K. 2018. Liver toxicity. *Veterinary toxicology.* Elsevier.

Braissant, O., Astasov-Frauenhoffer, M., Waltimo, T. & Bonkat, G. 2020. A review of methods to determine viability, vitality, and metabolic rates in microbiology. *Frontiers in Microbiology,* 11**,** 547458.

Bray, F., Ferlay, J., Soerjomataram, I., Siegel, R. L., Torre, L. A. & Jemal, A. 2018. Global cancer statistics 2018: GLOBOCAN estimates of incidence and mortality worldwide for 36 cancers in 185 countries. *CA Cancer J Clin,* 68**,** 394-424.

Bray, F., Laversanne, M., Sung, H., Ferlay, J., Siegel, R. L., Soerjomataram, I. & Jemal, A. 2024. Global cancer statistics 2022: GLOBOCAN estimates of incidence and mortality worldwide for 36 cancers in 185 countries. *CA: a cancer journal for clinicians,* 74**,** 229-263.

Calderaro, J., Ziol, M., Paradis, V. & Zucman-Rossi, J. 2019. Molecular and histological correlations in liver cancer. *Journal of hepatology,* 71**,** 616-630.

Cavalcante, G. C., Schaan, A. P., Cabral, G. F., Santana-Da-Silva, M. N., Pinto, P., Vidal, A. F. & Ribeiro-Dos-Santos, Â. 2019. A cell's fate: an overview of the molecular biology and genetics of apoptosis. *International journal of molecular sciences,* 20**,** 4133.

Ceci, R., Maldini, M., Olson, M. E., Crognale, D., Horner, K., Dimauro, I., Sabatini, S. & Duranti, G. 2022. Moringa oleifera leaf extract protects C2C12 myotubes against H2O2-induced oxidative stress. *Antioxidants,* 11**,** 1435.

Cerny, M., Chernyak, V., Olivié, D., Billiard, J. S., Murphy-Lavallée, J., Kielar, A. Z., Elsayes, K. M., Bourque, L., Hooker, J. C., Sirlin, C. B. & Tang, A. 2018. LI-RADS Version 2018 Ancillary Features at MRI. *Radiographics,* 38**,** 1973-2001.

Chen, J., Jiang, S., Wang, J., Renukuntla, J., Sirimulla, S. & Chen, J. 2019. A comprehensive review of cytochrome P450 2E1 for xenobiotic metabolism. *Drug metabolism reviews,* 51**,** 178-195.

Chen, J., Zhong, K., Qin, S., Jing, Y., Liu, S., Li, D. & Peng, C. 2023. Astragalin: A food-origin flavonoid with therapeutic effect for multiple diseases. *Frontiers in Pharmacology,* 14**,** 1265960.

Chepng'etich, J., Ngule, C., Jepkorir, M., Mwangangi, R., Njuguna, D. K., Ndung'u, J. W., Kiboi, D. & Mwitari, P. 2018. Total phenolic content and in vitro antiproliferative activity of Tragia brevipes (Pax) and Tetradenia riparia (Hochst) leaves extract.

Conde De La Rosa, L., Goicoechea, L., Torres, S., Garcia-Ruiz, C. & Fernandez-Checa, J. C. 2022. Role of oxidative stress in liver disorders. *Livers,* 2**,** 283-314.

Đanić, M. & Mikov, M. 2020. Biotransformation of xenobiotics in living systems—metabolism of drugs: Partnership of liver and gut microflora. *Pharmaceutical Biocatalysis,* 1**,** 129-166.

Dao Thi, V. L., Wu, X., Belote, R. L., Andreo, U., Takacs, C. N., Fernandez, J. P., Vale-Silva, L. A., Prallet, S., Decker, C. C. & Fu, R. M. 2020. Stem cell-derived polarized hepatocytes. *Nature communications,* 11**,** 1677.

De Dios Alché, J. 2019. A concise appraisal of lipid oxidation and lipoxidation in higher plants. *Redox biology,* 23**,** 101136.

De Leon, J. a. D. & Borges, C. R. 2020. Evaluation of oxidative stress in biological samples using the thiobarbituric acid reactive substances assay. *JoVE (Journal of Visualized Experiments)***,** e61122.

De Oliveira, A. C., Simões, R. C., Tavares, C. P., Lima, C. A., Sá, I. S. C., Da Silva, F. M., Figueira, E. A., Nunomura, S. M., Nunomura, R. C. & Roque, R. A. 2022. Toxicity of the essential oil from Tetradenia riparia (Hochstetter.) Codd (Lamiaceae) and its principal constituent against malaria and dengue vectors and non-target animals. *Pesticide Biochemistry and Physiology,* 188**,** 105265.

Di Meo, S., Reed, T. T., Venditti, P. & Victor, V. M. 2016. Role of ROS and RNS sources in physiological and pathological conditions. *Oxidative medicine and cellular longevity,* 2016.

Dietz, C. & Dekker, M. 2017. Effect of green tea phytochemicals on mood and cognition. *Current pharmaceutical design,* 23**,** 2876-2905.

Donato, M. T., Tolosa, L. & Gómez-Lechón, M. J. 2015. Culture and functional characterization of human hepatoma HepG2 cells. *Protocols in in vitro hepatocyte research***,** 77-93.

Dong, N., Li, Y., Qi, J., Chen, Y. & Hao, Y. 2018. Nitric oxide synthase-dependent nitric oxide production enhances chilling tolerance of walnut shoots in vitro via involvement chlorophyll fluorescence and other physiological parameter levels. *Scientia Horticulturae,* 230**,** 68-77.

Dosunmu-Ogunbi, A., Yuan, S., Reynolds, M., Giordano, L., Sanker, S., Sullivan, M., Stolz, D. B., Kaufman, B. A., Wood, K. C. & Zhang, Y. 2022. SOD2 V16A amplifies vascular dysfunction in sickle cell patients by curtailing mitochondria complex IV activity. *Blood, The Journal of the American Society of Hematology,* 139**,** 1760-1765.

Downey, A. M. 2019. *The Male Germ Cell Response to Cyclophosphamide Treatment: A Potential Role for Zinc.* McGill University (Canada).

Feng, Y., Xiong, Y., Qiao, T., Li, X., Jia, L. & Han, Y. 2018. Lactate dehydrogenase A: A key player in carcinogenesis and potential target in cancer therapy. *Cancer medicine,* 7**,** 6124-6136.

Feno, S., Butera, G., Vecellio Reane, D., Rizzuto, R. & Raffaello, A. 2019. Crosstalk between calcium and ROS in pathophysiological conditions. *Oxidative medicine and cellular longevity,* 2019**,** 1-18.

Ferlay, J., Colombet, M., Soerjomataram, I., Parkin, D. M., Piñeros, M., Znaor, A. & Bray, F. 2021. Cancer statistics for the year 2020: An overview. *International journal of cancer,* 149**,** 778-789.

Galluzzi, L., Vitale, I., Aaronson, S. A., Abrams, J. M., Adam, D., Agostinis, P., Alnemri, E. S., Altucci, L., Amelio, I. & Andrews, D. W. 2018. Molecular mechanisms of cell death: recommendations of the Nomenclature Committee on Cell Death 2018. *Cell Death & Differentiation,* 25**,** 486-541.

Gao, W., Guo, L., Yang, Y., Wang, Y., Xia, S., Gong, H., Zhang, B.-K. & Yan, M. 2022. Dissecting the crosstalk between Nrf2 and NF-κB response pathways in drug-induced toxicity. *Frontiers in cell and developmental biology,* 9**,** 809952.

Gaobotse, G., Venkataraman, S., Brown, P. D., Masisi, K., Kwape, T. E., Nkwe, D. O., Rantong, G. & Makhzoum, A. 2023. The use of African medicinal plants in cancer management. *Frontiers in Pharmacology,* 14.

Gazim, Z. C., Rodrigues, F., Amorin, A. C. L., De Rezende, C. M., Soković, M., Tešević, V., Vučković, I., Krstić, G., Cortez, L. E. R. & Colauto, N. B. 2014. New natural diterpene-type abietane from Tetradenia riparia essential oil with cytotoxic and antioxidant activities. *Molecules,* 19**,** 514-524.

Ghani, M. A., Barril, C., Bedgood Jr, D. R. & Prenzler, P. D. 2017. Measurement of antioxidant activity with the thiobarbituric acid reactive substances assay. *Food chemistry,* 230**,** 195-207.

Ghuman, S., Ncube, B., Finnie, J., Mcgaw, L., Njoya, E. M., Coopoosamy, R. & Van Staden, J. 2019. Antioxidant, anti-inflammatory and wound healing properties of medicinal plant extracts used to treat wounds and dermatological disorders. *South African Journal of Botany,* 126**,** 232-240.

Greten, F. R. & Grivennikov, S. I. 2019. Inflammation and Cancer: Triggers, Mechanisms, and Consequences. *Immunity,* 51**,** 27-41.

Guerrache, A. & Micheau, O. 2024. TNF-Related Apoptosis-Inducing Ligand: Non-Apoptotic Signalling. *Cells,* 13**,** 521.

Guo, J., Zhu, X., Badawy, S., Ihsan, A., Liu, Z., Xie, C. & Wang, X. 2021. Metabolism and mechanism of human cytochrome P450 enzyme 1A2. *Current Drug Metabolism,* 22**,** 40-49.

Hsieh, C.-H., Hsieh, H.-C., Shih, F.-H., Wang, P.-W., Yang, L.-X., Shieh, D.-B. & Wang, Y.-C. 2021. An innovative NRF2 nano-modulator induces lung cancer ferroptosis and elicits an immunostimulatory tumor microenvironment. *Theranostics,* 11**,** 7072.

Idowu, K. A. 2020. *Pharmacokinetic influences of selected phytochemical compounds from herbal medicine used by HIV-positive patients on drugs-metabolising proteins of HIV-1 protease inhibitor drugs.*

Idris, A. M. 2021. *Antioxidative and antidiabetic activity and phytochemicals, analysis of some selected Sudanese traditional medicinal plants.*

Ighodaro, O. & Akinloye, O. 2018. First line defence antioxidants-superoxide dismutase (SOD), catalase (CAT) and glutathione peroxidase (GPX): Their fundamental role in the entire antioxidant defence grid. *Alexandria journal of medicine,* 54**,** 287-293.

Imran, M., Rauf, A., Abu-Izneid, T., Nadeem, M., Shariati, M. A., Khan, I. A., Imran, A., Orhan, I. E., Rizwan, M. & Atif, M. 2019. Luteolin, a flavonoid, as an anticancer agent: A review. *Biomedicine & Pharmacotherapy,* 112**,** 108612.

Jesús, A. D. D. L. 2020. Evaluation of oxidative stress in biological samples using the thiobarbituric acid reactive substances assay.

Jomova, K., Raptova, R., Alomar, S. Y., Alwasel, S. H., Nepovimova, E., Kuca, K. & Valko, M. 2023. Reactive oxygen species, toxicity, oxidative stress, and antioxidants: Chronic diseases and aging. *Archives of toxicology,* 97**,** 2499-2574.

Juan, C. A., Pérez De La Lastra, J. M., Plou, F. J. & Pérez-Lebeña, E. 2021. The chemistry of reactive oxygen species (ROS) revisited: outlining their role in biological macromolecules (DNA, lipids and proteins) and induced pathologies. *International journal of molecular sciences,* 22**,** 4642.

Jung, S., Jeong, H. & Yu, S.-W. 2020. Autophagy as a decisive process for cell death. *Experimental & Molecular Medicine,* 52**,** 921-930.

Kabakov, A. E. & Gabai, V. L. 2018. Cell death and survival assays. *Chaperones: methods and protocols***,** 107-127.

Kamiloglu, S., Sari, G., Ozdal, T. & Capanoglu, E. 2020. Guidelines for cell viability assays. *Food Frontiers,* 1**,** 332-349.

Klaunig, J. E. 2018. Oxidative stress and cancer. *Current pharmaceutical design,* 24**,** 4771-4778.

Koukourakis, M. I. & Giatromanolaki, A. 2019. Warburg effect, lactate dehydrogenase, and radio/chemo-therapy efficacy. *International Journal of Radiation Biology,* 95**,** 408-426.

Krüger, M. & Richter, P. 2022. To die or not to die: Cell death in biology and disease. MDPI.

Kumar, P., Nagarajan, A. & Uchil, P. D. 2018a. Analysis of cell viability by the lactate dehydrogenase assay. *Cold Spring Harb. Protoc,* 2018**,** 465-468.

Kumar, P., Nagarajan, A. & Uchil, P. D. 2018b. Analysis of cell viability by the MTT assay. *Cold spring harbor protocols,* 2018**,** pdb. prot095505.

Kupcho, K., Shultz, J., Hurst, R., Hartnett, J., Zhou, W., Machleidt, T., Grailer, J., Worzella, T., Riss, T. & Lazar, D. 2019. A real-time, bioluminescent annexin V assay for the assessment of apoptosis. *Apoptosis,* 24**,** 184-197.

Kurashova, N., Madaeva, I. & Kolesnikova, L. 2020. Expression of HSP70 heat-shock proteins under oxidative stress. *Advances in Gerontology,* 10**,** 20-25.

Kurien, B. T. & Scofield, R. H. 2015. Western blotting: an introduction. *Western blotting: Methods and protocols***,** 17-30.

Kuwabara, M., Niwa, K., Toyoda, T., Shirai, T., Tateno, S., Ohuchi, H., Tanaka, Y., Ichida, F., Fujisawa, T., Akagi, T. & Mori, Y. 2018. Liver Cirrhosis and/or Hepatocellular Carcinoma Occurring Late After the Fontan Procedure - A Nationwide Survey in Japan. *Circ J,* 82**,** 1155-1160.

Li, H. & Lampe, J. N. 2019. Neonatal cytochrome P450 CYP3A7: A comprehensive review of its role in development, disease, and xenobiotic metabolism. *Archives of biochemistry and biophysics,* 673**,** 108078.

Licata, A. 2016. Adverse drug reactions and organ damage: the liver. *European journal of internal medicine,* 28**,** 9-16.

Liu, D., Zhong, Z. & Karin, M. 2022. NF-κB: A double-edged sword controlling inflammation. *Biomedicines,* 10**,** 1250.

Liu, H., Xu, Y., Xiang, J., Long, L., Green, S., Yang, Z., Zimdahl, B., Lu, J., Cheng, N., Horan, L. H., Liu, B., Yan, S., Wang, P., Diaz, J., Jin, L., Nakano, Y., Morales, J. F., Zhang, P., Liu, L. X., Staley, B. K., Priceman, S. J., Brown, C. E., Forman, S. J., Chan, V. W. & Liu, C. 2017. Targeting Alpha-Fetoprotein (AFP)-MHC Complex with CAR T-Cell Therapy for Liver Cancer. *Clin Cancer Res,* 23**,** 478-488.

Liu, Y., Shi, Y., Han, R., Liu, C., Qin, X., Li, P. & Gu, R. 2023. Signaling pathways of oxidative stress response: the potential therapeutic targets in gastric cancer. *Frontiers in immunology,* 14**,** 1139589.

Livak, K. J. & Schmittgen, T. D. 2001. Analysis of Relative Gene Expression Data Using Real-Time Quantitative PCR and the 2−ΔΔCT Method. *Methods,* 25**,** 402-408.

Lou, J.-S., Zhao, L.-P., Huang, Z.-H., Chen, X.-Y., Xu, J.-T., Tai, W. C.-S., Tsim, K. W., Chen, Y.-T. & Xie, T. 2021. Ginkgetin derived from Ginkgo biloba leaves enhances the therapeutic effect of cisplatin via ferroptosis-mediated disruption of the Nrf2/HO-1 axis in EGFR wild-type non-small-cell lung cancer. *Phytomedicine,* 80**,** 153370.

Luanda, A. & Ripanda, A. 2022. Recent trend on Tetradenia riparia (Hochst.) Codd (Lamiaceae) for management of medical conditions. *Phytomedicine Plus***,** 100382.

Luanda, A. & Ripanda, A. 2023. Recent trend on Tetradenia riparia (Hochst.) Codd (Lamiaceae) for management of medical conditions. *Phytomedicine Plus,* 3**,** 100382.

Mahlangu, S. G. 2019. *The antimicrobial activity of secondary metabolites produced by bacterial endophytes isolated from Pellaea calomelanos*, University of Johannesburg (South Africa).

Mak, D., Sengayi, M., Chen, W. C., Babb De Villiers, C., Singh, E. & Kramvis, A. 2018. Liver cancer mortality trends in South Africa: 1999-2015. *BMC Cancer,* 18**,** 798.

Małyszko, J., Kozłowska, K., Kozłowski, L. & Małyszko, J. 2017. Nephrotoxicity of anticancer treatment. *Nephrology Dialysis Transplantation,* 32**,** 924-936.

Mandal, R., Barrón, J. C., Kostova, I., Becker, S. & Strebhardt, K. 2020. Caspase-8: The double-edged sword. *Biochimica et Biophysica Acta (BBA)-Reviews on Cancer,* 1873**,** 188357.

Maruma, L. N., Somboro, A. M., Amoako, D. G., Khumalo, H. M. & Khan, R. B. 2022. Molecular mechanisms underlying Warburgia salutaris effects on oxidative stress and apoptotic parameters in Human Hepatoma Cells. *bioRxiv***,** 2022.03. 05.483129.

Mas-Bargues, C., Escriva, C., Dromant, M., Borras, C. & Vina, J. 2021. Lipid peroxidation as measured by chromatographic determination of malondialdehyde. Human plasma reference values in health and disease. *Archives of biochemistry and biophysics,* 709**,** 108941.

Megersa, M., Jima, T. T. & Goro, K. K. 2019. The use of medicinal plants for the treatment of toothache in Ethiopia. *Evidence-Based Complementary and Alternative Medicine,* 2019.

Mhlanga, P., Perumal, P. O., Somboro, A. M., Amoako, D. G., Khumalo, H. M. & Khan, R. B. 2019. Mechanistic insights into oxidative stress and apoptosis mediated by tannic acid in human liver hepatocellular carcinoma cells. *International Journal of Molecular Sciences,* 20**,** 6145.

Milato, J. V., Silva, R. S. F., De Souza Figueiredo, F., De Almeida Azevedo, D., Ribeiro, C. a. B. & Leitão, G. G. 2018. Use of counter-current chromatography as a selective extractor for the diterpenequinone 7α-hydroxyroyleanone from Tetradenia riparia. *Journal of Chromatography A,* 1537**,** 135-140.

Miyai, T., Toyono, T., Kitamoto, K., Fukushima, M., Yoshida, J., Shirakawa, R., Nakagawa, S., Jurkunas, U. V. & Usui, T. 2018. Endoplasmic reticulum stress decreases mitochondrial membrane potential and upregulates PARK2 expression in corneal endothelium. *Investigative Ophthalmology & Visual Science,* 59**,** 4436-4436.

Moujalled, D., Strasser, A. & Liddell, J. R. 2021. Molecular mechanisms of cell death in neurological diseases. *Cell Death & Differentiation,* 28**,** 2029-2044.

Mposula, S., Amoako, D. G., Somboro, A. M., Arhin, I., Kumalo, H. M. & Khan, R. B. 2021. Apoptosis-inducing effects of Terminalia phanerophlebia leaf extracts on human renal cells. *South African Journal of Botany,* 139**,** 273-280.

Nagura-Ikeda, M., Imai, K., Tabata, S., Miyoshi, K., Murahara, N., Mizuno, T., Horiuchi, M., Kato, K., Imoto, Y. & Iwata, M. 2020. Clinical evaluation of self-collected saliva by quantitative reverse transcription-PCR

(RT-qPCR), direct RT-qPCR, reverse transcription–loop-mediated isothermal amplification, and a rapid antigen test to diagnose COVID-19. *Journal of clinical microbiology,* 58**,** 10.1128/jcm. 01438-20.

Nawaz, H., Shad, M. A., Rehman, N., Andaleeb, H. & Ullah, N. 2020. Effect of solvent polarity on extraction yield and antioxidant properties of phytochemicals from bean (Phaseolus vulgaris) seeds. *Brazilian Journal of Pharmaceutical Sciences,* 56**,** e17129.

Ndlovu, S., Nagiah, S., Abdul, N. S., Ghazi, T. & Chuturgoon, A. A. 2021. Deoxynivalenol downregulates NRF2-induced cytoprotective response in human hepatocellular carcinoma (HepG2) cells. *Toxicon,* 193**,** 4-12.

Netshitangani, T. F. 2022. *Momordica foetida facilitates glucose uptake independent of AMPK2 and PI3K to attenuate hyperglycemia-induced oxidative stress via a JNK-STAT3 mediated pathway in HepG2 cells.*

Njau, E.-F. & Ndakidemi, P. 2017. The Genus Tetradenia (Lamiaceae): A Review of Its Ethnomedicinal, Botanical, Chemical and Pharmacological Activities. *International Journal of Biology,* 9**,** 35.

Nunes, C., Almeida, L., Barbosa, R. M. & Laranjinha, J. 2017. Luteolin suppresses the JAK/STAT pathway in a cellular model of intestinal inflammation. *Food & function,* 8**,** 387-396.

Nxumalo, M. B., Ntanzi, N., Kumalo, H. M. & Khan, R. B. 2024. Mitigating Hyperglycaemic Oxidative Stress in HepG2 Cells: The Role of Carica papaya Leaf and Root Extracts in Promoting Glucose Uptake and Antioxidant Defence. *Nutrients,* 16**,** 3496.

Nyahada, M. R. 2021. *Terminalia phanerophlebia crude aqueous leaf extract activates the NRF2-mediated antioxidant defence to prevent oxidative stress in human hepatocellular carcinoma cells.*

Ortega-Alonso, A. & Andrade, R. J. 2018. Chronic liver injury induced by drugs and toxins. *Journal of Digestive Diseases,* 19**,** 514-521.

Ozioma, E.-O. J. & Chinwe, O. a. N. 2019. Herbal medicines in African traditional medicine. *Herbal medicine,* 10**,** 191-214.

Pan, X., Zhou, J., Chen, Y., Xie, X., Rao, C., Liang, J., Zhang, Y. & Peng, C. 2020. Classification, hepatotoxic mechanisms, and targets of the risk ingredients in traditional Chinese medicine-induced liver injury. *Toxicology letters,* 323**,** 48-56.

Panda, S. K., Gazim, Z. C., Swain, S. S., Bento, M. C. V. D. A., Sena, J. D. S., Mukazayire, M. J., Van Puyvelde, L. & Luyten, W. 2022. Ethnomedicinal, phytochemical and pharmacological investigations of Tetradenia riparia (Hochst.) Codd (Lamiaceae). *Frontiers in Pharmacology,* 13**,** 896078.

Pappas, G., Wilkinson, M. L. & Gow, A. J. 2023. Nitric oxide regulation of cellular metabolism: Adaptive tuning of cellular energy. *Nitric Oxide,* 131**,** 8-17.

Patil, A. A., Bhor, S. A. & Rhee, W. J. 2020. Cell death in culture: Molecular mechanisms, detections, and inhibition strategies. *Journal of Industrial and Engineering Chemistry,* 91**,** 37-53.

Petrick, J. L. & Mcglynn, K. A. 2019. The changing epidemiology of primary liver cancer. *Current epidemiology reports,* 6**,** 104-111.

Pfeffer, C. M. & Singh, A. T. 2018. Apoptosis: a target for anticancer therapy. *International journal of molecular sciences,* 19**,** 448.

Prasad, S. B. 2022. Cancer and apoptosis. *Understanding Cancer.* Elsevier.

Procházková, M., Killinger, M., Prokeš, L. & Klepárník, K. 2022. Miniaturized bioluminescence technology for single-cell quantification of caspase-3/7. *Journal of pharmaceutical and biomedical analysis,* 209**,** 114512.

Rai, Y., Pathak, R., Kumari, N., Sah, D. K., Pandey, S., Kalra, N., Soni, R., Dwarakanath, B. & Bhatt, A. N. 2018. Mitochondrial biogenesis and metabolic hyperactivation limits the application of MTT assay in the estimation of radiation induced growth inhibition. *Scientific reports,* 8**,** 1531.

Riaz, A., Rasul, A., Hussain, G., Zahoor, M. K., Jabeen, F., Subhani, Z., Younis, T., Ali, M., Sarfraz, I. & Selamoglu, Z. 2018. Astragalin: a bioactive phytochemical with potential therapeutic activities. *Advances in pharmacological sciences,* 2018.

Rosenzweig, R., Nillegoda, N. B., Mayer, M. P. & Bukau, B. 2019. The Hsp70 chaperone network. *Nature reviews molecular cell biology,* 20**,** 665-680.

Ruan, J., Shi, Z., Cao, X., Dang, Z., Zhang, Q., Zhang, W., Wu, L., Zhang, Y. & Wang, T. 2024. Research Progress on Anti-Inflammatory Effects and Related Mechanisms of Astragalin. *International Journal of Molecular Sciences,* 25**,** 4476.

Sakamuru, S., Attene-Ramos, M. S. & Xia, M. 2016. Mitochondrial membrane potential assay. *High-throughput screening assays in toxicology*, 17-22.

Salbitani, G., Bottone, C. & Carfagna, S. 2017. Determination of reduced and total glutathione content in extremophilic microalga Galdieria phlegrea. *Bio-protocol,* 7, e2372-e2372.

Satyo, L., Amoako, D. G., Somboro, A. M., Sosibo, S. C., Kumalo, H. M., Mhlongo, N. N. & Khan, R. B. 2020. Molecular insights into Di (2-Picolyl) amine–induced cytotoxicity and apoptosis in human kidney (HEK293) cells. *International journal of toxicology,* 39, 341-351.

Sauzay, C., Petit, A., Bourgeois, A. M., Barbare, J. C., Chauffert, B., Galmiche, A. & Houessinon, A. 2016. Alpha-foetoprotein (AFP): A multi-purpose marker in hepatocellular carcinoma. *Clin Chim Acta,* 463, 39-44.

Scabini, M., Stellari, F., Cappella, P., Rizzitano, S., Texido, G. & Pesenti, E. 2011. In vivo imaging of early stage apoptosis by measuring real-time caspase-3/7 activation. *Apoptosis,* 16, 198-207.

Schrödl, W., Büchler, R., Wendler, S., Reinhold, P., Muckova, P., Reindl, J. & Rhode, H. 2016. Acute phase proteins as promising biomarkers: Perspectives and limitations for human and veterinary medicine. *PROTEOMICS–Clinical Applications,* 10, 1077-1092.

Shen, Y., Risch, H., Lu, L., Ma, X., Irwin, M. L., Lim, J. K., Taddei, T., Pawlish, K., Stroup, A. & Brown, R. 2020. Risk factors for hepatocellular carcinoma (HCC) in the northeast of the United States: results of a case–control study. *Cancer Causes & Control,* 31, 321-332.

Shimira, F. 2022. Tetradenia riparia, an ethnobotanical plant with diverse applications, from antimicrobial to anti-proliferative activity against cancerous cell lines: A systematic review. *Journal of Herbal Medicine,* 32, 100537.

Shunmugam, L. 2016. *Moringa oleifera crude aqueous leaf extract induces apoptosis in human hepatocellular carcinoma cells via the upregulation of NF-kB and IL-6/STAT3 pathway.*

Sia, D., Villanueva, A., Friedman, S. L. & Llovet, J. M. 2017. Liver cancer cell of origin, molecular class, and effects on patient prognosis. *Gastroenterology,* 152, 745-761.

Sies, H. 2018. On the history of oxidative stress: Concept and some aspects of current development. *Current Opinion in Toxicology,* 7, 122-126.

Sies, H. & Jones, D. P. 2020. Reactive oxygen species (ROS) as pleiotropic physiological signalling agents. *Nature reviews Molecular cell biology,* 21, 363-383.

Singh, P. & Lim, B. 2022. Targeting apoptosis in cancer. *Current oncology reports,* 24, 273-284.

Soond, S. M., Kozhevnikova, M. V., Savvateeva, L. V., Townsend, P. A. & Zamyatnin Jr, A. A. 2021. Intrinsically connected: therapeutically targeting the cathepsin proteases and the Bcl-2 family of protein substrates as co-regulators of apoptosis. *International Journal of Molecular Sciences,* 22, 4669.

Stockdale, A. J., Kreuels, B., Henrion, M. Y., Giorgi, E., Kyomuhangi, I., De Martel, C., Hutin, Y. & Geretti, A. M. 2020. The global prevalence of hepatitis D virus infection: systematic review and meta-analysis. *Journal of hepatology,* 73, 523-532.

Suk, K. T. & Kim, D. J. 2015. Staging of liver fibrosis or cirrhosis: The role of hepatic venous pressure gradient measurement. *World J Hepatol,* 7, 607-15.

Sun, J., Liu, F., Yu, W., Jiang, Q., Hu, J., Liu, Y., Wang, F. & Liu, X. 2019. Highly sensitive glutathione assay and intracellular imaging with functionalized semiconductor quantum dots. *Nanoscale,* 11, 5014-5020.

Sung, H., Ferlay, J., Siegel, R. L., Laversanne, M., Soerjomataram, I., Jemal, A. & Bray, F. 2021. Global cancer statistics 2020: GLOBOCAN estimates of incidence and mortality worldwide for 36 cancers in 185 countries. *CA: a cancer journal for clinicians,* 71, 209-249.

Süntar, I. 2020. Importance of ethnopharmacological studies in drug discovery: role of medicinal plants. *Phytochemistry Reviews,* 19, 1199-1209.

Sykes, W. 2021. *An investigation of the impact of universal Hepatitis B Virus (HBV) vaccination among young blood donors in South Africa.*

Taylor, R. S., Taylor, R. J., Bayliss, S., Hagström, H., Nasr, P., Schattenberg, J. M., Ishigami, M., Toyoda, H., Wong, V. W.-S. & Peleg, N. 2020. Association between fibrosis stage and outcomes of patients with nonalcoholic fatty liver disease: a systematic review and meta-analysis. *Gastroenterology,* 158, 1611-1625. e12.

Thompson, J. B. & Hawkins, J. A. 2025. Phylogeny and bioprospecting: The diversity of medicinal plants used in cancer management. *PLANTS, PEOPLE, PLANET,* 7, 147-158.

Truong, D.-H., Nguyen, D. H., Ta, N. T. A., Bui, A. V., Do, T. H. & Nguyen, H. C. 2019. Evaluation of the use of different solvents for phytochemical constituents, antioxidants, and in vitro anti-inflammatory activities of Severinia buxifolia. *Journal of food quality,* 2019**,** 8178294.

Ulasov, A. V., Rosenkranz, A. A., Georgiev, G. P. & Sobolev, A. S. 2022. Nrf2/Keap1/ARE signaling: Towards specific regulation. *Life sciences,* 291**,** 120111.

Van Wyk, A. & Prinsloo, G. 2018. Medicinal plant harvesting, sustainability and cultivation in South Africa. *Biological Conservation,* 227**,** 335-342.

Von Staden, L. 2016. Tetradenia riparia (Hochst.) Codd. National Assessment: Red List of South African Plants version *Accessed on 2024/12/16*.

Wu, X.-Y., Xu, W.-W., Huan, X.-K., Wu, G.-N., Li, G., Zhou, Y.-H. & Najafi, M. 2023. Mechanisms of cancer cell killing by metformin: a review on different cell death pathways. *Molecular and Cellular Biochemistry,* 478**,** 197-214.

Yamashita, T. & Kaneko, S. 2016. [Liver Cancer]. *Rinsho Byori,* 64**,** 787-796.

Yang, M., Li, W.-Y., Xie, J., Wang, Z.-L., Wen, Y.-L., Zhao, C.-C., Tao, L., Li, L.-F., Tian, Y. & Sheng, J. 2021. Astragalin inhibits the proliferation and migration of human colon cancer HCT116 cells by regulating the NF-κB signaling pathway. *Frontiers in Pharmacology,* 12**,** 639256.

Yasgar, A., Shultz, J., Zhou, W., Wang, H., Huang, F., Murphy, N., Abel, E. L., Digiovanni, J., Inglese, J. & Simeonov, A. 2010. A high-throughput 1,536-well luminescence assay for glutathione S-transferase activity. *Assay and drug development technologies,* 8**,** 200-211.

Youn, B.-Y., Kim, J.-H., Jo, Y.-K., Yoon, S., Im, J.-Y., Kim, H.-J., Lee, J.-D. & Ko, S.-G. 2023. Current Characteristics of Herbal Medicine Interventions for Cancer on Clinical Databases: A Cross-Sectional Study. *Integrative Cancer Therapies,* 22**,** 15347354231218255.

Younes, N., Alsahan, B. S., Al-Mesaifri, A. J., Da'as, S. I., Pintus, G., Majdalawieh, A. F. & Nasrallah, G. K. 2022. JC-10 probe as a novel method for analyzing the mitochondrial membrane potential and cell stress in whole zebrafish embryos. *Toxicology research,* 11**,** 77-87.

Yu, H., Lin, L., Zhang, Z., Zhang, H. & Hu, H. 2020. Targeting NF-κB pathway for the therapy of diseases: mechanism and clinical study. *Signal transduction and targeted therapy,* 5**,** 209.

Zhang, T., Ma, C., Zhang, Z., Zhang, H. & Hu, H. 2021. NF-κB signaling in inflammation and cancer. *MedComm,* 2**,** 618-653.

Zhao, H., Wu, L., Yan, G., Chen, Y., Zhou, M., Wu, Y. & Li, Y. 2021a. Inflammation and tumor progression: signaling pathways and targeted intervention. *Signal transduction and targeted therapy,* 6**,** 263.

Zhao, M., Ma, J., Li, M., Zhang, Y., Jiang, B., Zhao, X., Huai, C., Shen, L., Zhang, N. & He, L. 2021b. Cytochrome P450 enzymes and drug metabolism in humans. *International journal of molecular sciences,* 22**,** 12808.

Zhao, R. Z., Jiang, S., Zhang, L. & Yu, Z. B. 2019. Mitochondrial electron transport chain, ROS generation and uncoupling. *International journal of molecular medicine,* 44**,** 3-15.

Zhao, S., Tang, Y., Wang, R. & Najafi, M. 2022. Mechanisms of cancer cell death induction by paclitaxel: an updated review. *Apoptosis,* 27**,** 647-667.

Zorova, L. D., Popkov, V. A., Plotnikov, E. Y., Silachev, D. N., Pevzner, I. B., Jankauskas, S. S., Babenko, V. A., Zorov, S. D., Balakireva, A. V. & Juhaszova, M. 2018. Mitochondrial membrane potential. *Analytical biochemistry,* 552**,** 50-59.

APPENDICES

APPENDIX 1: CELL VIABILITY OF HEPG2 CELLS

Table A1: HepG2 cells were treated with a range concentration of *TRALE* (0 – 500 µM) for 24 hours.

TRALE **Concentration (µg/ml)**	**% Viability**	**Log[TRALE]**
0	100.000000	0.000000
250	86.551730	2.397940
500	105.000000	2.698970
1000	59.482760	3.000000
2000	20.172410	3.301030
3000	10.172410	3.477121
4000	9.482759	3.602060
5000	9.482759	3.698970

APPENDIX 2: NITRATE STANDARD CURVE

Table A2: determination of the nitrates and nitrites standard reference curve

Nitrite Standard Concentration (µM)	**Absorbance (triplicate)**	**Average Absorbance**
0	-0.004 -0.0004 -0.001	-0.0018
12.5	0.117 0.213 0.224	0.184667
25	0.369 0.468 0.452	0.429667
50	0.682 0.902 0.824	0.802667
75	1.021 1.042 1.248	1.103667
10	1.401 1.493 1.612	1.502
150	2.13 2.212 2.472	2.271333
200	2.718 2.975 3.14	2.944333

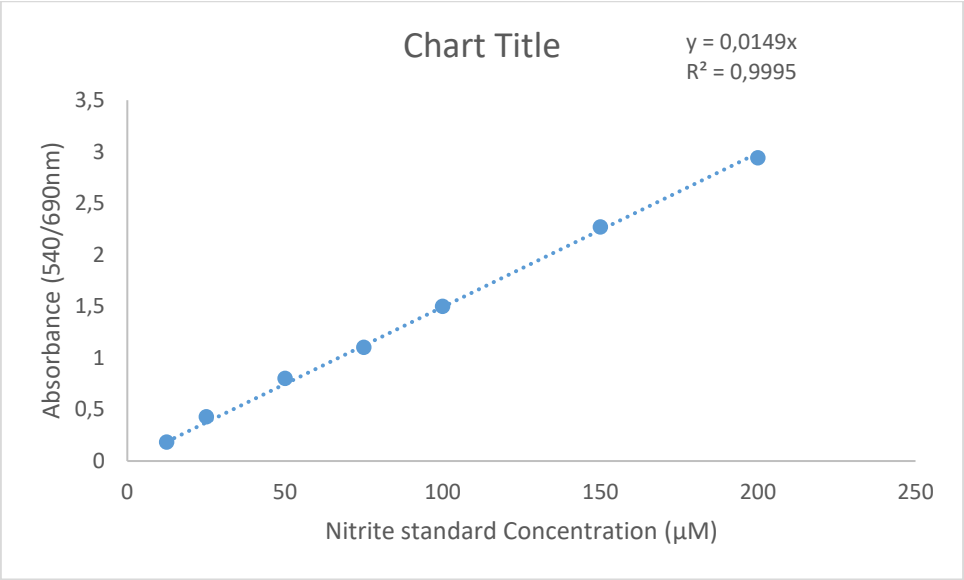

Figure A1: Standard curve generated from nitrates and nitrites standards and was used to determine nitrates and nitrites concentration in samples.

APPENDIX 3 : PROTEIN PREPARATION FOR WESTERN BLOTTING

Table A3: Protein Quantification and Standardisation using Bovine Serum Albumin (BSA)

Protein Standard(mg/ml)	**OD1**	**OD2**	**OD3**	**Average OD**
0	0.146	0.181	0.176	0.16766667
0.2	0.367	0.406	0.379	0.384
0.4	0.626	0.622	0.569	0.605667
0.6	0.754	0.831	0.864	0.816333
0.8	1.028	1.032	1.053	1.037666667
0.1	1.252	1.211	1.281	1.248

Table A4: Standardisation of protein samples to 1mg/ml using standard curve of BSA concentrations

Treatment	**OD1**	**OD2**	**OD3**	**Average**	**[Protein]**	**V1 (Sample)**	**V2-V1(Cytobuster)**
Control	2.1760	2.4030	2.8290	2.469333	2.12629	197.53	2.47
IC_{50}	3.3310	3.0770	3.0910	3.166333	2.770527	151.60	48.40
Normalised Control	2.0083	2.2353	2.6613	2.301667	2.126229	197.53	2.47
Normalised IC_{50}	3.1633	2.9093	2.9233	2.998667	2.770466	151.60	48.40

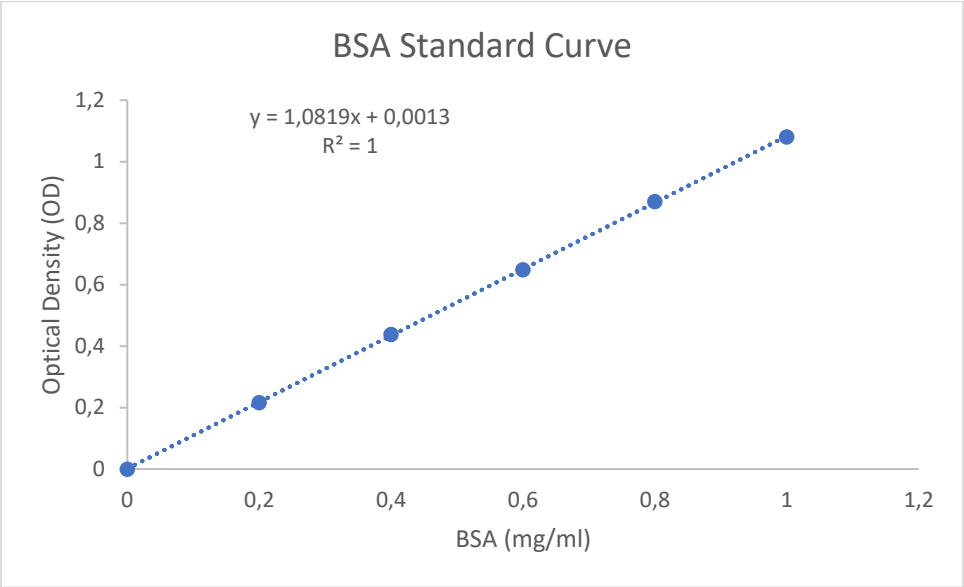

Figure A2: standard curve generated from BSA standard and used to determine protein concentrations in samples.

APPENDIX 4 : PCR

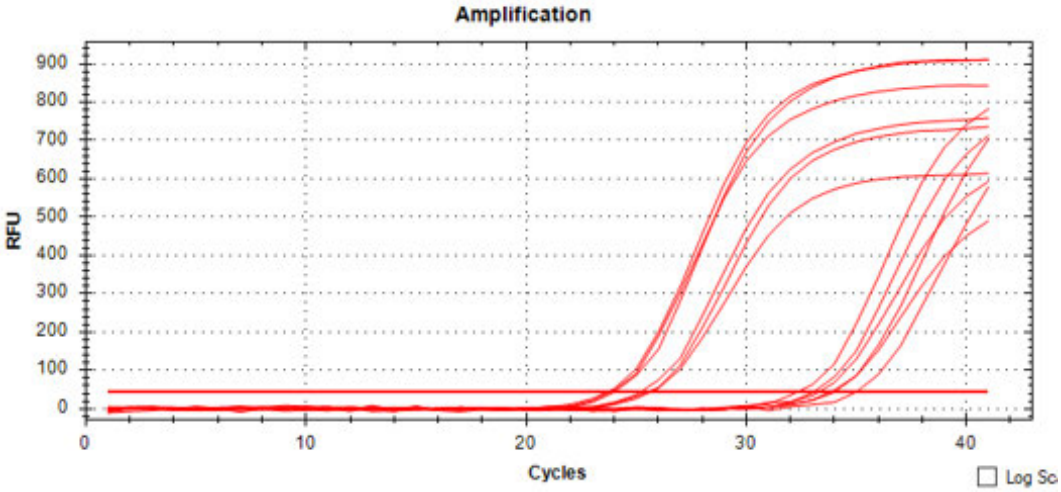

Figure A3: Gene amplification of *Gpx1*.

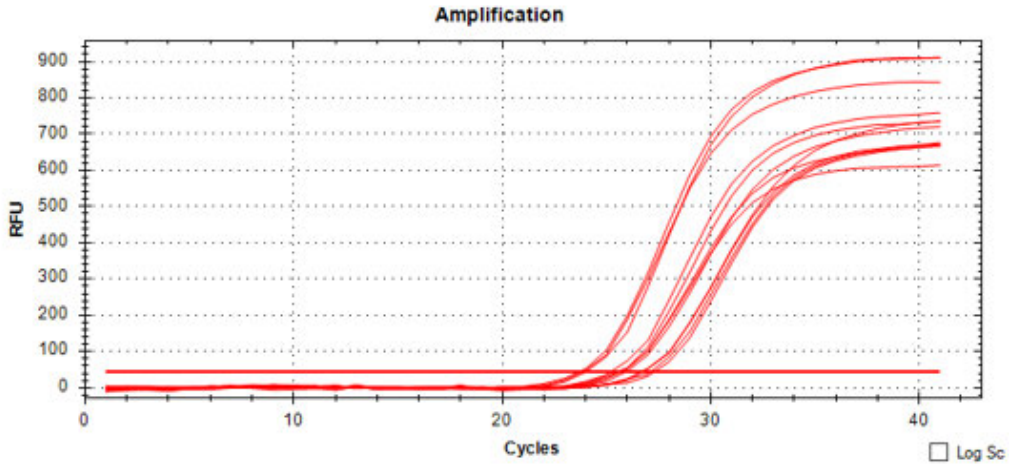

Figure A4: Gene amplification of *NF-κB.*

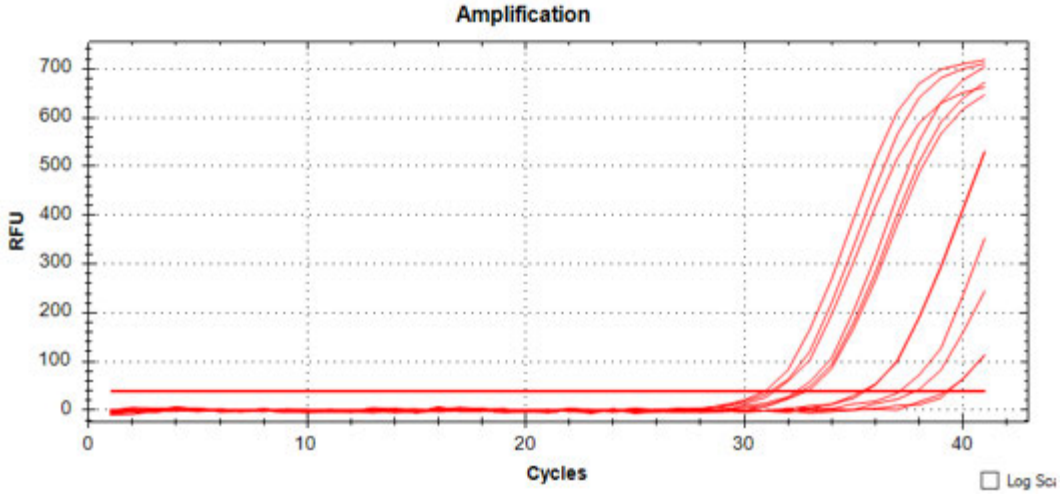

Figure A5: Gene amplification of *Catalase*.

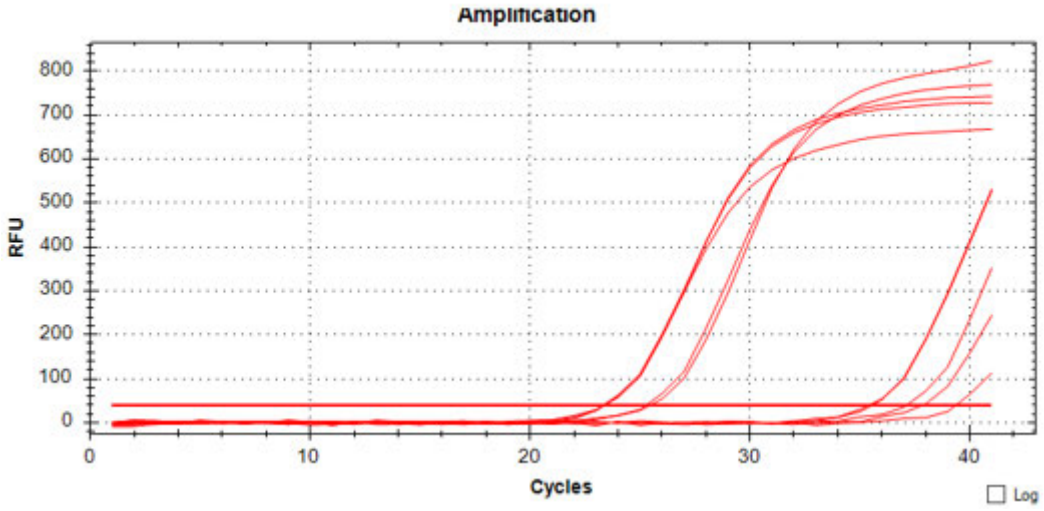

Figure A6: Gene amplification of BCL-2.

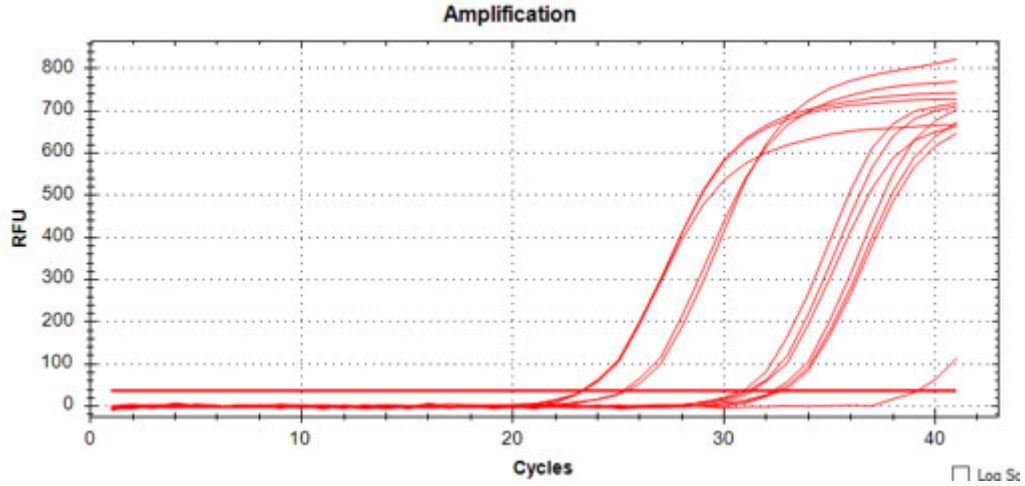

Figure A7: Gene amplification of *SOD2*.

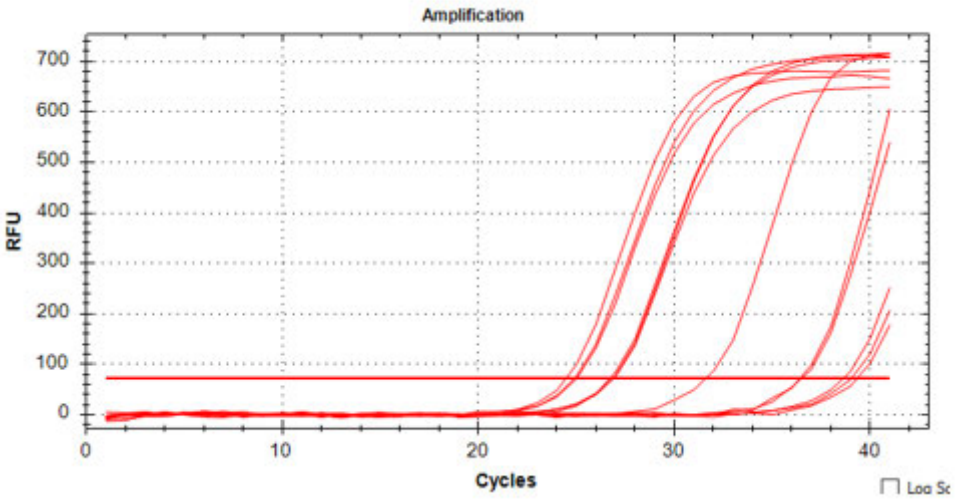

Figure A8: Gene amplification of *iNOS*.

APPENDIX 5 : ETHICS

UNIVERSITY OF KWAZULU-NATAL
INYUVESI YAKWAZULU-NATALI

02 October 2023

Mr Seluleko Gcaba (218045487)
School of Lab Med & Medical Sc

Dear Mr Gcaba,

Protocol reference number: BREC/00006185/2023
Project title: The Cytotoxic and inflammatory effects of Tetradenia riparia plant (iboza) in hepatocellular carcinoma (HepG2) cancer cells
Degree: Masters

EXPEDITED APPLICATION: APPROVAL LETTER

A sub-committee of the Biomedical Research Ethics Committee has considered and noted your application.

The conditions have been met and the study is given full ethics approval and may begin as from 02 October 2023. Please ensure that any outstanding site permissions are obtained and forwarded to BREC for approval before commencing research at a site.

This approval is valid for one year from 02 October 2023. To ensure uninterrupted approval of this study beyond the approval expiry date, an application for recertification must be submitted to BREC on RIG on the appropriate BREC form 2-3 months before the expiry date.

Any amendments to this study, unless urgently required to ensure safety of participants, must be approved by BREC prior to implementation.

Your acceptance of this approval denotes your compliance with South African National Research Ethics Guidelines (2015), South African National Good Clinical Practice Guidelines (2020) (if applicable) and with UKZN BREC ethics requirements as contained in the UKZN BREC Terms of Reference and Standard Operating Procedures, all available at http://research.ukzn.ac.za/Research-Ethics/Biomedical-Research-Ethics.aspx.

BREC is registered with the South African National Health Research Ethics Council (REC-290408-009). BREC has US Office for Human Research Protections (OHRP) Federal-wide Assurance (FWA 678).

The sub-committee's decision will be noted by a full Committee at its next meeting taking place on 14 November 2023.

Yours sincerely,

[redacted]

Prof D Wassenaar
Chair: Biomedical Research Ethics Committee

Biomedical Research Ethics Committee
Chair: Professor D R Wassenaar
UKZN Research Ethics Office Westville Campus, Govan Mbeki Building
Postal Address: Private Bag X54001, Durban 4000
Email: BREC@ukzn.ac.za
Website: http://research.ukzn.ac.za/Research-Ethics/Biomedical-Research-Ethics.aspx

APPENDIX 6 : TURNITIN / PLAGIARISM REPORT

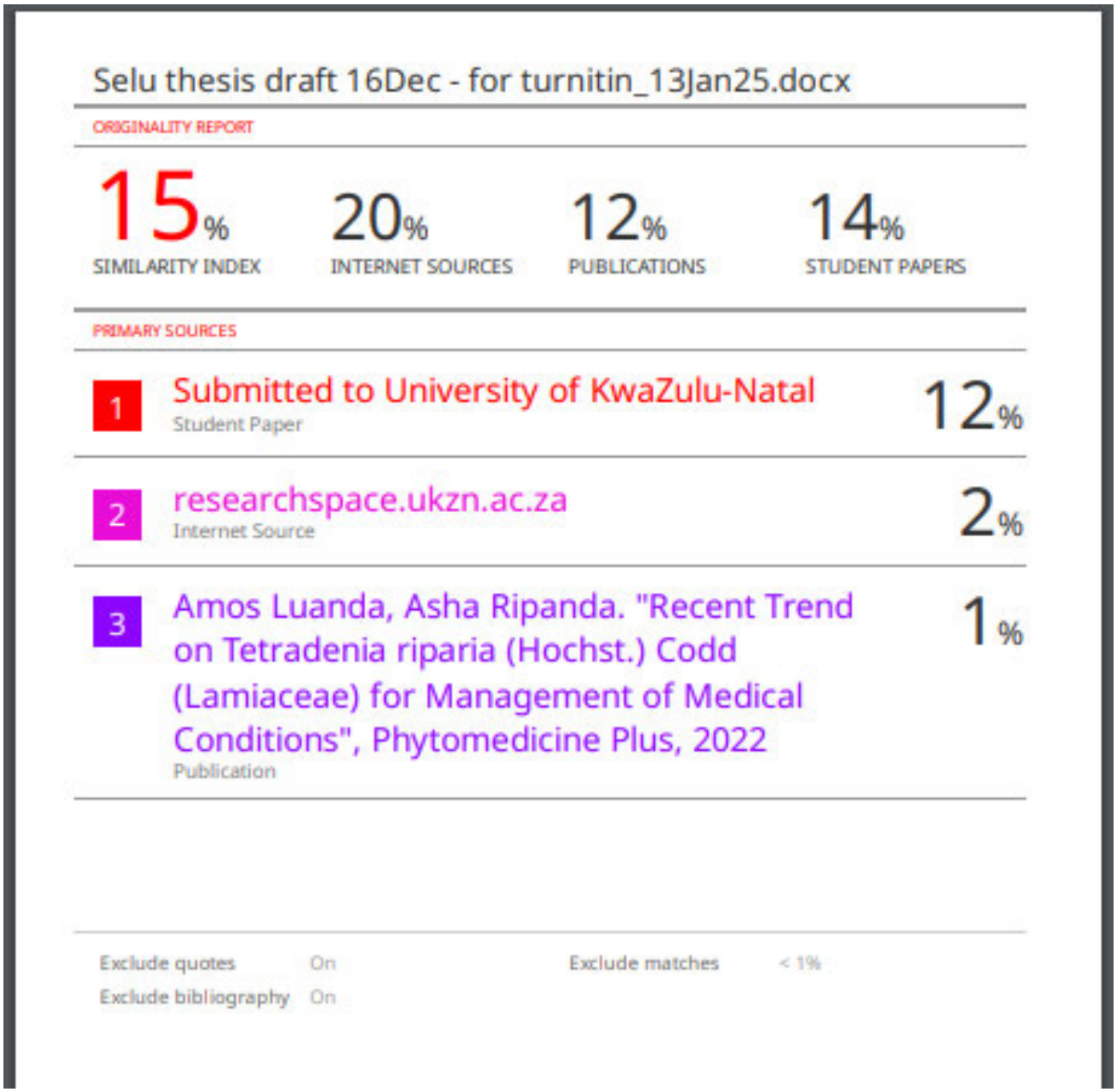

Selu thesis draft 16Dec - for turnitin_13Jan25.docx

ORIGINALITY REPORT

15%	20%	12%	14%
SIMILARITY INDEX	INTERNET SOURCES	PUBLICATIONS	STUDENT PAPERS

PRIMARY SOURCES

1	Submitted to University of KwaZulu-Natal Student Paper	12%
2	researchspace.ukzn.ac.za Internet Source	2%
3	Amos Luanda, Asha Ripanda. "Recent Trend on Tetradenia riparia (Hochst.) Codd (Lamiaceae) for Management of Medical Conditions", Phytomedicine Plus, 2022 Publication	1%

Exclude quotes	On	Exclude matches	< 1%
Exclude bibliography	On		